Crack width of reinforced concrete structures under imposed deformations

F. Yilmaz

TU Delft

Crack width of reinforced concrete structures under imposed deformations

by

F. Yilmaz

to obtain the degree of Master of Science
at the Delft University of Technology,
to be defended publicly on Wednesday 4 May 2022 at 16:00.

Student number:	4738071	
Graduation date:	4 May 2022	
Thesis committee:	Dr. ir. M. Lukovic,	TU Delft (Chair)
	Dr. ir. C.B.M. Blom,	TU Delft
	Prof. dr. ir. E. Schlangen,	TU Delft
	Ir. S. Mustafa,	TU Delft

This thesis is confidential and cannot be made public until 4 May 2022.

TU Delft

Preface

In order to obtain a Master's degree at the Faculty of Civil Engineering and Geosciences, it is required to write a Master's thesis on a subject of one's own interest. This reports covers my interest regarding crack widths due to imposed deformations. The main focus of this research is the difference between the crack width prediction of reinforced concrete structures under imposed loads or imposed deformations and the applicability of the current design codes.

First of all, I would like to express my gratitude to the members of my thesis committee dr. ir. Mladena Lukovic, prof. dr. ir. Erik Schlangen, ir. Shozab Mustafa and dr. ir. Kees Blom whose guidance and patience was very important during this research. I also want to thank dr. ir. Rene Braam and dr. ir. Max Hendriks for providing the required documents and their advice during my research.

Furthermore, my outmost appreciation goes out to my family, friends and girlfriend for their infinite support and encouraging words every day.

Fidel Yilmaz
Delft, 4 May 2022

Abstract

When concrete is subjected to imposed deformations, stresses may develop. If at any point in time this stress exceeds the tensile strength of the material, the concrete will crack. Early-age cracking of concrete structures may lead to problems with durability, serviceability and aesthetics. During hardening of concrete the material properties are still in development. Therefore, to be able to predict the crack width, understanding of the stress- and strength development is required. In addition, concrete is a visco-elastic material which means that stresses are affected by phenomena such as creep or relaxation. If the design codes predict the crack width in concrete structures under imposed deformations accurately remain subject of debate. The CROW report published in 2021 [9] provided the starting point for this research.

The aim of this study was to gain more insight on the background of the design codes, and to explain the fundamentals of the crack width prediction in case of imposed deformations. For this purpose, the following research question was formulated:

"What is the applicability of the design codes regarding the crack width prediction of reinforced concrete structures under imposed deformations?"

From the literature study it became clear that the main difference between the design codes was related to which boundary conditions and cracking theory were applied. The majority of the design codes applied the well known tension bar model theory where both ends are fully restrained. In addition, there were also codes using the continuous base restraining theory in which the tensile member is continuously restrained along one edge. This made a huge difference in the prediction of the crack width.

From the finite element analysis which was performed, it turned out that there is a difference between the steel stress development of imposed loading and imposed deformations. In addition, in case of imposed loading less cracks were developed than under imposed deformations. However, from this specific numerical analysis it turned out that the maximum crack spacing and crack width is smaller in the imposed loading model in comparison to the imposed deformation model. The only explanation for this is that in case of imposed loading the cracks are more evenly distributed.

A case study was used to simulate the hardening process of concrete in combination with autogenous shrinkage as imposed deformation and compared with a finite element analysis. The goal was to determine a set of model properties that are useful for future engineers. The accuracy of the input parameters was verified with the experimental work carried out by M. Sule. Overall, when performing a non-linear finite element analysis a lot of knowledge was required. It turned out that specific choices such as the constitutive model type, the kinematic and equilibrium condition have a major impact on the outcome. Using the modified Bar model of Lokhorst in combination with this numerical approach resulted in good agreement with the experimental findings.

The parameter study showed that regarding the tension bar models, the bar diameter has the largest influence on the crack width prediction. While with respect to the continuous models there was no one-sided answer to the question which parameter had the largest influence on the crack width prediction. In one of the design codes based on the continuous model theory named CIRIA [8] the degree of restraint clearly stands out as the most important parameter. Whereas in the another design code based on this theory, namely the ICE [4], all parameters that were investigated in this thesis have limited effect on the crack width prediction.

The design codes considered in this master thesis do not yet fully represent the crack width due to the hardening of concrete or due to autogenous shrinkage. The design codes are applicable for the crack width prediction of reinforced concrete structures under imposed deformations if conservative assumptions such as a weak bond between concrete and steel reinforcement are taken into account.

It is clear that the problem treated in this report has more complexity than what one initially may think. Opinions on how to determine the crack width of reinforced concrete tensile members under imposed deformations differ. The difference is related to the type of restraint and the cracking theory which are suggested in most used analytical design models. This report contributes to a better understanding of the crack width development under imposed deformations through non-linear finite element analyses and verification with experiments.

The results from this master thesis suggest that an approach to a more consistent crack width prediction under imposed deformations should investigate how bond in the interface between concrete and steel influences cracking. This has lacked attention in the current formulas in the design codes.

Contents

List of Figures

Notations

Latin upper case

A_c	Cross-sectional area of concrete
A_n	Cross-sectional area of new (restrained) concrete
A_o	Cross-sectional area of old (restrained) concrete
A_s	Cross-sectional area of reinforcement
E_c	Modulus of elasticity of concrete
E_n	Modulus of elasticity of new pour concrete
E_o	Modulus of elasticity of the old concrete
E_s	Modulus of elasticity of steel
K_1	Effect of creep on stress and strain relaxation
K_2	Effect of sustained loading on tensile properties
N_{cr}	Cracking force
T_1	Early age temperature change in the concrete
T_2	Long term ambient tenmperature change
R_{ax}	Restraint factor

Latin lower case

c	Concrete cover
d	Effective depth
$f_{cm,cube}$	Mean cube compressive strength
f_{ctm}	Mean concrete tensile strength
$f_{ct,eff}$	Effective mean concrete tensile strength
h_{cr}	Depth of the tensile zone immediately prior to cracking
k	Coefficient which takes into account self-equilibrating effects
k_c	Coefficient which takes into account the stress distribution in the concrete
l_m	Mean crack spacing
l_t	Transfer length

Greek letters

α_c	Thermal expansion coefficient
α_e	Young's modulus ratio
β	Emperical coefficient to asses the mean strain
ϵ_c	Concrete strain
ϵ_{ca}	Autogenous shrinkage
ϵ_{cd}	Drying shrinkage
ϵ_{cm}	Mean strain in concrete
ϵ_{cr}	Cracking strain of concrete
ϵ_{ctu}	Ultimate strain capacity of concrete in tension
ϵ_{free}	Free strain
ϵ_s	Steel strain
ϵ_{sh}	Shrinkage strain
ϵ_{sm}	Mean strain in reinforcement
ρ_s	Reinforcement ratio
$\rho_{s,eff}$	Effective reinforcement ratio
$\emptyset_s$	Reinforcement bar diameter
σ_{cr}	Concrete tensile stress at onset of cracking
σ_s	Steel stress in a crack
$\sigma_{s,cr}$	Steel stress directly after cracking
τ_{bm}	Mean bond stress
γ_s	Factor for scatter
γ_∞	Enhancement factor

Abbreviations

CM	Continuous models
FEM	Finite element modelling
MC 10	Model code 2010
RC	Reinforced concrete
TBM	Tension bar models

1 Introduction

Concrete is the most widely used construction material in the world. The freedom of shape and the high durability of concrete are characteristics that make designers choose for concrete so often. A disadvantage of concrete is its low tensile strength and that is why it is used in combination with steel bars, also known as reinforcement. Reinforced concrete structures are designed in such a way that concrete cracks. However, in order to prevent and reduce durability problems, crack widths should be controlled and limited. Concrete will crack at the moment that the tensile strain capacity is exceeded. Due to the cracking of the concrete, stresses must be taken over by the reinforcement at the location of the crack. Cracks occur throughout the whole life of a structure, and appear differently at an early age and later on at mature age. Cracks are caused by imposed loads or under imposed deformations. Imposed deformations are special forms of loading that get much less attention than mechanical loading due to imposed loads. Imposed deformations are due to shrinkage of concrete and temperature variations. The boundary conditions play an important role when analyzing stresses due to imposed deformation. Generally, the analytical calculation of stresses and deformations caused by imposed loads are straight forward. When cracks occur under imposed deformations, the situation becomes more complex. The complexity is related to the interaction between the structural behaviour and the magnitude of the forces caused by the imposed deformations. Cracking due to imposed deformations at early age may be from autogenous shrinkage and thermal contractions, resulting from the chemical reaction in the hydrating cement paste. At later age, imposed deformations may occur due to thermal effects or from long-term drying shrinkage, which is caused by the external water loss during the drying process. In addition to the analytical crack width prediction using design codes, there is a large variety of finite element modelling (FEM) software to predict the crack width under imposed deformations. In this thesis DIANA is chosen as FEM software because of the variety of cracking models to simulate the complex mechanisms of reinforced concrete structure.

1.1. Problem statement

Design codes can be consulted to predict the crack width under imposed deformations. The information provided in these codes is often very brief and condensed. The reason for this is most likely that imposed deformations were almost never responsible for the collapse of a structure. In addition, although there are many different types of crack width prediction methods, there is no consensus on which one is the best. To solve this problem a CROW-CUR rapport 1:2020 has been set up. CROW is a Dutch non profit institute on the design, construction and management of infrastructure. The aim of the CROW committee [9] was to collect experimental data and to develop a uniform crack width prediction approach in order to prevent errors. The report considered prediction methods which were often used in the Netherlands and other European countries. This report provided the starting point regarding the prediction models that should at least had to be taken into account in this research. The focus of this thesis will be on the background of these models, and on trying to understand if there are fundamental differences between crack width calculations in case of imposed loading or imposed deformations.

1.2. Research questions and sub-questions

In this research, the focus is on reinforced concrete structures that are subjected to imposed loads and to imposed deformations. The main goal of this thesis is summarized in the following research question:

"What is the applicability of the design codes regarding the crack width prediction of reinforced concrete structures under imposed deformations?"

In order to formulate an answer to this research question the following sub-questions have been stated:

- Which design codes are used to predict the maximum crack width under imposed loads and imposed deformations?
- Is there a difference in the steel stress and its growth at the location of cracks when cracking occurs due to imposed loads or under imposed deformations?
- Which parameters are essential to simulate the hardening process of concrete in combination with autogenous shrinkage as imposed deformations using finite element analyses?
- What are the most important parameters that influence crack prediction according to the design codes?
- Is there a difference between the crack width predicted using the design codes and numerically predicted crack width?

1.3. Research strategy

For the structure of the thesis and in order to answer all the research questions a certain strategy is followed. It is important to mention that regarding the numerical models the finite element analyses (FEA) were performed using DIANA version 10.5. The thesis is subdivided in the following activities:

II A literature study is performed to gain more insight in the background of the different analytical crack width prediction models. In addition, general assumptions and fundamental differences are explained.

III Multiple finite element analyses are performed to find out what the differences are in the crack width of a tensile bar loaded under imposed loading or loaded under imposed deformations.

IV To predict the early age cracking due to the hardening of concrete and autogenous shrinkage a finite element analysis is performed. The goal here is to determine a set of model properties that are useful for future engineers. The accuracy of the input parameters is verified with the experimental work carried out by M. Sule [21].

V A parameter study is performed to determine which parameters influence the crack occurrence the most. This study will also contribute to the comparison between the analytical and the numerical models.

VI After the parameter study was performed, a comparison is made between the numerically calculated crack width prediction and the crack width prediction according to various design codes.

VII The results presented throughout this thesis, as well as the way they were obtained, were critically analysed and discussed.

VIII The answers to the sub-questions were described. Thereafter, the main conclusions and the answer on the research question were given. In the end some recommendations on the future research were presented

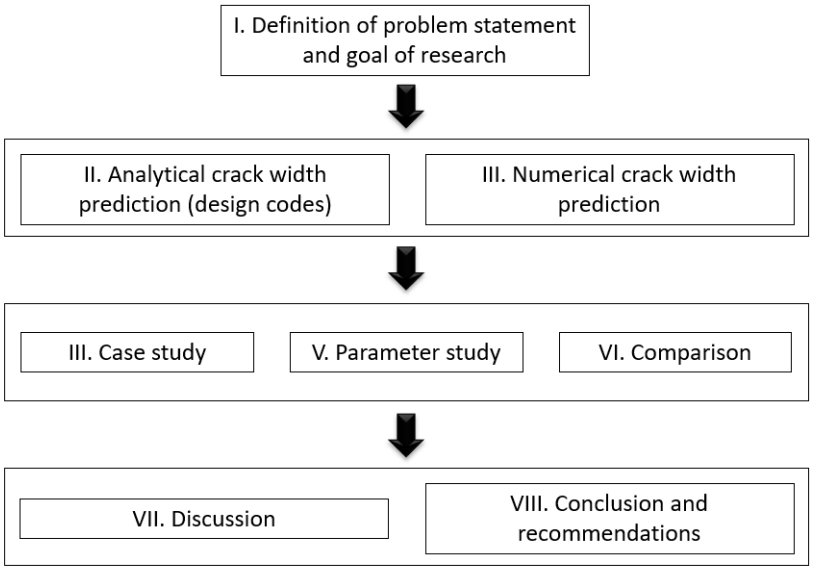

Figure 1.1: Overview research strategy

1.4. Outline

The previously discussed sub activities of the study are elaborated in different chapters in the report. The outline of the total report is prescribed in this section.

Chapter 2 - Analytical crack width prediction models
Chapter 2 explains the concept of a tensile bar under imposed deformations. In addition, the cracking theory and the different prediction models for calculating the crack width are individually discussed. Finally, a comparison is made between the different models and the general assumptions and conclusions are mentioned. The models included in the research are:

- EN 1992-1-1 (Eurocode 2)
- EN 1992-3 (Eurocode 2)
- Model Code 2010
- K. van Breugel (Pink book)
- CIRIA C660
- ICE 0706/012

Chapter 3 - Numerical crack width prediction (imposed loading versus imposed deformation)
The numerical analysis in chapter 3 is performed to find out whether there is a difference in the steel stress, when cracking in a tensile bar model occurs due to imposed loads or under imposed deformations. In addition a validation with DIANA is performed to check what the relation between the crack width and the deformation due to imposed loading or under imposed deformation is. These results will later on also contribute to the comparison between the analytical and the finite element models.

Chapter 4 - Case study: numerical prediction of early age cracking due to hardening of concrete
In this chapter first the methodology and the main findings of the experimental work, carried out during a Ph.D.thesis by M. Sule are highlighted. [16]. Thereafter, a finite element analysis is performed to simulate the hardening process of concrete in combination with autogenous shrinkage as imposed deformation. Finally, the experimental results are used to verify the accuracy of the input parameters.

Chapter 5 - Parameter study
Chapter 5 focuses on a parameter study which was carried out to determine which parameters influence the crack occurrence the most. The maximal crack widths and corresponding stresses and strains are displayed by the use of spreadsheet models in Excel. The spreadsheets models contributed to the comparison between the analytical crack width predictions models and the numerically predicted crack width.

Chapter 6 - Comparison between numerical crack width prediction and crack width prediction using design codes
This chapter compares the crack width prediction due autogenous shrinkage, calculated numerically with the crack width prediction according to various design codes. The design codes included in the comparison have been discussed earlier in chapter 2. In this part the influence of the assumptions made earlier in the parameter study are discussed in more detail.

Chapter 7 - Discussion
In this chapter, the results presented throughout this thesis, as well as the way they were obtained, are critically analysed and discussed.

Chapter 8 - Conclusions and recommendation
Finally, in chapter 8 the answers to the sub-question were given and the main conclusions and the answer on the research question are drawn. In the end of the thesis recommendations are made for further research needed.

2

Analytical crack width prediction models

This literature study is conducted to obtain a better understanding of the background of the different crack width prediction models. First of all, the concept of a tensile bar under imposed deformations is explained. Thereafter, the cracking theory and the different prediction models for calculating the crack width are discussed individually. Finally, a comparison is made between the different models and the general assumptions and conclusions are mentioned.

2.1. Description of imposed deformation

In this paragraph the concept of imposed deformations is described. The term imposed deformation often gives rise to confusion and misunderstanding. Therefore, the term ''restrained deformation'' would better reflect what is meant actually. Figure 2.1 shows what is meant with restrained deformation. In figure 2.1a a prismatic bar with length L is shown. The bar is fixed at one end and it is completely free to deform at the other end. This figure emphasizes that if unrestrained changes in volume or length are possible, no stresses will be generated and no cracks will appear. In figure 2.1b the bar is fixed at both ends. In this case volume or length changes are restrained, which may cause cracks in the concrete if the stress reaches the tensile strength. This case is denoted as ''imposed deformation''. Since there is no observable deformation of the bar, this may be confusing. To make the situation clearer a fictitious cut is made at the end of the bar. In case (a), a shrinkage strain will cause the bar to shorten freely by an increment $\Delta(\epsilon_{shr})$ without any stresses in the bar. In case (b) the boundary conditions do not allow the bar to shorten freely and a tensile force P has to be introduced, in order to restore the original situation. This force generates an elongation of the bar which is equal to:

$$\Delta L(\Delta\epsilon_{shr}) + \Delta L(\Delta P) = 0 \quad or: (\Delta\epsilon_{shr}) \cdot L + P \cdot \frac{L}{EA} = 0 \quad \rightarrow P = -\Delta\epsilon_{shr} \cdot EA \tag{2.1}$$

Due to the restoring force P, there is a deformation of the bar ΔL. This deformation by the force P is actually the imposed deformation. Therefore, the term ''imposed deformation'' refers to the situation of free deformation of the bar [24].

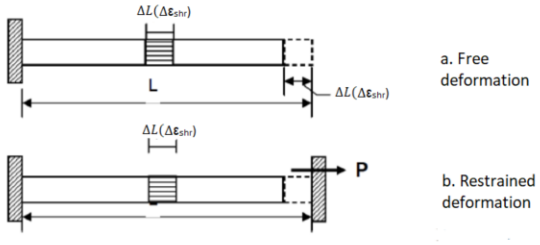

Figure 2.1: Schematic representation of a prismatic bar under imposed deformation (van Breugel et al., 2013)
a. Bar fixed at one end, shortened by imposed strain. No stresses.
b. Bar fixed at both ends, prevented to shorten under shrinkage strain

2.2. Cracking theory (Tensile bar model)

In the previous paragraph the concept of imposed deformation is described using an example. In this example the stiffness of the element was assumed to be constant. While in reality, the axial stiffness EA, decreases if cracking occurs. For this reason, axial forces are reduced due to the formation of cracks, at least in some part of the structures. How to deal with cracks caused by imposed deformations requires a clear understanding of the relationship between stiffness, deformation and cracking. In this section, the cracking behaviour of a *tensile bar* under an imposed load is explained.

In general, most prediction models that are used to calculate the crack width are based on the basic case of a prismatic reinforced concrete bar, subjected to axial tension. In figure 2.2 the basic behaviour of a tensile bar subjected to increasing axial load is shown. At the location of the crack, the stress and the elongation in the concrete is zero and the steel reinforcement has to carry the full tensile load. Due to bond stresses between the steel and the concrete, acting at both sides of the crack, the concrete is reactivated to carry the tensile force. At a transfer length l_t at both sides of the crack, the undisturbed area is reached again.

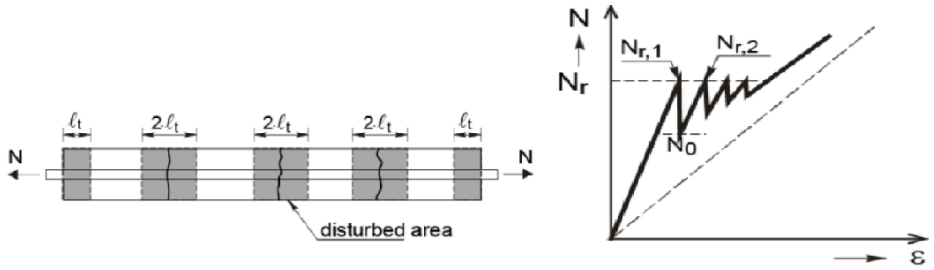

Figure 2.2: Behaviour of reinforced prismatic bar subjected to axial tension (Model Code, 2010)

The response of a reinforced concrete tensile bar to an axial load depends mainly on the cracking behavior of the member. The characteristic response of a tensile bar is shown in figure 2.3 and can be divided in four stages. In the next section the different stages and corresponding equations will be explained.

I - Uncracked stage

The first stage is the uncracked stage. In this stage the tensile force is smaller than the cracking force $N < N_{cr}$ of the cross-section and no cracks will occur. In addition, there will be no strain difference between the reinforcement steel and the concrete ($\epsilon_c = \epsilon_s$). The tensile force carried by the concrete and reinforcement can be calculated with the following equation:

$$N = N_c + N_s = \quad E_c \cdot A_c \cdot \epsilon_c + E_s \cdot A_s \cdot \epsilon_s = \quad \epsilon_c \cdot E_c \cdot A_c \cdot (1 + \rho\alpha_e), \tag{2.2}$$

where:

- E_c Young's modulus of concrete
- A_c Area of concrete
- ϵ_c Concrete strain
- E_s Young's modulus of steel
- A_s Area of reinforcement
- ϵ_s Steel strain
- ρ Reinforcement ratio $\frac{A_s}{A_c}$
- α_e Young's modulus ratio $\frac{E_s}{E_c}$

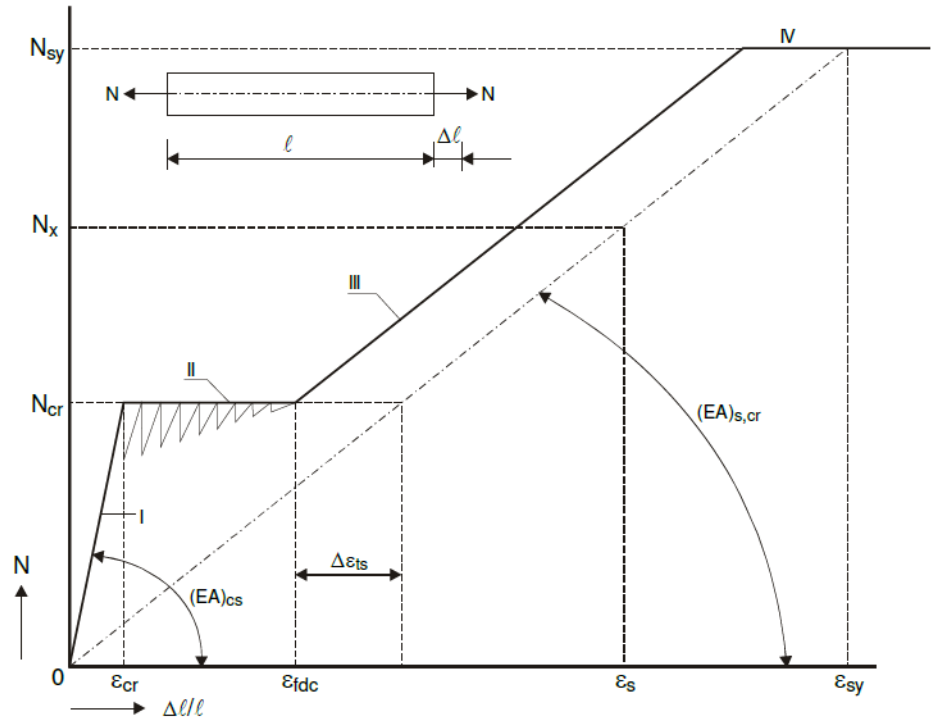

Figure 2.3: Load-deformation diagram of a reinforced concrete tensile bar (van Breugel et al., 2013)

II - Crack formation stage

Stage II is denoted as the crack formation stage. In this stage cracks will occur if the tensile force reaches the cracking force $N = N_{cr}$. The tensile force does not increase, because after the occurrence of a new crack, it falls back. If so many cracks have been formed that no intermediate areas (white areas in figure 2.2) are left, the concrete cannot reach the tensile strength anymore, so no new cracks will appear. The crack pattern is then fully developed. An important assumption is that the tensile force is constant until the stabilized cracking stage is reached. In reality, the dashed line which corresponds to the tensile force will not be horizontal but inclined ranging from a first crack for 5 percent fractile tensile strength $f_{ct,0.05}$ to an upper value of 95 percent fractile tensile strength $f_{ct,0.95}$ [CEB-FIB]. This assumption makes the calculation less complex because all cracks that occur at $N = N_{cr}$ have the same theoretical crack width.

In figure 2.4 the force transmission in a distributed area next to a crack is shown. It is important to note that the relationships are simplified by linearization. As can be seen, at the place of the crack the stress in the concrete is zero. As a result of this all the forces in the crack must be transmitted by the reinforcement. The stress in the reinforcement in the disturbed area can be calculated by dividing the cracking force with the area of reinforcement. If, for simplicity, the calculations are based on the mean concrete tensile strength f_{ctm}, the stress in the steel at the start of a new crack is:

$$\sigma_s = \sigma_{sr} = \frac{N_{cr}}{A_s} \quad = \frac{\epsilon_{cr} \cdot E_c \cdot A_c}{A_s}(1 + \rho \cdot \alpha_e) \quad = \frac{f_{ctm}}{\rho} \cdot (1 + \rho \cdot \alpha_e), \tag{2.3}$$

where f_{ctm} is the mean axial tensile strength.

The steel stress in the concrete outside the disturbed area σ_{se} is directly proportional to the concrete stress:

$$\epsilon_c = \epsilon_s \rightarrow \quad \frac{\sigma_{se}}{E_s} = \frac{f_{ctm}}{E_c} \rightarrow \quad \sigma_{se} = f_{ctm} \cdot \alpha_e, \tag{2.4}$$

where α_e is the young's modulus ratio $\frac{E_s}{E_c}$.

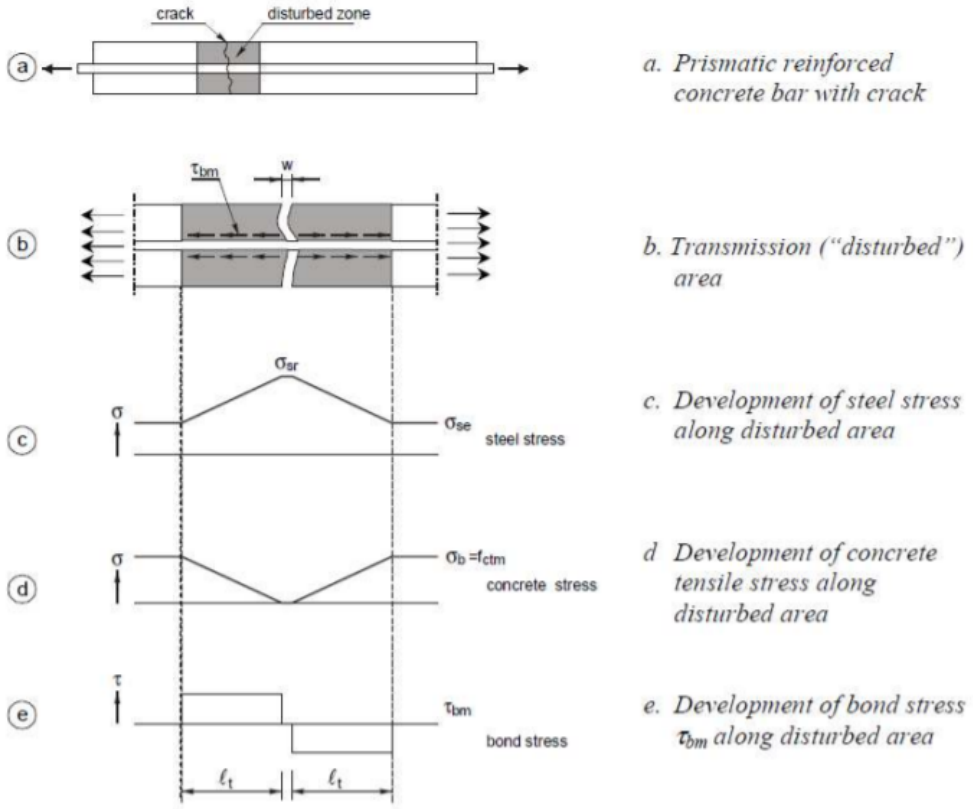

Figure 2.4: Cracking behaviour of concrete (Walraven et al., 2019)

Since the concrete tensile stress σ_{ct} in a crack is zero and at the end of the transfer length the concrete stress is f_{ctm} (figure 2.4d), the force transmitted by bond over that length can be expressed as:

$$N = A_c \cdot f_{ctm} \tag{2.5}$$

Now the force is transmitted by bond over the transfer length l_t:

$$N = \tau_{bm} \cdot l_t \cdot m \cdot \pi \cdot \emptyset, \tag{2.6}$$

where

A_c	Concrete area
m	Number of reinforcing bars
$\emptyset$	Diameter
τ_{bm}	Mean bond stress

By combining equation 2.5 and 2.6 the transfer length l_t can be determined:

$$\tau_{bm} \cdot l_t \cdot \pi \cdot \emptyset = A_c \cdot f_{ctm} \tag{2.7}$$

$$\frac{\tau_{bm} \cdot l_t \cdot \pi \cdot \emptyset}{A_s} = \frac{A_c \cdot f_{ctm}}{A_s} = \frac{f_{ctm}}{\rho}, \tag{2.8}$$

where $A_s = \frac{1}{4} \cdot m \cdot \pi \cdot \emptyset^2$

This results in the following expression for the transfer length:

$$l_t = \frac{1}{4} \frac{f_{ctm}}{\tau_{bm}} \frac{\emptyset}{\rho} \tag{2.9}$$

The crack width is defined as the difference of elongation between the steel and the concrete over a disturbed area. The maximum length of the disturbed area is two times the transfer length.

$$w = 2 \cdot l_t \cdot (\epsilon_{sm} - \epsilon_{cm}) \tag{2.10}$$

where ϵ_{sm} is the mean steel strain and ϵ_{cm} the mean concrete strain along the transfer length l_t. The development of the stresses at both sides of the crack is shown in figure 2.4. The strains can now be calculated from these stresses. The mean steel strain is:

$$\epsilon_{sm} = \frac{1}{2 \cdot E_s} \cdot (\sigma_{sr} + \sigma_{se}) \tag{2.11}$$

Substituting equation 2.4 into this will give the following equation:

$$\epsilon_{sm} = \frac{1}{2 \cdot E_s} \cdot (\sigma_{sr} + \alpha_e \cdot f_{ctm}) \tag{2.12}$$

The mean concrete strain over the transfer length is:

$$\epsilon_{cm} = \frac{f_{ctm}/2}{E_c} = \frac{1}{2 \cdot E_s} \cdot \alpha_e \cdot f_{ctm} \tag{2.13}$$

Substituting the mean steel strain and mean concrete strain from equation 2.12 and 2.13 in equation 2.10 will result in:

$$w_{max} = \frac{1}{4} \cdot \frac{f_{ctm}}{\tau_{bm}} \cdot \frac{\emptyset}{\rho} \cdot \frac{1}{E_s} \cdot \sigma_{sr} \tag{2.14}$$

III - Stabilized cracking stage
Stage III is the stabilized cracking stage. This stage is reached when the tensile force is larger than the cracking force $N > N_{cr}$ of the cross-section. An increase in tensile forces will not result in new cracks but will widen the existing cracks. This means that the number of cracks remains the same. The increase in the steel stress is then:

$$\Delta\sigma_s = \sigma_s - \sigma_{sr} \tag{2.15}$$

The increase of the steel stress can be converted to an increase of the crack width by the following equation:

$$\Delta w = \frac{\sigma_s - \sigma_{sr} \cdot 2l_t}{E_s} \tag{2.16}$$

Now the total crack width in the stabilized cracking stage can be obtained by adding equation 2.16 to equation 2.14:

$$w_{max} = \frac{1}{2} \cdot \frac{f_{ctm}}{\tau_{bm}} \cdot \frac{\emptyset}{\rho} \cdot \frac{1}{E_s} \cdot (\sigma_s - 0,5 \cdot \sigma_{sr}) \tag{2.17}$$

Since it is assumed that in the crack formation stage the steel stress σ_s is equal to the steel stress directly after cracking σ_{sr}, equation 2.17 can be denoted as the general expression for the calculation of the maximum crack width for both the stabilized cracking stage and the crack formation stage.

IV - Yielding stage
Stage IV starts when the yield strength of the steel is reached. Once the yield strength of the steel in one of the cracks is reached, the deformation increases significantly, even if the load is kept constant. This behaviour is shown by stage IV in figure 2.3.

2.3. Crack width prediction models (Design Codes)

The following part of the literature explains how to determine the crack width for each prediction method. In section 2.4 the fundamental differences are discussed. At the end of the literature study the general conclusions are listed (2.5).

2.3.1. EN 1992-1-1

The first prediction model that will be explained is the EN1992-1-1 [1]. This code is part of Eurocode 2 and relates to the design of concrete buildings. In chapter 7 of the code, the checks for the serviceability limit state (SLS) are given. This chapter covers the following three limit states: stress limitation, crack control and deflection control. In this research, only the checks relating to the crack control are discussed.

In the Eurocode some general considerations are made:

- Cracks must be limited in such a way that they do not affect the function and durability of the structure.
- Cracks are normal in reinforced concrete structures that are subject to bending, shear, torsion or stress as a result of direct loading.
- Cracks caused by other causes, such as plastic shrinkage or expansive chemical reactions are beyond the scope of this section.
- If the cracks do not compromise the function of the structure, they may arise without control.
- For the calculated crack width w_k, a limit value, w_{max}, must be taken into account. The maximum crack width is shown in figure 2.5 and depends on the exposure class and the reinforcement conditions.

Exposure class	Reinforced members and prestressed members without bonded tendons	Prestressed members with bonded tendons
	Quasi-permanent load combination	Frequent load combination
X0, XC1	0,4[1]	0,2
XC2, XC3, XC4	0,3	0,2[2]
XD1, XD2, XD3, XS1, XS2, XS3		Decompression

Note 1: For XO, XC1 exposure classes, crack width has no influence on durability and his limit is set to give generally acceptable appearance. In the absence of appearance conditions this limit may be relaxed.
Note 2: For these exposure classes, in addition, decompression should be checked under the quasi-permanent combination of loads.

Figure 2.5: Recommended values of w_{max} [mm] (Table 7.1N - Eurocode 2, 2004)

The code provides two methods to validate the crack width w_k.The first method determines the crack width without direct calculation also known as the **indirect** method (EC2 art. 7.3.3). This method provides the maximum bar diameter (figure 2.6) or the maximum bar spacing (figure 2.7). These stated limit values depend only on the steel stress in the serviceability limit state. Assumptions have been made to calculate the values in the table. If practical values deviate from these assumed values, the bar diameter read from figure 2.6 must be corrected on the base of equation 2.4 and 2.19.

Steel stress [MPa]²	Maximum bar size [mm]		
	w_k = 0,4 mm	w_k = 0,3 mm	w_k = 0,2 mm
160	40	32	25
200	32	25	16
240	20	16	12
280	16	12	10
320	12	10	8
360	10	8	6
400	8	6	4
450	6	5	-
Note: 1. The values in the table are based on the following assumptions: c = 25mm; $f_{ct,eff}$ = 2,9 MPa; h_{cr} = 0,5h; (h-d) = 0,1h; k_1 = 0,8; k_2 = 0,5; k_c 0,4; k = 1,0; k_t = 0,4 and k_4= 1,0 2. Under the relevant combinations of actions			

Figure 2.6: Maximum bar diameter for crack control (Table 7.2N - Eurocode 2, 2004)

Steel stress [MPa]²	Maximum bar spacing [mm]		
	w_k = 0,4 mm	w_k = 0,3 mm	w_k = 0,2 mm
160	300	300	200
200	300	250	150
240	250	200	100
280	200	150	50
320	150	100	-
360	100	50	-
Note: 1. The values in the table are based on the following assumptions: c = 25mm; $f_{ct,eff}$ = 2,9 MPa; h_{cr} = 0,5h; (h-d) = 0,1h; k_1 = 0,8; k_2 = 0,5; k_c 0,4; k = 1,0; k_t = 0,4 and k_4= 1,0 2. Under the relevant combinations of actions			

Figure 2.7: Maximum bar spacing for crack control (Table 7.3N - Eurocode 2, 2004)

In case of member loaded in bending the following equation should be used to determine the bar diameter:

$$\emptyset_s = \emptyset_s^* \frac{f_{ct,eff}}{2.9} \frac{k_c h_{cr}}{(2(h-d)}, \tag{2.18}$$

In case of member loaded in tension the following equation should be used to determine the maximum bar diameter:

$$\emptyset_s = \emptyset_s^* \frac{f_{ct,eff}}{2.9} \frac{h_{cr}}{(8(h-d)}, \tag{2.19}$$

where

$\emptyset_s$ Adjusted maximum bar diameter

$\emptyset_s^*$ Maximum bar size given in figure 2.6

$f_{ct,eff}$ Effective mean concrete tensile strength

k_c Coefficient which takes into account of the stress distribution

h Overall depth of the section

h_{cr} Depth of the tensile zone immediately prior to cracking

d Effective depth to the centroid of the outer layer of reinforcement

The second method determines the crack width w_k by calculating it **directly**. This approach is based on the before mentioned hidden tensile member. The characteristic crack width w_k, can be determined by integrating the strain difference between the reinforcement and concrete over the maximum crack spacing.

$$w_k = \int_0^{s_{r,max}} (\epsilon_s(x) - \epsilon_c(x))dx = s_{r,max}(\epsilon_{sm} - \epsilon_{cm}), \tag{2.20}$$

$$s_{r,max} = k_3 \cdot c + k_1 \cdot k_2 \cdot k_4 \cdot \frac{\emptyset}{\rho_{p,eff}}. \tag{2.21}$$

$$\epsilon_{sm} - \epsilon_{cm} = \frac{\sigma_s - k_t \frac{f_{ct,eff}}{\rho_{p,eff}}(1 + \alpha_e \rho_{p,eff})}{E_s} \geq 0,6\frac{\sigma_s}{E_s}. \tag{2.22}$$

where

w_k Characteristic crack width.

$s_{r,max}$ Maximum crack spacing.

ϵ_{sm} Mean strain in the reinforcement under the relevant combination of loads.

ϵ_{cm} Mean strain in the concrete between cracks.

σ_s stress in the tension reinforcement assuming a cracked section.

$f_{ct,eff}$ Effective concrete tensile strength.

$\rho_{p,eff}$ Effective reinforcement percentage. $\frac{A_s}{A_{c,eff}}$.

$A_{c,eff}$ Effective area of concrete in tension surrounding the reinforcement.

α_e Young's modulus ratio $\frac{E_s}{E_{cm}}$.

k_t Coefficient which takes into account the duration of the load.

k_1 Coefficient which takes into account the bond properties.

k_2 Coefficient which takes into account the distribution of strain.

k_3 Constant parameter which is defined for each country; 3,4 for the Netherlands.

k_4 Constant parameter which is defined for each country; 0,425 for the Netherlands.

c concrete cover

$\emptyset$ Adjusted maximum bar diameter

2.3.2. EN 1992-3

The next prediction model is the EN-1992-3 [2]. This method is another part of the Eurocode 2 but this code relates to the design of concrete liquid retaining and containment structures. In chapter 7 of the code the checks for the serviceability limit state (SLS) are given. The code provides two methods to determine the crack width. It makes a distinction between an indirect method and a method to calculate the crack width due to restraint of imposed deformations. With regard to the indirect method the code provides two figures where the maximum bar diameters (figure 2.8) and maximum spacing bar (figure 2.9) according to the service stress in the reinforcement are given. This approach is very similar to the EN1992-1-1 [1]. The service stress in the reinforcement can be calculated from the following formula:

$$\sigma_s = \frac{k_c \cdot k \cdot f_{ct,eff}}{\rho_{eff}}, \tag{2.23}$$

where:

k_c Coefficient which takes into account the stress distribution in the concrete

k Coefficient which takes into account self-equilibrating effects

$f_{ct,eff}$ Effective mean concrete tensile strength

ρ_{eff} Effective reinforcement ratio

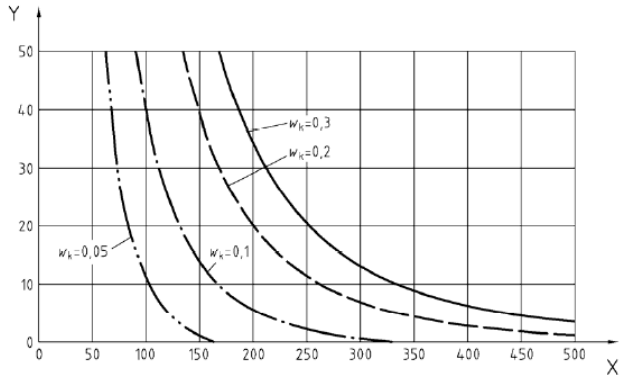

Figure 2.8: Maximum bar diameters in mm (Y-axis) for crack control in members subject to axial tension. Reinforcement stress σ_s in MPa (X-axis) (Figure 7.103N - EC2)

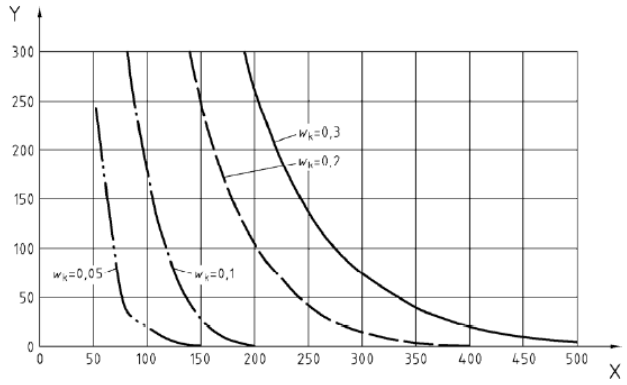

Figure 2.9: Maximum bar spacings in mm (Y-axis) for crack control in members subject to axial tension. Reinforcement stress σ_s in MPa (X-axis)(Figure 7.104N - EC2)

The maximum bar diameter given by figure 2.8 may be determined using the formula below:

$$\emptyset_s = \emptyset_s^* \cdot \frac{f_{ct,eff}}{2.9} \cdot \frac{h}{(10(h-d)}, \tag{2.24}$$

where

$\emptyset_s$ Adjusted maximum bar diameter

$\emptyset_s^*$ Maximum bar size given in figure 2.8

$f_{ct,eff}$ Effective mean concrete tensile strength

h Overall depth of the section

d Effective depth to the centroid of the outer layer of reinforcement

In Annex M of the EN1992-3 the direct calculation of crack width due to restraint of imposed deformations is given. The code deals with two specific conditions of restraint as shown in Figure 2.10. The forms of imposed deformation covered in this code are shrinkage and early thermal movements due to cooling of members during the days immediately after casting.

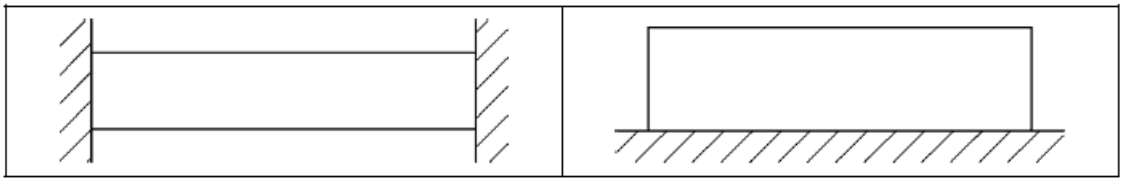

(a) restraint of a member at its ends (b) restraint along one edge

Figure M.1 — Types of restraint to walls

Figure 2.10: Types of restraint to walls (Figure M1 - Eurocode 2, 2006)

EN1992-3 refers to EN1992-1-1 for the calculation of characteristic crack width. The general formula is given in equation 2.20. This equation holds for both restraint conditions, the only difference is the way the crack strain is estimated.

(a) The crack strain in case a member is restrained at both ends:

$$(\epsilon_{sm} - \epsilon_{cm}) = \frac{0.5k \cdot k_c \cdot f_{ct,eff} \cdot \alpha_e}{E_s}((\frac{1}{\alpha_e \rho} + 1). \tag{2.25}$$

(b) The crack strain in case a member is restrained along one edge:

$$(\epsilon_{sm} - \epsilon_{cm}) = R_{ax} \cdot \epsilon_{free}, \tag{2.26}$$

where

R_{ax} Restraint factor

ϵ_{free} Strain which would occur if the member was completely unrestrained

In Annex L of the EN 1992-3 different situations are given with a corresponding factor of restraint. It states that the degree of restraint varies over the height of the structure. The variation depends on the ratio between the length and the height $\frac{L}{H}$. The code states that if $\frac{L}{H} = 2$ the restraint at the top equals zero. While if $\frac{L}{H} > 8$ the restraint at the top equals the restraint at the joint.

2.3.3. *fib* Model Code 2010

The *fib* Model Code for Concrete Structures 2010 [10] is a recommendation for the design of reinforced concrete which is intended to be a guidance document for future codes. It states that before the crack width can be calculated, it must be determined which crack stage applies. According to the simplified representation shown in figure 2.3 the stabilized cracking stage applies when the load is larger than the cracking load ($N > N_{cr}$). The crack formation stage applies when, for imposed deformation, the strain ϵ satisfies the following condition:

$$\epsilon_{cr} \leq \epsilon \leq \epsilon_{fdcp}, \tag{2.27}$$

where the concrete strain at onset of cracking ϵ_{cr} and the concrete strain at which the crack pattern is fully developed ϵ_{fdcp} can be calculated by the following equations:

$$\epsilon_{cr} = \frac{f_{ctm}}{E_c} \tag{2.28}$$

$$\epsilon_{fdcp} = \frac{f_{ctm} \cdot (0.6 + \alpha_e \cdot \rho)}{E_s \cdot \rho} \tag{2.29}$$

The code assumes that in general, if only imposed deformation occurs, the crack formation stage applies. The crack width w_k for all stages of cracking may be calculated by using the following equations:

$$w_k = 2 \cdot l_{st} \cdot (\epsilon_{sm} - \epsilon_{cm} - \epsilon_{cs}), \tag{2.30}$$

$$l_{st} = \frac{1}{4} \cdot \frac{f_{ctm}}{\tau_{bm}} \cdot \frac{\phi_s}{\rho_s}, \tag{2.31}$$

$$\epsilon_{sm} - \epsilon_{cm} - \epsilon_{cs} = \frac{\sigma_s - \beta \cdot \sigma_{sr}}{E_s} - \eta_r \cdot \epsilon_{sh} \tag{2.32}$$

where

l_{st}	Length over which slip between concrete and steel occurs
k	Empirical parameter to take the influence of the concrete cover into consideration (k = 1)
c	Concrete cover
ϵ_{sm}	Mean strain in the reinforcement
ϵ_{cm}	Mean strain in the concrete
ϵ_{cs}	Strain of the concrete due to shrinkage
τ_{bm}	Mean bond stress
ϕ_s	Reinforcement bar diameter
ρ_s	Reinforcement percentage
β	Empirical coefficient to asses the mean strain
η_r	Coefficient taking account of shrinkage condition
ϵ_{sh}	Shrinkage strain
σ_s	Steel stress in a crack
σ_{sr}	Maximum steel stress in a crack in the crack formation stage

The maximum steel stress σ_{sr} in a crack in the crack formation stage is:

$$\sigma_{sr} = \frac{f_{ctm}}{\rho_{s,eff}}(1 + \alpha_e \cdot \rho_{s,eff}) \tag{2.33}$$

The maximum steel stress $\sigma_{s,cr}$ in a stabilized cracking stage is:

$$\sigma_{s,cr} = \frac{f_{ctm}}{\rho_{s,eff}}(1 + \alpha_e \cdot \rho_{s,eff}) + E_s(\epsilon - \epsilon_{fdc}) \tag{2.34}$$

The values for mean bond strength τ_{bm} and the coefficients β and η_r are given in figure 2.11.

	Crack formation stage	Stabilized cracking stage
Short term, instantaneous loading	$\tau_{bn} = 1.8\ f_{ctm}(t)$ $\beta = 0.6$ $\alpha = 0$	$\tau_{bn} = 1.8\ f_{ctm}(t)$ $\beta = 0.6$ $\alpha = 0$
Long term, repeated loading	$\tau_{bn} = 1.35\ f_{ctm}(t)$ $\beta = 0.6$ $\eta_r = 0$	$\tau_{bn} = 1.8\ f_{ctm}(t)$ $\beta = 0.4$ $\eta_r = 1$

Figure 2.11: Values for β and η_r for deformed reinforcing bars (Model Code, 2010)

The Model Code 2010 also provides a method to determine the crack width without calculation. This method will not be discussed because it largely corresponds to the indirect method of EN 1992-1-1 (see paragraph 2.3.1)

2.3.4. Van Breugel

One of the more comprehensive crack prediction models is that of Professor K. van Breugel [24]. According to Van Breugel, it is essential to check whether a member subjected to an imposed deformation is indeed in the crack formation stage. In other words, it should be checked if the imposed strain is larger than the cracking strain and smaller than the strain at which the fully developed crack pattern is reached ($\epsilon_{cr} < \epsilon < \epsilon_{fdcp}$). The strain at which the fully developed crack pattern is reached is approximated with the following equation:

$$\epsilon_{fdcp} \approx (60 + 2,4 \cdot \sigma_{sr}) \cdot 10^{-6} \tag{2.35}$$

In case that the member is in the **crack formation stage**, the mean crack width w_{mo} can be determined by equation 2.36.

$$w_{mo} = 2 \cdot [\frac{0,4 \cdot \emptyset}{f_{cm,cube} \cdot E_s} \cdot (\frac{\sigma_{cr}}{\rho})^2 \cdot (1 + \alpha_e \cdot \rho)]^{0,85} \tag{2.36}$$

In equation 2.37 the mean crack width is given as function of the steel stress σ_{sr} directly after cracking.

$$w_{mo} = 2 \cdot [\frac{0,4 \cdot \emptyset}{f_{cm,cube} \cdot E_s} \cdot \sigma_{sr} \cdot (\sigma_{sr} - \alpha_e \cdot \sigma_{sr})]^{0,85} \tag{2.37}$$

where

$\emptyset$ Bar diameter

$f_{cm,cub}$ Mean cube compressive strength

E_s Modulus of elasticity of steel

α_e Ratio of young moduli

ρ Reinforcement ratio

σ_{cr} Concrete tensile stress at onset of cracking

From the force equilibrium in the cracked cross section it is possible to calculate the steel stress directly after cracking. This equilibrium can be expressed as follows:

$$A_c \cdot \sigma_{cr} \cdot (1 + \alpha_e \cdot \rho) = A_s \cdot \sigma_{s,cr} \tag{2.38}$$

The steel stress after cracking can now be determined:

$$\sigma_{s,cr} = \frac{\sigma_{cr}}{\rho} \cdot (1 + \alpha_e \cdot \rho) \tag{2.39}$$

Van Breugel states that the transfer length l_{st} now can be calculated using the following formula:

$$l_{st} = 1,2 \cdot w_{mo} \cdot \frac{E_s}{\sigma_{s,cr}} \tag{2.40}$$

When the member is in the stabilized cracking stage which means that the crack pattern is fully developed, the crack spacing varies between l_{st} and $2l_{st}$. It is assumed that the mean crack spacing remains constant at about $1.5 \cdot l_{st}$ when the load further increases. The mean crack spacing is now:

$$l_m = 1,8 \cdot w_{mo} \cdot \frac{E_s}{\sigma_{s,cr}} \tag{2.41}$$

The mean crack width w_{mv} in case the member is in the **stabilized cracking stage** can be determined with the following equation:

$$w_{mv} = \frac{l_m}{E_s} \cdot (\sigma_s - 0,5 \cdot \sigma_{s,cr}) \tag{2.42}$$

where

l_m mean crack spacing

σ_s Steel stress in the crack (in SLS if $N > N_{cr}$)

$\sigma_{s,cr}$ Steel stress directly after cracking (for $N = N_{cr}$)

In case of a non fully developed crack pattern caused by an imposed deformation and a steel stress $\sigma_s \leq 295N/mm^2$ the characteristic crack width is:

$$w_k = w_{m0} \cdot \gamma_s \cdot \gamma_\infty \tag{2.43}$$

In case of a fully developed crack pattern and $\sigma_s \leq 295N/mm^2$ the characteristic crack width is:

$$w_k = w_{mv} \cdot \gamma_s \cdot \gamma_\infty, \tag{2.44}$$

where

γ_s factor for scatter (crack formation stage 1.3; stab. cracking stage tension 1.5 and flexure 1.7)

γ_∞ enhancement factor ($\sigma_s <$ 295 MPa = 1.3 and $\sigma_s >$ 295 MPa = formula 2.45

Formula enhancement factor

$$\gamma_\infty = \frac{1}{1 - 9 \cdot \sigma_s^3 \cdot 10^{-9}} \tag{2.45}$$

2.3.5. CIRIA C660

The CIRIA C660 [3] is an English guideline that has been developed complimentary to the Eurocode 2. The main objective of the CIRIA C660 is to provide a method for the control of early-age cracking, while also being adequate for controlling cracks that may develop due to long-term deformations caused by temperature change and shrinkage.The CIRIA C660 makes a distinction between the following situations: (I) a member restrained along one edge; (II) a member restrained at ends only. For both situations the maximum crack spacing $s_{r,max}$ can be calculated using equation 2.46. This equation corresponds with the Eurocode 2.

$$s_{r,max} = k_3 \cdot c + k_1 \cdot k_2 \cdot k_4 \cdot \emptyset / \rho_{p,eff} \tag{2.46}$$

I - For a member restrained along one edge, the crack width w_k can be calculated using the following equations:

$$w_k = s_{r,max} \cdot \epsilon_{cr} \tag{2.47}$$

$$\epsilon_{cr} = K_1(\alpha_c T_1 + \epsilon_{ca})R_1 + \alpha_c T_2 R_2 + \epsilon_{cd} R_3 \tag{2.48}$$

where

- T_1 Early age temperature change in the concrete
- T_2 Long term ambient temperature change
- α_c Thermal expansion coefficient
- ϵ_{ca} Autogenous shrinkage
- ϵ_{cd} Drying shrinkage
- K_1 Effect of creep on stress and strain relaxation
- R_i Degree of restraint

II - For a member restrained at ends only the crack width w_k is:

$$w_k = s_{r,max} \cdot \epsilon_{sm} - \epsilon_{cm} \tag{2.49}$$

$$(\epsilon_{sm} - \epsilon_{cm}) = \frac{0.5k \cdot k_c \cdot f_{ct,eff} \cdot \alpha_e}{E_s}((\frac{1}{\alpha_e \rho} + 1) \tag{2.50}$$

This approach corresponds with the EN 1992-3 described in section 2.3.2

In CIRIA C660 the following formula is given to determine the degree of restraint R when a member is restrained along one edge:

$$R_j = \frac{1}{1 + (\frac{A_n}{A_o}\frac{E_n}{E_o})} \tag{2.51}$$

where

- A_n Cross sectional area of the new (restrained) concrete
- A_o Cross sectional area of the old (restrained) concrete
- E_n Modulus of elasticity of the new concrete
- E_o Modulus of elasticity of the old concrete

2.3.6. ICE 0706/012

The ICE 0706/012 [4] is a further development of the calculation method described in the EN 1992-3 and CIRIA C660. The ICE provides a unified approach that assumes that the maximum potential crack width w_p may only occur on conditions of end restraint, and in case a member is restrained along the edge, a reduction in maximum potential crack width is assumed because of the following:

1. A part of the load is transferred from the concrete into the restraining member, so this reduces the stress which should be transferred to the reinforcement.
2. The edge restraint inhibits the extent to which a crack can open. The higher the edge restraint, the less strain relief can occur and therefore the smaller the crack width that may develop.
3. A new crack may be affected by the presence or lack of existing cracks which may determine the degree of stress relaxation between the cracks.

The ICE method makes a distinction between two cracking stages. The first cracking stage starts when the tensile strain capacity of the concrete ϵ_{ctu} is exceeded. In the first stage is assumed that the crack opens instantaneously to a value w_{k1}. In this stage a part of the load is transferred from the concrete to the steel. At the second stage, the crack gets wider by a value of w_{k2}, as the concrete is assumed to continue to shrink relatively to the reinforcement. The full crack width can now be determined with the following equation:

$$w_k = w_{k1} + w_{k2} \tag{2.52}$$

For the calculation of the crack width in stage 1, equations 2.53 and 2.54 are based on the current methods for the members subject to end restraint with a modification factor $(1 - R_{edge})$ to take into account the effect of edge restraint in both attracting load and preventing crack opening (figure 2.13). The code takes also the relative lengths of the cracked zone S into account and the uncracked zone.

I - For a member restrained at ends only the crack width w_{k1} in stage 1 is:

$$w_{k1} = s_{r,max} \cdot \frac{0.5k \cdot k_c \cdot f_{ct,eff} \cdot \alpha_e}{E_s}\left(\left(\frac{1}{\alpha_e \rho} + 1\right)\right) \tag{2.53}$$

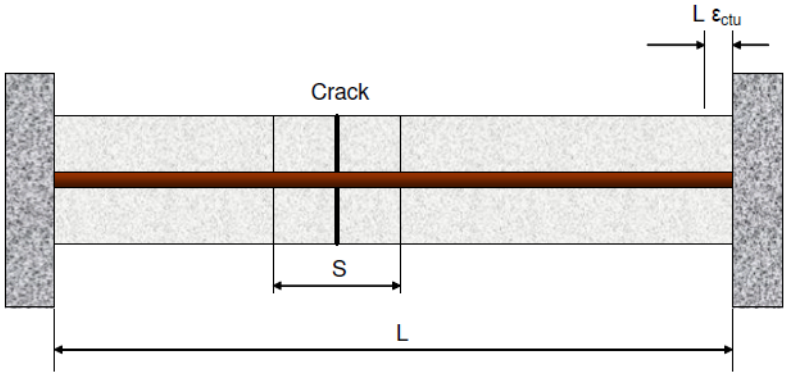

Figure 2.12: End restraint (Figure A2.1 - ICE 0706, 2010)

II - For a member restrained along one edge, the crack width w_{k1} in stage 1 can be calculated using the following equation:

$$w_{k1} = s_{r,max} \cdot \frac{0,5L \cdot \epsilon_{ctu} \cdot (1 - R_{edge})B}{1 - \frac{S \cdot R_{edge}}{k_L \cdot H}[1 - 0,5(B + \frac{1}{1 - R_{edge}})]}, \tag{2.54}$$

where,

ϵ_{ctu} Ultimate strain capacity of concrete in tension $\epsilon_{ctu} = \alpha_e \cdot \frac{f_{ct,eff}}{E_s}$

B Strain relief $B = (\frac{k \cdot k_c}{\alpha_e \cdot \rho} + 1)$

S Length of the cracked zone

$(1 - R_{edge})$ Modification factor

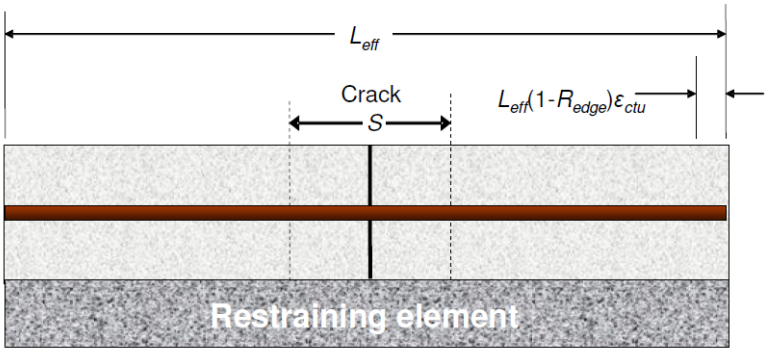

Figure 2.13: Edge restraint (Figure A3.1 - ICE 0706, 2010)

The second cracking stage occurs as the concrete continues to contract after the development of the crack. The steel in the cracked zone is maintained under stress by contraction of the concrete outside the cracked zone. It is assumed that the concrete in the cracked zone contracts relatively to the steel, causing the crack to grow (figure 2.14).

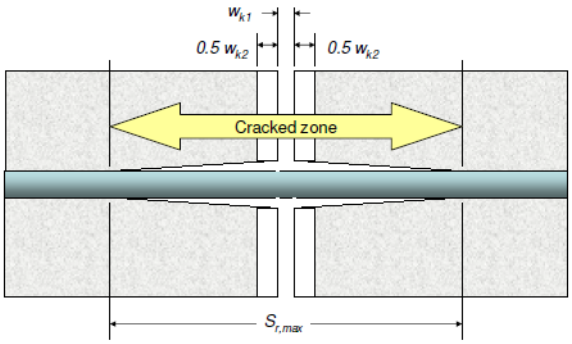

Figure 2.14: Development of second cracking stage (ICE 0706, 2010)

The restraint local to the crack, prevents contraction of the concrete in the cracked zone. The restraint to contraction of the concrete is zero at the crack (the concrete is locally debonded) and it builds up linearly to its pre-cracked value outside the cracking zone. The code states that the average restraint within the cracking zone is therefore $0.5R_{edge}$. The extra crack w_{k2} will therefore be proportional to $(1 - 0.5R_{edge})$. This results in the following equation:

$$w_{k2} = s_{r,max} \cdot (1 - 0,5R_{edge})K_1(\epsilon_{free} - \frac{\epsilon_{ctu}}{R_{edge} \cdot K_1}) \tag{2.55}$$

2.4. Fundamental differences

In this section, the fundamental differences between the crack width prediction models will be contemplated. In this comparison, the focus is on the approach and the theoretical background on which the models are based. In the parametric analysis (chapter 3) the influence of individual parameters are discussed in more detail.

2.4.1. Direct versus indirect crack width prediction

From the literature study it turned out that the Eurocode 2 and Model Code 2010, make a distinction between two different approaches to calculate the crack width. In the first approach the crack width is calculated indirectly without direct calculations. The models provide tables or figures in which the crack width criteria can be satisfied on the base of the maximum bar diameter or bar spacing according to the service stress in the reinforcement. In these tables and figures assumptions have been made to determine the maximum crack width. If practical values deviate, equations are given to determine the maximum bar diameter and associated crack width. It must be taken into account that if cracks occur due to *imposed deformations* the bar size criteria should be satisfied and the steel stress is the value obtained immediately after cracking. While, in case cracks occur due to *imposed loads* either the maximum bar size or the maximum bar spacing criteria must be complied with. In this case the steel stress should be calculated assuming a cracked section.

The second approach implies that the crack width is calculated directly. The majority of the models state that the characteristic crack width can be determined by multiplying the maximum crack spacing with the difference between the reinforcement and concrete elongation (crack strain). This characteristic crack width is limited by a maximum crack width. The maximum allowed crack width varies between 0,2 and 0,4 mm and depends on the exposure class and the reinforcement conditions.

The indirect approach is initially more convenient for engineers because it saves time. However, previous studies [17] have shown that the indirect methods turned out to be quite conservative. In addition, none of the indirect approaches explains clearly the difference between cracks which occur due to imposed loads or imposed deformations. Therefore, only the direct methods will be discussed in the continuation of this thesis.

2.4.2. Tension bar model versus continuous restraining model theory

Figure 2.15 provides an overview of the crack width prediction models which were discussed in the literature study. It turned out that a distinction can be made between prediction models which are based on the tension bar model theory and models based on continuous restraining model theory.

MODEL	TENSION BAR MODEL	CONTINUOUS MODEL
EN 1992-1-1	X	
EN 1992-3 – I	X	
EN 1992-3 – II		X
MODEL CODE 2010	X	
VAN BREUGEL	X	
CIRIA C660 – I	X	
CIRIA C660 - II		X
ICE/0707/012		X

Figure 2.15: Overview crack width prediction models

As mentioned before the tension bar model is a theoretical model of a concrete tensile member with one reinforcing bar in the middle subjected to a uniform tensile load. It is assumed that at the location of the crack, the stress and strain in the concrete is zero and the steel reinforcement has to carry the full tensile load. Over a certain transfer length, the stress is transferred from the steel reinforcement to the concrete by means of bond. At the end of the transfer length, the axial strain of concrete matches that of the reinforcement steel.

In case that the stabilized cracking stage is reached, the distances between the cracks, also called the crack spacing, are all less than twice the transfer length. This indicates that there is no longer a position along the tensile member where the axial strain of the concrete equals the cracking strain ϵ_{cr}. The crack width is determined by integrating the strain difference between the reinforcement and concrete over the transfer length (crack formation stage) or over the crack spacing (stabilized cracking stage). The differences between the prediction models in the way the strain difference and the transfer length or crack spacing are determined is explained in section 2.4.3. Most of the prediction models based on the tension bar theory assume a constant bond slip relationship, which translates into the linear strain distribution as shown in figure 2.16.

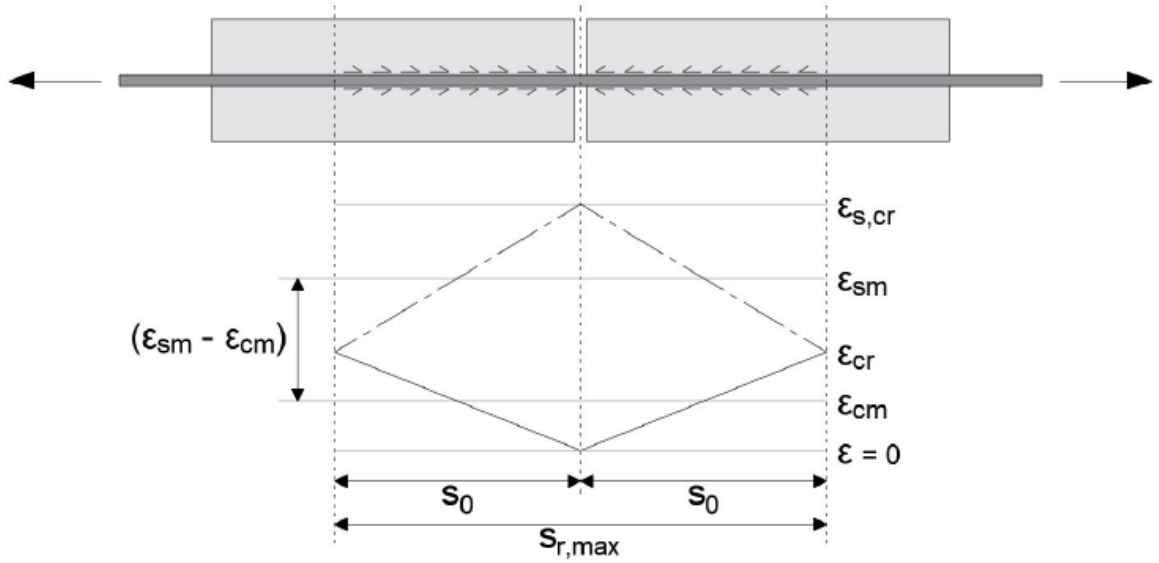

Figure 2.16: Schematic representation of strain distribution of tensile member in crack formation stage (Y Zondag, 2021)

The EN 1992-3-II, CIRIA C660-II and ICE apply the so called continuous restraining model. This model has some similarities with the tension bar model. First of all, it also consists of a single reinforcement bar surrounded by concrete and this reinforcement bar is also subjected to a uniform tensile load. However, this member is continuously restrained along one edge as shown in figure 2.17.

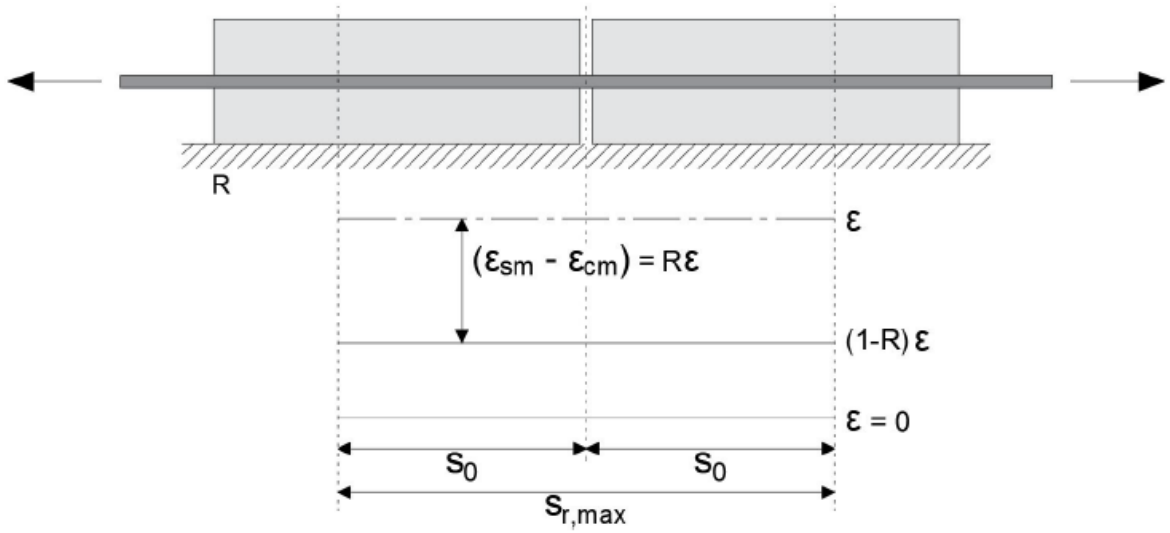

Figure 2.17: Schematic representation of strain distribution of tensile member according to continuous restraining model (Y Zondag, 2021)

Another difference with respect to the tensile bar model is that the continuous restraining model does not take into account that the axial load is transferred from the concrete to the reinforcement steel due to bonding [4]. This implies that the axial load is carried completely by the concrete and the mean strain difference is equal to the axial strain of the tensile member being restrained. For this reason, it can be concluded, once the crack strain is exceeded, that all the cracks will develop at the same time. No matter what the degree of restraint is. [26].

Remarkably, only the ICE which is a further development of the CIRIA argues that part of the load is transferred from the concrete into the restraining member, and this reduces the stress which should be transferred to the reinforcement. It can be concluded that the ICE method combines the two theoretical models. As mentioned before in section 2.3.6 this method considers two stages. The crack width in the first stage is calculated on the basis of a revision of the tensile bar model which takes into account the strain relief of the undisturbed area. While, the determination of the crack width in the second stage is more in line with the continuous restraining model. In the second stage the cracks continuously develop as the imposed deformation allows the concrete to continue to contract relatively to the reinforcement.

2.4.3. Crack spacing theory

In paragraph 2.3 of the literature study it is emphasized that the crack widths are a function of the crack spacing and the crack spacing depends mainly on the transfer length. According to Beeby [6], the major differences between the prediction models can be explained on the basis of the following three theories:

- ”slip” theory
- ”no slip” theory
- combinations of ”slip” and ”no slip” theory

In the following section, the three different theories will be explained and subsequently the differences between the crack width prediction models will be discussed.

2.4.3.1 ”Slip theory”

The ”slip theory” is a theory that was proposed by prof. Salinger in 1936 for the first time. [22]. This theory was developed for members which were subjected to pure tension, and in the theory it was assumed that at each crack, bond failure occurs and that plane sections within the concrete remain plane. Which means that cracks are formed parallel throughout the section thickness. According to the ”slip” theory the crack width is equal to the elongation of the reinforcement relative to the concrete over a slip length (transfer length) on either side of the crack as is illustrated in figure 2.18. The distribution of the forces transferred between the concrete and the reinforcement interface is a function of the ultimate bond strength f_b.

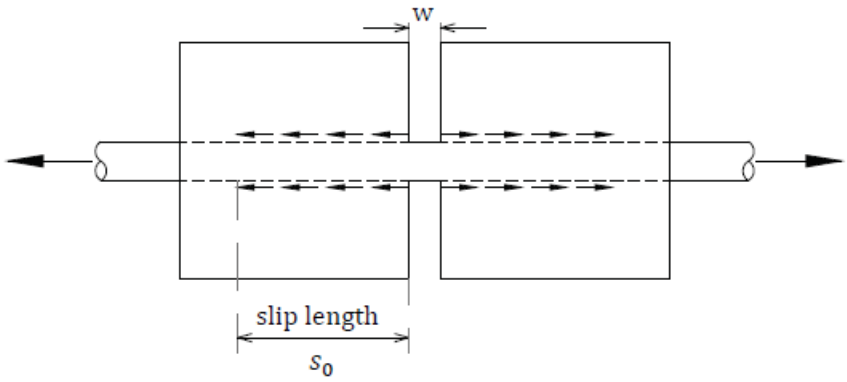

Figure 2.18: Schematic representation of the ”slip” cracking theory (Micallef, 2016)

As mentioned before in section 2.2, the force transmitted by bond over the slip length s_0 can be expressed as:

$$A_{ct} \cdot f_{ct} = s_0(\pi \emptyset f_b) \tag{2.56}$$

The reinforcement ratio is given by the following equation:

$$\rho = \frac{A_s}{A_{ct}} = \frac{\pi \emptyset^2}{4A_{ct}} \tag{2.57}$$

Substituting equation 2.56 into equation 2.57 and rewriting it in the general form of the ”slip” theory will result in the following expression:

$$s_0 = C_1 \cdot \frac{f_{ct}}{f_b} \cdot \frac{\emptyset}{\rho}, \tag{2.58}$$

where C_1 is a coefficient which depends on the shape of the bond stress distribution and is derived empirically. It can be concluded that according to the ”slip” theory the slip length (transfer length) is proportional to $\frac{\emptyset}{\rho}$.

2.4.3.2 ”No slip” theory

The ”no slip” theory is described in a report written by Base et al. in 1966 [5]. In contrast to the ”slip” theory, this theory assumes that there is perfect bond between the concrete and the steel reinforcement. According to the ”no slip” theory the transfer length of stresses is proportional to the concrete cover to reinforcement. The transfer length s_0 can be derived with the following equation:

$$s_0 = C_2 \cdot c, \tag{2.59}$$

where C_2 is a constant and c is the concrete cover. This theory argues that the crack widths are minimal at the bar surface and as they approach the concrete surface the crack width will increase. In figure 2.19 a schematic representation of the ”no-slip” cracking theory is shown.

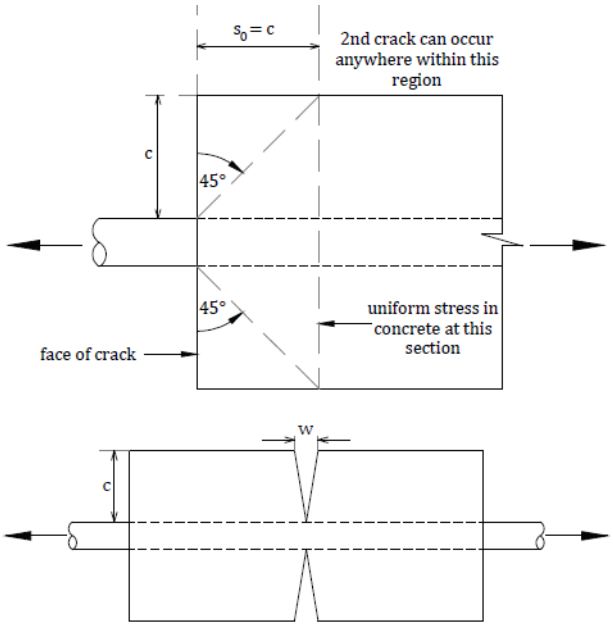

Figure 2.19: Schematic representation of the ”no slip” cracking theory (Micallef, 2016)

2.4.3.3 Combined ”slip” and ”no slip” theory

In 1979, professor Beeby [6] argued that it would be more reasonable to combine the ”slip” and ”no slip” cracking theories. He stated that the transfer length s_0 had to be a function of both the ratio between the bar diameter and the reinforcement percentage ($\frac{\emptyset}{\rho}$) and the concrete cover to reinforcement. The expression of the transfer length is given by the following equation:

$$s_0 = C_3 \cdot c + C_4 \cdot \frac{\emptyset}{\rho}, \tag{2.60}$$

where C_3 and C_4 are non-dimensional coefficients. In figure 2.20 a schematic representation of the combined cracking theories is given.

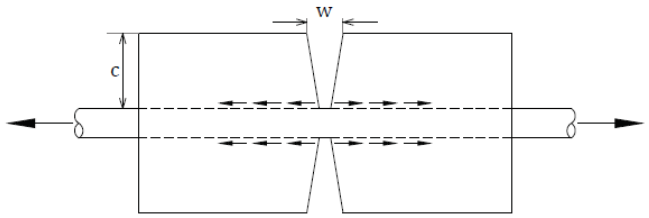

Figure 2.20: Schematic representation of the combined cracking theories (Micallef, 2016)

2.4.3.4 Comparison between the prediction models

In figure 2.21 an overview of the applied formulas for the transfer length and maximum crack spacing is given. It must be noted that the crack spacing mentioned here only refers to the stabilized cracking stage. The reason for this is that the crack spacing in the crack formation stage is variable because new cracks still develop. It can be concluded that all models with the exception of Van Breugel and the Model Code apply the combined cracking theory. According to Van Breugel and the Model Code, the ”slip” theory applies which means that the concrete cover will not influence the crack spacing. Furthermore, it is remarkable that most of the prediction models assume a maximum crack spacing that exceeds the theoretical upper limit of two times the transfer length. These models state that this is because of the bond strength along the tensile member and due to the scatter in the crack stress causing the transfer length to vary. The codes argue that this results in a larger crack spacing.

Code	Transfer length	Maximum crack spacing
Eurocode 2, CIRIA and ICE	$s_0 = 1{,}5 \cdot c + 0{,}15 \cdot \frac{ø}{\rho_{s,eff}}$	$s_{r,max} = 2{,}26 \cdot s_0$
Model Code 2010	$s_0 = 0{,}14 \cdot \frac{ø}{\rho_{s,eff}}$	$s_{r,max} = 2{,}0 \cdot s_0$
Van Breugel	$s_0 = 0{,}15 \cdot \frac{ø}{\rho_{s,eff}}$	$s_{r,max} = 2{,}25 \cdot s_0$

Figure 2.21: Transfer length and crack spacing equation of the crack width prediction models

2.5. General assumptions

In the Model Code 2010 and Van Breugel, which are the more comprehensive crack width prediction models, is assumed that the crack width due to imposed deformations can also be determined by the **tensile member model** as shown in figure 2.22. The assumption is that the starting point is the horizontal axis. At a given imposed deformation, the response of the tensile member is found by determining the intersection with the curve and reading the **fictitious** steel stress on the vertical axis. This fictitious steel stress is used to determine the maximum crack width. However, the effect of an imposed deformation in the crack formation stage is different from that in the stabilized cracking stage.

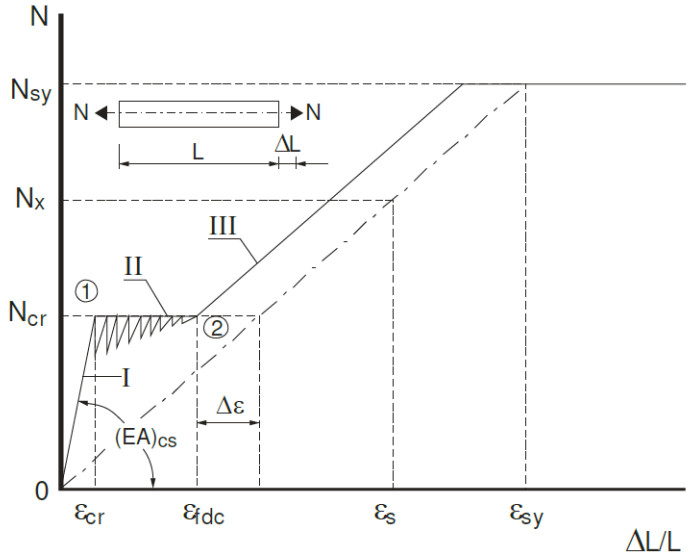

$$N_{cr} = \varepsilon_{cr}\, E_c\, A_c\, (1 + \alpha_e \rho)$$
$$\varepsilon_{fdc} = (60 + 2.4\, \sigma_{s,cr}) \cdot 10^{-6}$$
$$\sigma_{s,cr} = N_{cr}/A_s$$
$$\varepsilon_{s,cr} = \sigma_{s,cr}/A_s$$
$$\Delta\varepsilon_{ts} = \varepsilon_{s,cr} - \varepsilon_{fdc}$$

Figure 2.22: Load-deformation diagram of a reinforced concrete tensile member (van Breugel et al.,2013)

If an imposed deformation occurs in the crack formation stage while simultaneously the external imposed strain remains constant, the number of cracks tends to increase. Since the external force can not exceed the cracking load in the crack formation stage, the existing crack width will not increase. The result is that only additional cracks will develop and the maximum crack width does not change. The maximum crack width in the crack formation stage corresponds to the previously given equation 2.14 and is as follows:

$$w_{max} = \frac{1}{4} \cdot \frac{f_{ctm}}{\tau_{bm}} \cdot \frac{\emptyset}{\rho} \cdot \frac{1}{E_s} \cdot \sigma_{sr} \tag{2.61}$$

While in the stabilized cracking stage, it is assumed that imposed deformations have influence on the maximum crack width. Because in the stabilized cracking stage no new cracks are formed, and if imposed deformations are present they cause widening of the existing cracks. The widening of the cracks will cause an increase in the steel stress which can be defined as:

$$\Delta\sigma_s = \epsilon_{imposed} \cdot E_s \tag{2.62}$$

The general form of the equation for the maximum crack width in the stabilized cracking stage is as follows:

$$w_{max} = \frac{1}{2} \cdot \frac{f_{ctm}}{\tau_{bm}} \cdot \frac{\emptyset}{\rho} \cdot \frac{1}{E_s} \cdot (\sigma_s - \alpha \cdot \sigma_{sr} + \beta \cdot \epsilon_{imposed} \cdot E_s) \tag{2.63}$$

where α depends on the duration of the load and the cracking stage and β is taking account of the imposed deformation condition.

In addition, it is important to emphasize that imposed deformations such as shrinkage strains are considered as long term constant loads. It is assumed that in case of short-term loading the bonding stress between steel and concrete is equal to approximately two times the mean tensile strength of the concrete ($\tau_{bm} = 2 \cdot f_{ctm}$). While, under long term loading, it is stated that the bond stress decreases and that this could result in an increase in the transfer length of approximately 25%.

2.6. Conclusion

The impact of imposed deformations is described in a limited scope in the EN 1992-1-1 and EN 1992-3. Overall, both parts of the Eurocode are very vague and inconsistent in the determination of the effective tensile zone for cross-sections with multiple layers or varying reinforcement. In addition, the codes do not take into account whether the cracks are formed in the crack formation stage or the stabilized cracking but instead the codes make a distinction between the load duration (short or long term loading). These aspects are described in more detail in the Model Code 2010 and Van Breugel and are very important for the calculation of the crack width.

Only the EN 1992-3, CIRIA and ICE deal with the specific condition of a member which is restrained along one edge (CM). It must be noted that in the EN 1992-3 and CIRIA it is assumed that in the area beyond the maximum crack spacing there is no strain relief as result of the crack occurrence which could lead to a different crack width. This may be acceptable with full edge restraint but in reality most of the structures are only partially restrained and strain relief may occur. Only in the ICE the favourable effect of member's restrained edge on the reduction of crack spacing and crack width is taken into account.

Another important point of criticism relates to the determination of the degree of restraint. In the EN 1992-3 only a few practical axial restraint factors for common situations are given. The EN 1992-3 states that in many cases it will be clear that no significant curvature could occur and recommends to assume a restraint factor of 1,0. This assumption seems quite conservative and unrealistic. On the other hand, CIRIA and ICE provide a formula to determine the degree of restraint which is based on the relative size and stiffness of the restraint elements.

3

Numerical crack width prediction (imposed loading versus imposed deformation)

3.1. Introduction to finite element analysis (FEA)

This numerical analysis is performed to investigate the differences in crack width development in a tensile member loaded under an imposed load or loaded under an imposed deformation. In this master thesis the finite element analyses (FEA) are made with DIANA version 10.5. DIANA is an extensive multi-functional finite element software package that is applied to a wide variety of problems encountered in civil engineering, including structural, geotechnical, tunneling, earthquake and oil and gas engineering. This software has been developed by TNO which is a Dutch organization for applied scientific research. DIANA is chosen because it is one of the most practical and commercial tools in engineering practice.

When performing a non-linear finite element analysis (NLFEA), many choices have to be made such as the constitutive model type, the kinematic and equilibrium conditions. In addition, there are different options for modelling the bond and the behavior of the reinforcement. The finite element discretization includes the element type and the element size applied. Solving the system is also subject to choices about convergence criteria, load step size, and how many iterations are allowed. One of the difficulties in applying NLFEA is that the analyst's specific choices have a major impact on the outcome of the analysis. In [18] it was argued that the uncertainty of an NLFEA solution tends to increase as the analyst's skills and knowledge decline. This is the case for any analysis method, as there are always different types of models available. However, some of these choices are prescribed in normative documents such as the Dutch guideline for the assessment of existing concrete structures, the Rijkswaterstaat Technical Document (RTD) [19], which was initiated by Rijkswaterstaat out of concern for the safety of concrete bridges. Following this code procedure should reduce the scatter resulting from the user's choices.

The *fib* Model Code, a document published by the International Concrete Federation (*fib*), aims to help development and updating of codes. It is a semi-normative document that also takes into account new scientific developments. The 2010 edition [10] includes a section on NLFEA that focuses primarily on how to deal with safety formats, but does not provide guidance in choosing a solution strategy. The *fib* Model Code 2022 will include a comprehensive section on verification by non-linear analysis, where the so-called model uncertainty is used to assess the reliability of a NLFEA solution strategy.

In this section, first, the material properties that are of interest and the choices that are made are explained and elaborated.

3.1.1. Cracking models

In DIANA a distinction can be made between multiple cracking models. The material models which can be applied for cracking are the discrete and smeared cracking models. To apply discrete cracking models, the expected location of the crack should be known. This is often not the case so in this master thesis only smeared cracking models are discussed. Smeared cracking models are models in which every element of the model can crack.

The cracks can be formed in different directions. Within the smeared cracking models, the following two types are commonly used:

- Total strain crack model
- Multi directional fixed crack model

The total strain crack model is a constitutive model based on total strain that describes the stress as a function of the strain. The model is called a rotating crack model when the stress-strain relationship is evaluated in the principal direction of the strain vector. This type of modelling is eligible for reinforced concrete structures [16]. In case the aim is to model a more physical nature crack, the fixed crack model can be applied. This fixed crack model determines the cracks in a fixed coordinate system. If a fixed crack model is used, an adequate shear retention model should be used.

The basis of the multi directional fixed crack model is the decomposition of the total strain [ϵ] into an elastic strain [ϵ_e] and a crack strain [ϵ_{cr}]. Due to the sub-decomposition of the crack strain, it is possible to model cracks that occur simultaneously. The decomposition of the cracking strain is shown in figure 3.1. The multi directional fixed crack model is a combination of tension cut-off, tension softening and shear retention. In this model the main focus lies on how the cracks initiate and rotate simultaneously with the stresses.

In this master thesis it has been decided to apply the total strain crack model with a rotating crack orientation. This choice is based on the recommendation in the Dutch guideline for the assessment of existing concrete structure, the Rijkswaterstaat Technical Document (RTD) [19],

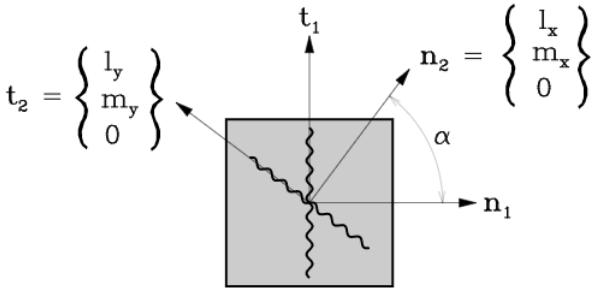

Figure 38.1: Multi-directional fixed crack model

Figure 3.1: Plane stress element including its fixed crack coordinate system (Slobbe, 2015)

3.1.2. Tensile behavior

With the help of a predefined tension softening function it is possible to model the tensile behavior of the concrete in DIANA. The available tension softening curves which are available are shown in figure 3.2. In this master thesis, it is assumed that the concrete tensile stress reduces exponentially to zero after cracking. The exponential-type softening diagrams such as the Hordijk relationship is preferred because this diagram will result in more localized cracks and consequently will avoid large areas of diffuse cracking [19].

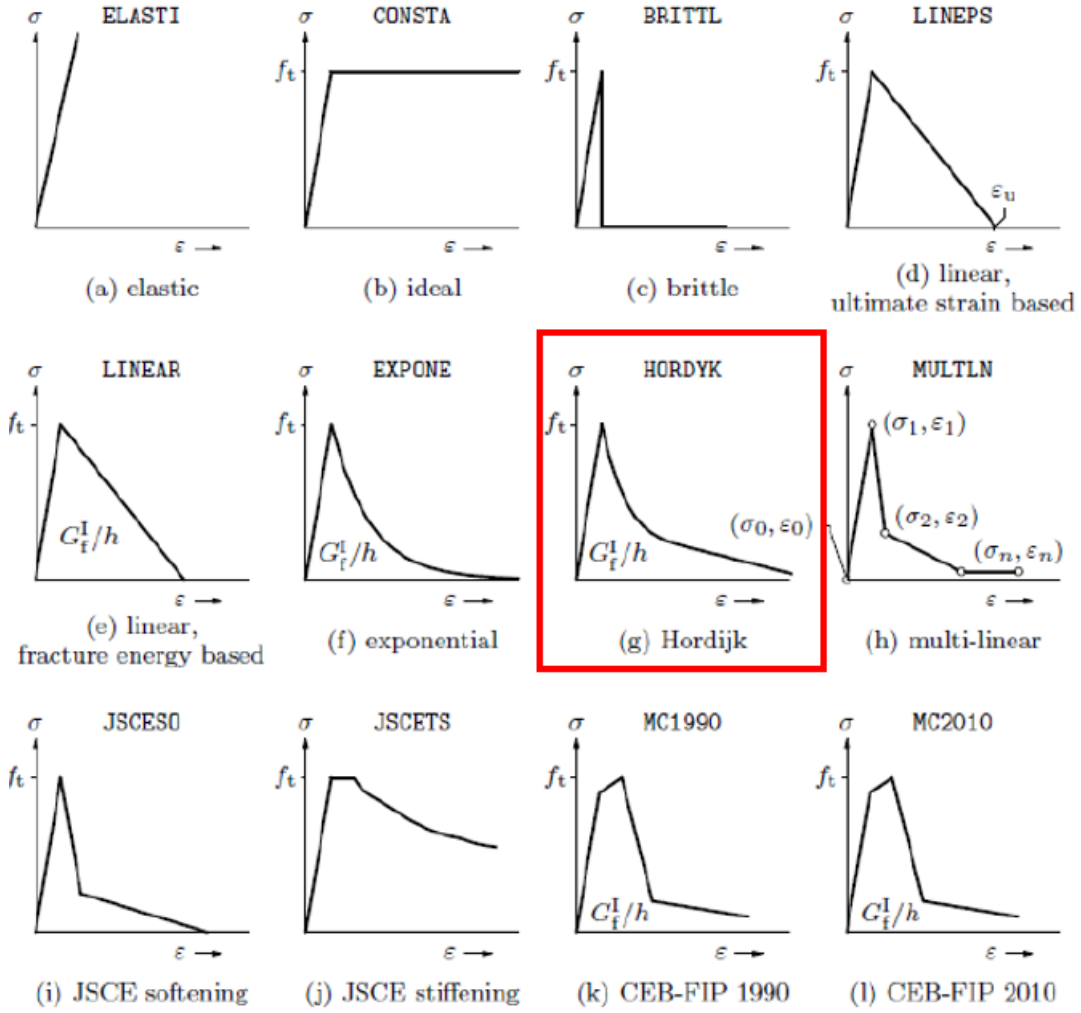

Figure 3.2: Tensile behavior (DIANA FEA MANUAL, 2021)

The damage based Poisson's ratio reduction option is selected, consequently the Poisson's ratio decreases to 0 when the concrete cracks. This is used to prevent unrealistic compression strains in the direction perpendicular to the crack, when large crack strains arise in the vicinity of the crack[25].

3.1.3. Compressive behavior

The compressive behavior of the concrete can be determined by different predefined models within DIANA. In this master thesis, as recommended in the RTD [19], the parabolic stress strain diagram with a softening branch is applied (figure 3.3). The softening branch is based on the compressive fracture energy G_c value in order to reduce mesh size sensitivity during compressive strain localization [19]. According to the RTD report [19], a value of 250 times the fracture energy G_f is advised. This value is based on research results from Nakamura and Higai [15].

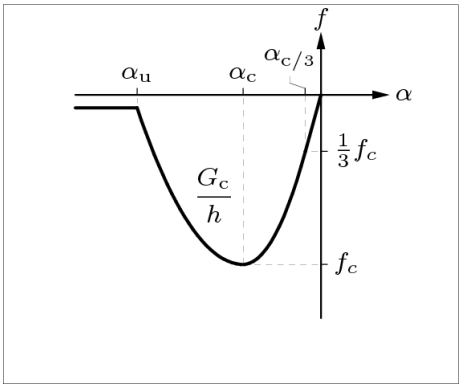

Figure 3.3: Compressive behavior curve according to DIANA, the parabolic compression curve has been applied (DIANA FEA MANUAL, 2021)

The length over which the strain localises is incorporated as an input parameter named the crack bandwidth (h) or also known as the equivalent length (h_{eq}). This could be conceived as the length of the fracture process zone of the crack. Bandwidth for a few element-shapes and crack orientations are depicted in figure 3.4.

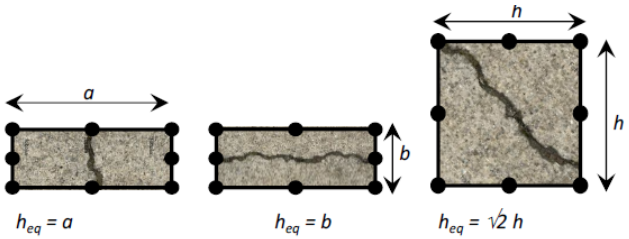

Figure 3.4: Examples of crack bandwidth or equivalent length on element dimensions and crack direction (RTD, 2017)

Since the RTD [19] states that a reduction of the compressive strength resulting from lateral cracking should be taken into account, the reduction model of Vecchio and Collins 1993 shown in figure 3.5 is used.

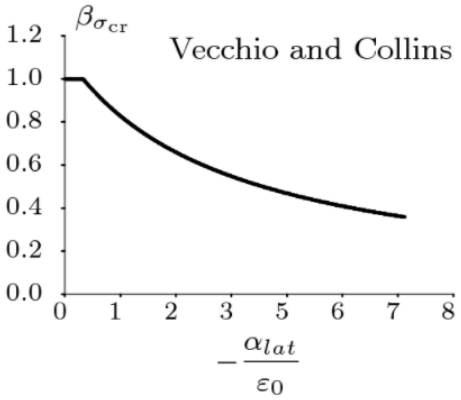

Figure 3.5: Vecchio and Collins reduction factor due to lateral cracking (RTD, 2017)

3.1.4. Bond-slip behavior

An important parameter to determine the crack width is the interaction between the concrete and reinforcement. In DIANA this interaction can be modelled using bond slip mechanisms. The Model Code 2010 slip relationship is applied for the bond-slip behavior in this master thesis. The Model Code 2010 [10] proposed a relation between the shear traction and slip with the back bone curve given in figure 3.6. The first section of the curve is from a slip of s_0 up to s_1 and can be formulated as a power function with an exponent α. The second section is from s_1 to s_2 and is assumed as a constant value of τ_{max}. In the third section from s_2 to s_3, the bond stress reduces linearly until the ultimate bond-slip stress τ_f is reached. A constant value of τ_f is considered after s_3. In this thesis, it is assumed that the bond conditions were moderate and if the load is not perpendicular to the direction of the reinforcement the concrete is assumed to be unconfined. The used parameters are listed in figure 3.9.

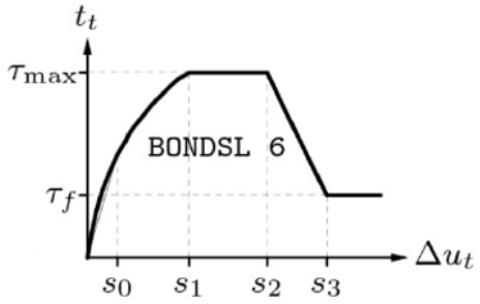

Figure 3.6: Bond-slip curve according to the Model Code 2010 (Model Code, 2010)

To calculate the normal and shear stiffness modulus of the interface for the bond-slip behavior the following equations, as suggested by the professionals at DIANA FEA have been applied:

$$k_n = 100 \cdot \frac{E}{l} = 100 \cdot \frac{32836}{25} \approx 130000 \frac{N}{mm^3} \tag{3.1}$$

$$k_t = 0.1 \cdot k_n = 0.1 \cdot 130000 = 13000 \frac{N}{mm^3} \tag{3.2}$$

Where k_n is the normal stiffness modulus, k_t is the shear stiffness modulus, E is the young's modulus and l is the average element edge length.

3.1.5. Mesh size

According to the guideline for non-linear finite element analysis (NLFEA) from Rijkswaterstaat [19] the maximum size of a 2D model is limited by the following rule:

maximum element size = $min(\frac{L}{50}; \frac{h}{6}) = min(\frac{2000}{50}; \frac{150}{6}) = min(40; 25) = 25mm.$

In order to evaluate the models sensitivity to mesh refinements four different mesh sizes are tested and the results are compared. The results obtained from mesh changes are summarized in figure 3.7. It can be seen that increasing the mesh causes a larger crack width. However, the difference between a mesh size of 25 and 30 mm is less than 5%. Due to this small difference and the significant reduction of the calculation time a mesh size of 30 mm is applied in the numerical models.

Mesh size [mm]	Maximum crack spacing [mm]	Maximum crack width [mm]
15	675	0.41
25	725	0.46
30	750	0.48
50	900	0.59

Figure 3.7: Result of mesh sensitivity models

3.2. Finite element analysis 1 - Imposed loading

Now the different model options have been discussed and chosen, the first analysis was carried out. In the first analysis a single reinforced concrete tensile member is subjected to an imposed load. In this part of the thesis 2D models were used in stead of 3D models. 3D models require a significant longer calculation time and consume much more disk space. In addition, using 2D models has no effect on the structural behavior. Important parameters for determining the structural behavior such as the bond slip interface and the tensile material properties remain exactly the same in 2D as in 3D models and therefore 3D modelling does not have significant benefits over 2D modelling.

3.2.1. Input geometrical and material properties

In figure 3.8 the model used for analysis 1 is given. The dimensions of the model are: length = 2000 mm, height = 150 mm and width = 150 mm. In this model a centrically placed reinforcement bar with a diameter of 25 mm is applied. The tensile member is loaded by a prescribed deformation of the rebar in the X-direction of 0.01 mm per load step. This prescribed deformation is considered as the imposed load and is applied at the tip of the reinforcement. At both ends of the reinforcement the model is restrained in X direction. At one end the model is restraint in Y-direction to prevent rotation. In the finite element program DIANA it is required to place a support in the direction of the prescribed deformation.

Figure 3.8: Model analysis 1 - Single reinforced tensile member subjected to imposed load (DIANA FEA)

The concrete and steel properties which are used in the model are given in figure 3.9. The concrete properties are given for concrete class C30. The steel properties are given for B500 reinforcement.

Material class	*Concrete and masonry*	*Material class*	*Reinforcements*
Material model	*Total strain-based crack model*	*Material model*	*Bond-slip reinforcement*
Linear material properties		**Reinforcement bar**	
Young's modulus	32836 N/mm^2	Young's modulus	200000 N/mm^2
Poisson ratio	0.2	Poisson ratio	0.3
Mass density	2500 kg/m^3	Mass density	7850 kg/m^3
Total strain-based crack model		Non-linear model	Von Mises Plasticity
Crack orientation	Rotating		
Tensile behavior			
Tensile curve	Hordijk		
Tensile strength	2.9 N/mm^2		
Mode-I fracture energy	0.1405 N/mm		
Crack bandwidth specification	Rots		
Poisson's reduction model	Damage based		
Compressive behavior		**Bond-slip interface**	
Compressive curve	Parabolic	Normal stiffness modulus	130000 N/mm^3
Compressive strength	30 N/mm^2	Shear stiffness modulus	13000 N/mm^3
Compressive fracture energy	35 N/mm	Bond-slip interface failure model	CEB-FIB 2010 bond-slip function
Reduction model	Vecchio and Collins 1993	Maximum shear stress	5.5 N/mm^2
Lower bound reduction curve	0.4	Ultimate shear stress	2.2 N/mm^2
Confinement model	No increase	Linearized initial slip section s0	0.1 mm
		Relative slip section s1	0.6 mm
		Relative slip section s2	0.6 mm
		Relative slip section s3	2.5 mm
		Exponent alpha	0.4

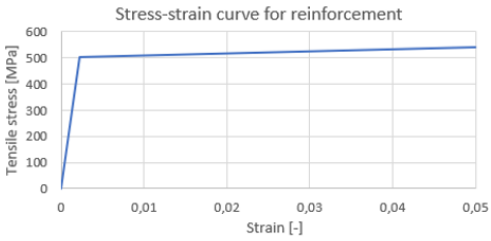

Figure 3.9: Material properties finite element analysis 1

3.2.2. Load displacement diagram

In figure 3.10 the load-displacement diagram of a tensile bar subjected to an imposed load is shown. It is important to note that this is the load taken by the steel at the support. It can be seen that the diagram can be subdivided into three stages. The first stage is the uncracked stage. In this stage there is no difference between the strain in the reinforcement and the concrete strain. Stage II is the crack formation stage. During this stage individual cracks develop and at some places the strain in the reinforcement and the concrete strain are different. Next, stage III is the stabilized cracking stage. Now in all places there is a strain difference between the reinforcement and concrete. No new cracks are formed but only existing cracks widen in this stage. This development is corresponding with the cracking theory which is discussed earlier in section 2.2.

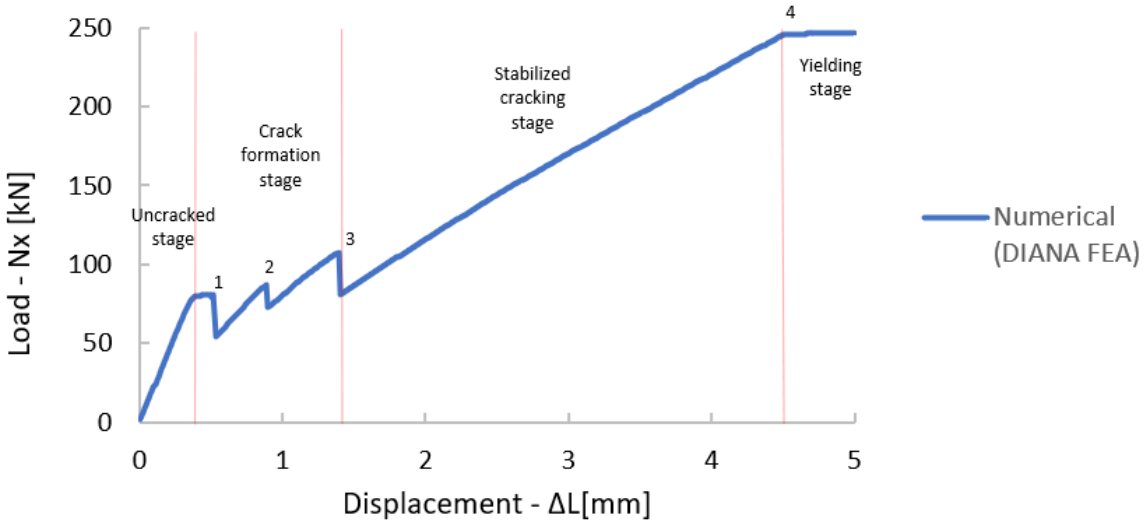

Figure 3.10: Load-displacement diagram model analysis 1 - imposed loading

3.2.3. Crack pattern and bond stress

In the following section the crack patterns and bond stress gradients are given and discussed. The first through cracks occur at a prescribed deformation of 0.53 mm. When these cracks occur, the tensile force of the concrete has to be carried by the reinforcement and therefore it can be seen that on both sides of the crack the maximum bond stress is reached and at the location of the crack the bond stress is zero. Important to mention is that micro cracks already developed earlier at a prescribed deformation of 0.34 mm when the cracking strain was reached. However, these micro cracks were negligibly small. Furthermore, it can be observed that the distance between the cracks and the ends of the tensile member is exactly the same. This symmetry is caused by the fact that both end supports have the same boundary conditions in the X-direction and the tensile load is applied centrically.

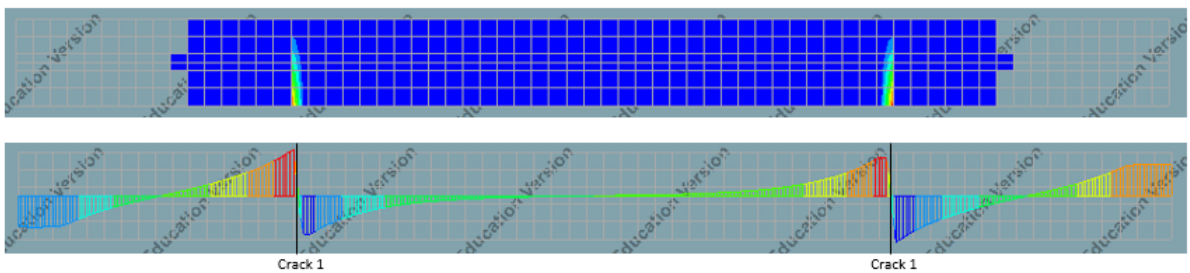

Figure 3.11: Crack pattern and bond stress crack 1 - load step 53 = ΔL = 0.53 mm (Crack Formation Stage)

In figure 3.12 the crack pattern and bond stress gradient of the consecutive cracks are shown. It can be seen that in addition to the first two cracks, two primary cracks have been developed in the middle of the tensile member. The cracks have occurred at a prescribed deformation of 0.90 mm.

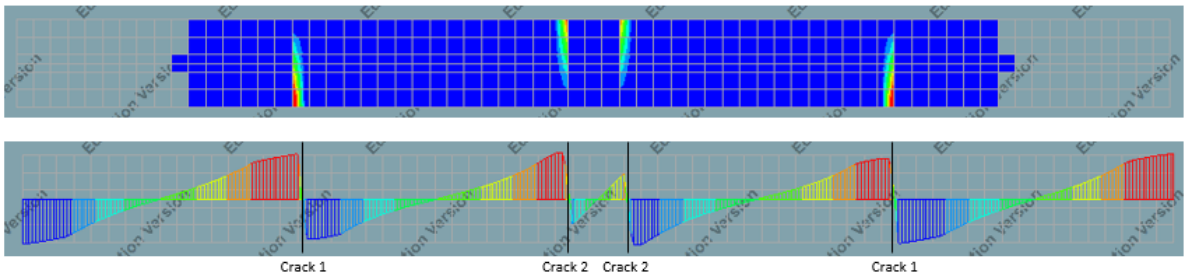

Figure 3.12: Crack pattern and bond stress crack 2 - load step 90 = ΔL = 0.90 mm (Crack Formation Stage)

Next, in figure 3.13 it can be seen that at a prescribed deformation of 1,4 mm, four new through cracks have been developed. At this point the end of the crack formation stage has been reached. From now, no new cracks should appear and only the existing cracks should widen.

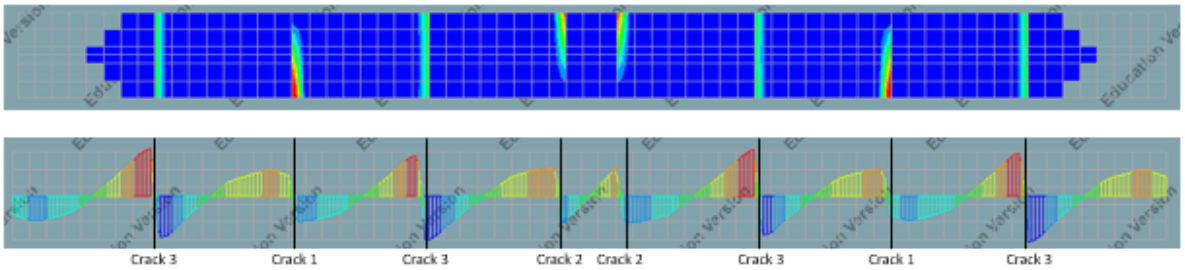

Figure 3.13: Crack pattern and bond stress crack 3 - load step 140 = ΔL = 1.40 mm (Crack Formation Stage)

Figure 3.14 shows the crack pattern and the bond stress gradient at the end of the stabilized cracking stage. It can be observed that no new cracks have developed and that only existing cracks have been widened. This is in line with the cracking theory as discussed in section 2.2.

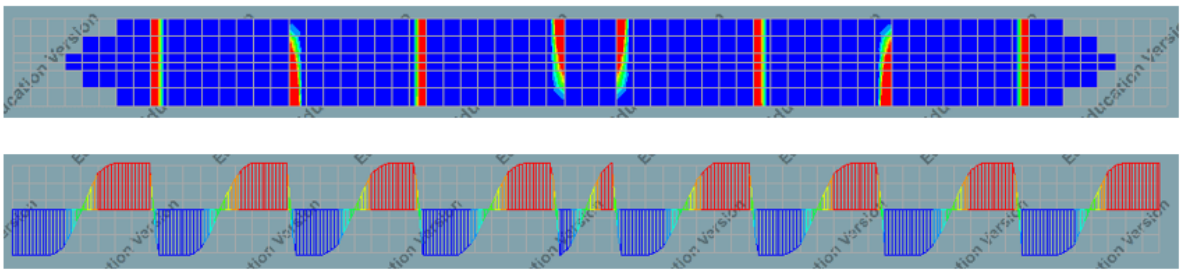

Figure 3.14: Crack pattern and bond stress end stabilized cracking stage - load step 450 = ΔL = 4.5 mm

3.2.4. Steel stress development

In figure 3.15 the crack width contour plot (top) and the steel stress development in the cracks (bottom) are shown. Due to symmetry only half of the contour plot of the tensile bar is presented. It is important to emphasize that the blue line is the steel stress taken at the support. It can be seen that when the first crack occurs, the steel stress in crack 1 increases (yellow line) and the steel stress at the support decreases. The reason for this is that there must be always an equilibrium of forces. The same phenomena can be seen in crack 2 (green line), 3a (red line) and crack 3b (blue dashed line). Crack 3a and 3b are two different cracks which initiated at the same time in the model. When these cracks develop, the steel stress increases and the stresses at the other points drop. In the stabilized cracking stage, the steel stress is in all the cracks the same.

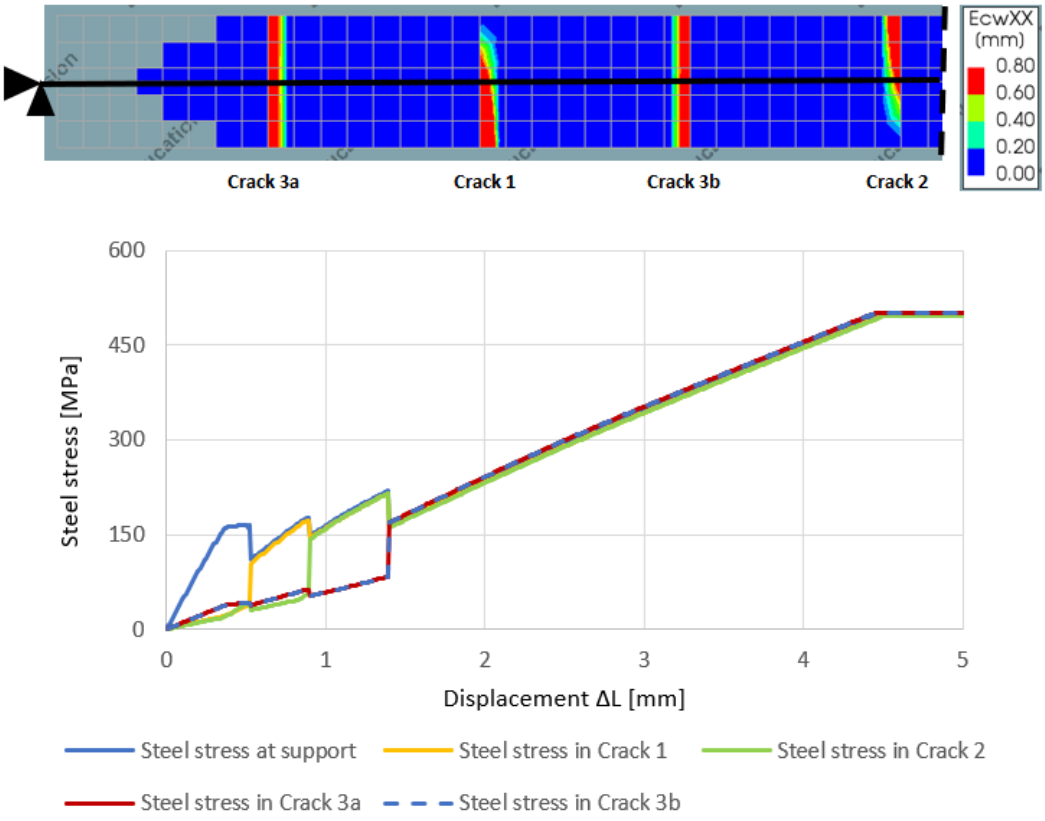

Figure 3.15: Steel stress in the cracks

3.2.5. Crack width development

In the top of figure 3.16 the contour plot of the crack pattern is shown. The location where the crack width is measured is highlighted. In the bottom of the figure, the maximum crack width development per individual crack is given. It can be observed that when crack 2 (green line) starts to open, the crack width in crack 1 (yellow line) decreases. The same can be seen when cracks 3a (red line) and 3b (dashed blue line) open, the crack width in crack 1 and 2 drops. After crack 3a and 3b have been developed the stabilized cracking stage is reached and the crack width in all cracks gradually increases.

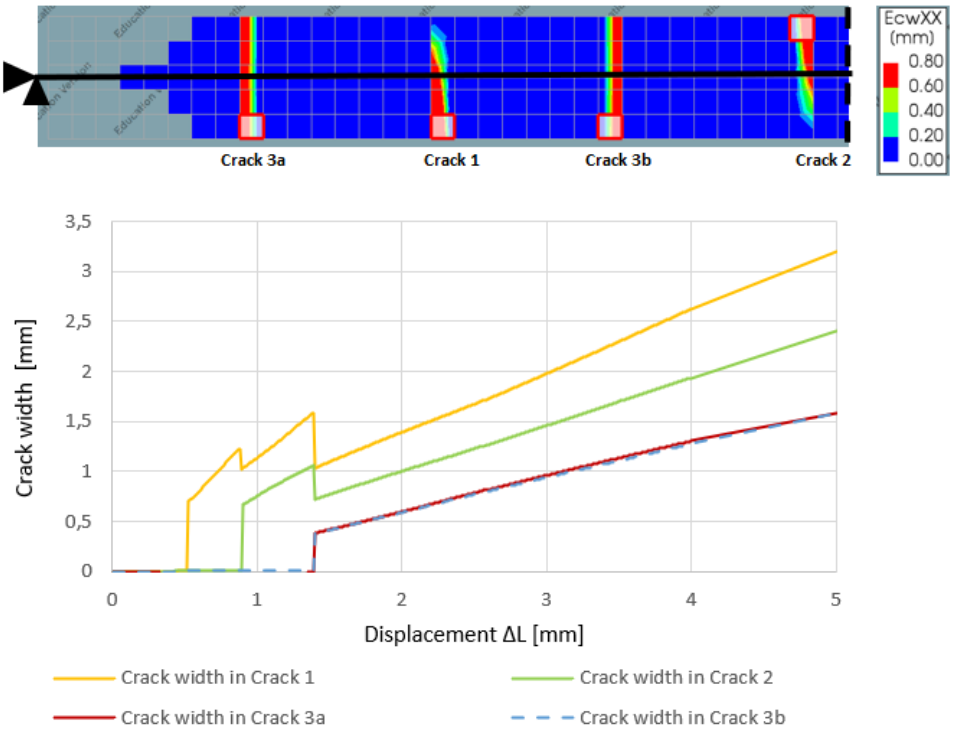

Figure 3.16: Crack width development

3.3. Verification with experiments of imposed loading model

To verify the accuracy and applicability of the finite element analysis in case of imposed loading, the experimental results from A. Kwan [12] were used. Unfortunately no load-displacement curves were given in Kwan's research, therefore only the maximum crack width development and crack pattern are used for the verification. In the experiment from A. Kwan two reinforced tensile members with a length of 700 mm and a cross section of 70 x 70 mm were subjected to an imposed tensile load. The elements were tensioned by a hydraulic press via reinforcement. The concrete and steel properties can be find in figure 3.17 and 3.18.

Specimen number	Compressive strength [MPa]	Tensile strength [MPa]	Elastic modulus [GPa]	Poisson's ratio	Fracture toughness ($MNm^{-2/3}$)
D8-RA	24.1	1.8	23244	0.2	1.3
D12-RA	24.1	1.8	23244	0.2	1.3

Figure 3.17: Concrete properties of tension specimens (Kwan, 2016)

Specimen number	Steel bar diameter [mm]	Steel ratio [%]	Elastic modulus [GPa]	Steel yield strength [MPa]	Steel ultimate strength [MPa]
D8-RA	8	1.03	200	400	500
D12-RA	12	2.31	200	400	500

Figure 3.18: Steel properties of tension specimens (Kwan, 2016)

The test set-up is shown in the top of figure 3.19. It can be observed that at both ends of the tensile bar a tension force T is applied. In the bottom of figure 3.19 the mesh size used in the finite element model is shown. Due to the fact that in this simulation not a prescribed deformation is applied but a prescribed tension force the boundary conditions are slightly different compared to the previous FEA.

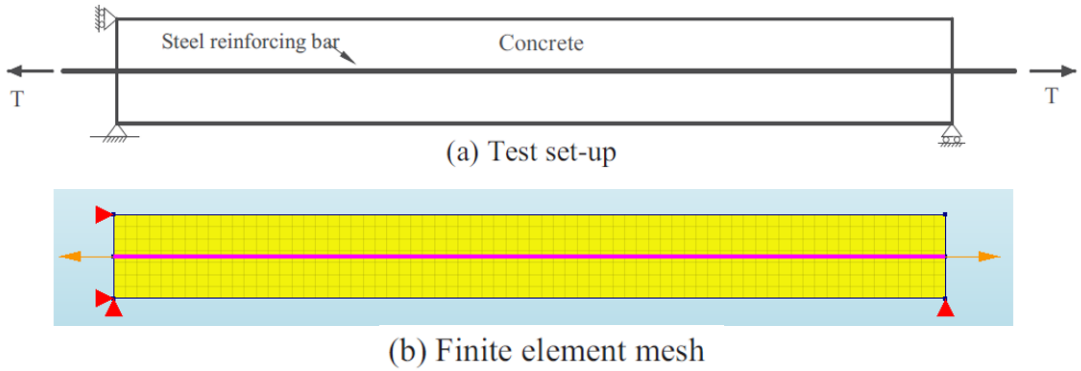

Figure 3.19: Test setup (Kwan, 2016)

3.3.1. Maximum crack width

In DIANA the crack width over an element is given as an output. It is important to emphasize that DIANA gives the maximum crack width in an integration point. The maximum crack width is calculated by multiplying the cracking strain in the integration point with the crack bandwidth of the total element. For specimen D8-RA and D12-RA, the numerically predicted and measured maximum crack widths are compared. The difference between these two models is the bar diameter which is respectively 8 and 12 mm.

Figure 3.20 presents the maximum crack width at different loading stages for specimen D8-RA. It can be observed that the maximum crack width predicted numerically at the first loading stage (T=17 kN) is 25% larger than the maximum crack width measured in the experiments. However at the next three loading stages (T = 22.6; T = 28.3; T = 33.9 kN) it can be seen that the difference becomes smaller up to 15%. In the final loading stage (T=39.5 kN), the numerically predicted maximum crack width differs only 7% from the measured maximum crack width. So in this particular case, with an increasing load the numerical results come closer to the experimentally measured maximum crack widths. This is presented by the graph in figure 3.20. In order to make a complete comparison the crack width is also calculated analytically according to the Model Code 2010. It can be seen that the design formula in the Model Code 2010 tends to overestimate the maximum crack width as the steel stress increases.

Load	Steel stress	Analytical (Model Code 2010)	Experimental result (A. Kwan)	Numerical result (DIANA)	Difference DIANA vs Kwan
T [kN]	σs [Mpa]	Wmax [mm]	Wmax [mm]	Wmax [mm]	%
17,0	150	0,20	0,10	0,13	-25
22,6	200	0,27	0,12	0,14	-14
28,3	250	0,33	0,13	0,15	-15
33,9	300	0,40	0,16	0,18	-12
39,6	350	0,46	0,21	0,22	-7

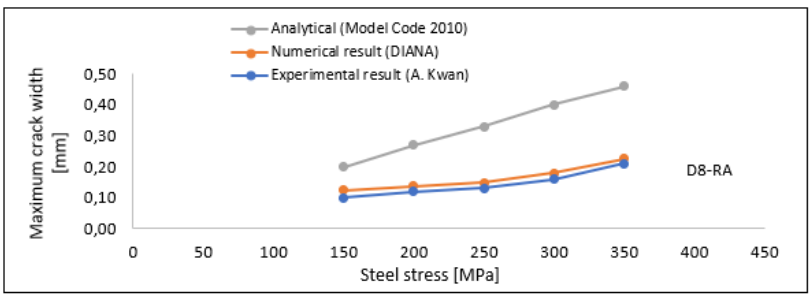

Figure 3.20: Verification D8-RA

For specimen D12-RA, the comparison between the numerically predicted and the experimentally measured maximum crack width is shown in figure 3.21. It can be seen that at the first three loading stages (T = 11.3; T=22.6 and T=28.3 kN), the numerically predicted maximum crack width is significantly larger than the measured maximum crack width. While in the last two loading stages (T = 33.9 and T = 39.6 kN) this difference diminishes to 4 and 9% respectively. In this case it can be observed that the maximum crack width prediction according to the Model Code 2010 in the first loading stage is quite accurate. However, with increasing tensile load the maximum crack width is more overestimated. This finding is also confirmed in Kwan's study [12].

Load	Steel stress	Analytical (Model Code 2010)	Experimental result (A. Kwan)	Numerical result (DIANA)	Difference DIANA vs Kwan
T [kN]	σs [Mpa]	Wmax [mm]	Wmax [mm]	Wmax [mm]	%
11,3	100	0,09	0,08	0,09	-14
22,6	200	0,18	0,10	0,12	-19
28,3	250	0,22	0,11	0,15	-32
33,9	300	0,27	0,18	0,19	-4
39,6	350	0,31	0,20	0,22	-9

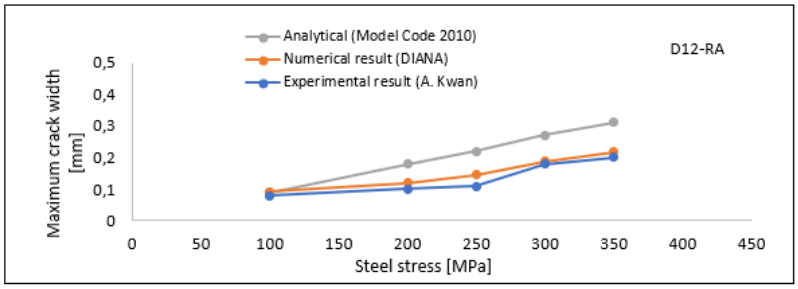

Figure 3.21: Verification D12-RA

Overall, it can be concluded that the numerically predicted and the experimentally measured maximum crack widths are corresponding reasonably well at the final loading stages. The difference at the final loading stage is only 9%. In addition, it can be seen that in general the numerically predicted results and to a greater extent the analytical prediction overestimate the real maximum crack width. One of the explanations for this overestimation is that when a crack is localised in one element, the cracking strain in the integration point is only maximum at one side of the element. This maximum cracking strain is used by DIANA to calculate the crack width. This approach might cause that the numerical calculated crack widths are higher than the measured crack widths.

In addition, another explanation might be the accuracy of the bond slip curve. For a more accurate prediction of the crack width of tensile members, the bond slip material properties must correspond exactly to reality. In these models multiple assumptions given in the experiments of A. Kwan [12] are used. These assumptions are related to the the maximum bond stress and the moment when the rebar starts to slip.

3.3.2. Crack pattern

After verifying the crack width, the number of cracks and crack patterns at different loading stages obtained by the numerical analysis and the measured crack patterns are compared. In the figures 3.22, 3.23 and 3.24 the crack patterns measured and obtained numerically of specimen D12-RA are shown. From figure 3.22, when the tensile load equals 20 kN, 5 cracks could be observed in the measured crack pattern while according to the numerical model only 4 cracks appeared. At T = 30 kN, the measured crack number was 8 whereas the numerical crack number is 7. Finally, at T = 40 kN, the measured number of cracks increased to 12 while according to numerical results the total number of cracks became also 12.

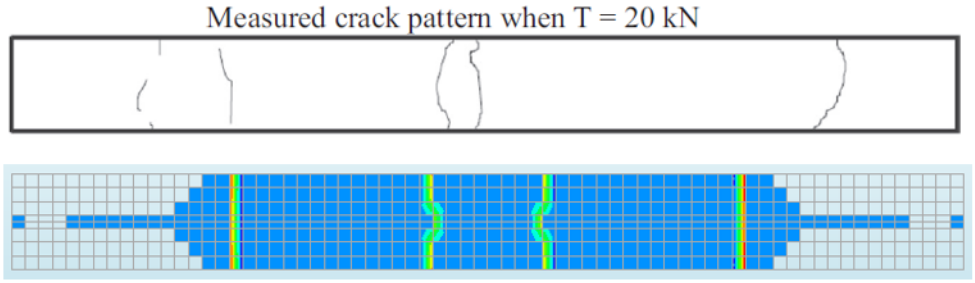

Figure 3.22: Measured crack pattern (Kwan, 2016) and numerical predicted crack pattern at T = 20 kN

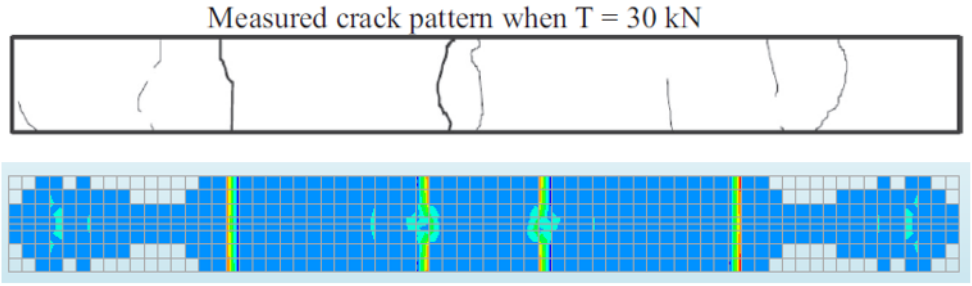

Figure 3.23: Measured crack pattern (Kwan, 2016) and numerical predicted crack pattern at T = 30 kN

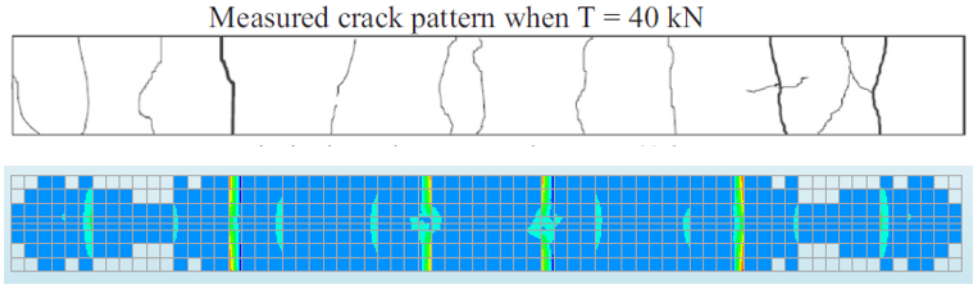

Figure 3.24: Measured crack pattern (Kwan, 2016) and numerical predicted crack pattern at T = 40 kN

Overall the measured number of cracks agree quite well with the numerical predictions. However, the measured crack patterns show more randomness compared to the numerical predicted crack patterns where the cracks are more evenly distributed.

3.4. Finite element analysis 2 - Imposed deformation

3.4.1. Input geometrical and material properties

In the second analysis exactly the same single reinforced concrete tensile member which is described in section 3.2.1 is used. The difference compared to finite element analysis 1 is that in analysis 2 the concrete is loaded under an imposed deformation. As imposed deformation a prescribed shrinkage strain of -5 · 10^{-6} per load step is applied.

3.4.2. Load displacement diagram

In figure 3.25 the load-displacement diagram of finite element analysis 2 is presented. The blue line is the load taken by the steel at the support. It can be observed that the diagram can be subdivided in three stages. In stage I the concrete is uncracked. When the concrete starts cracking, stage II applies which is denoted as the crack formation stage. And the final stage in the figure is stage III, this is the stabilized cracking stage. A remarkable observation is that the force drops, while the imposed strain increases and more cracks are developing. In the comparison in section 3.5 a possible explanation is described.

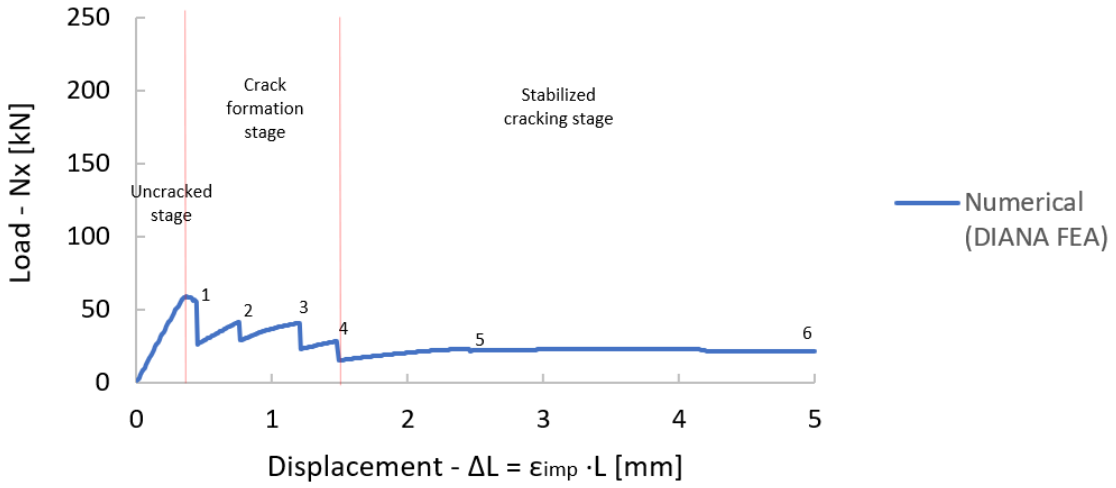

Figure 3.25: Load - displacement diagram finite element analysis 2 - imposed deformation

3.4.3. Crack pattern and bond stress

In this section the crack patterns and bond stress gradients from finite element analysis 2 are presented. In figure 3.26 the first through cracks occur at a prescribed deformation of 0.45 mm. Important to mention is that micro cracks already developed earlier at a prescribed deformation of 0.34 mm when the cracking strain was reached. However, these micro cracks were negligibly small.

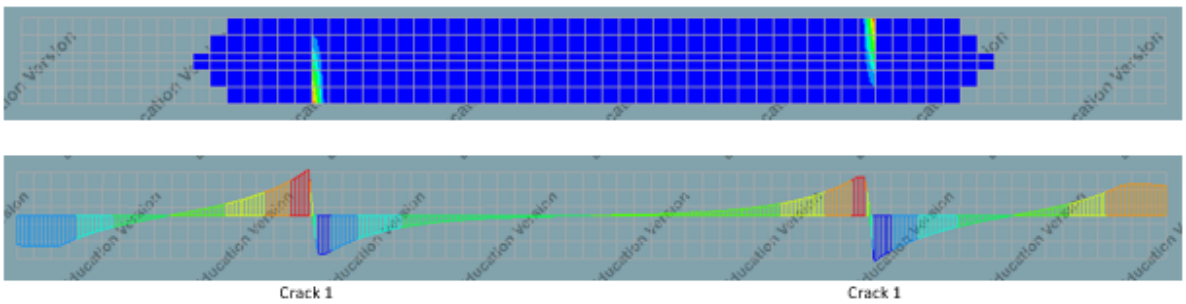

Figure 3.26: Crack pattern and bond stress crack 1 - load step 45 = ΔL = 0.45 mm (Crack Formation Stage)

In figure 3.27 the crack pattern and bond stress of the second moment of cracking are shown. It can be seen that in addition to the first two cracks, one primary crack has been developed in the middle of the tensile member. This crack was developed at a deformation of 0.77 mm.

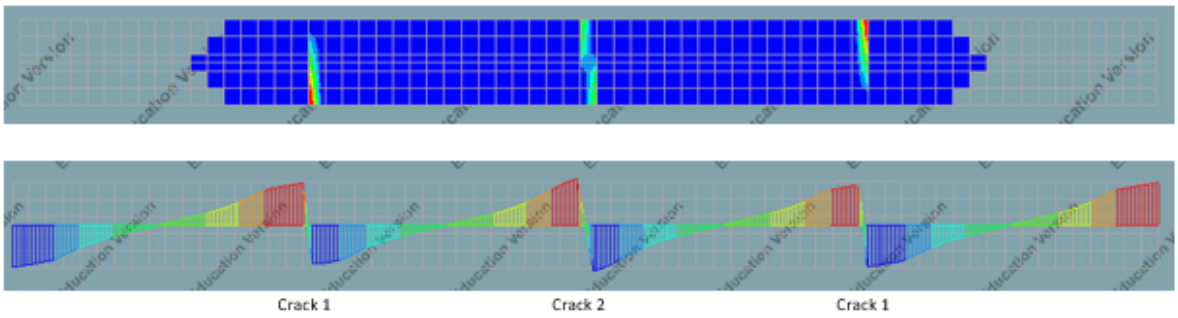

Figure 3.27: Crack pattern and bond stress crack 2 - load step 77 = ΔL = 0.77 mm (Crack Formation Stage)

From figure 3.28 it can be observed that at a deformation of 1.21 mm two more cracks have been developed.

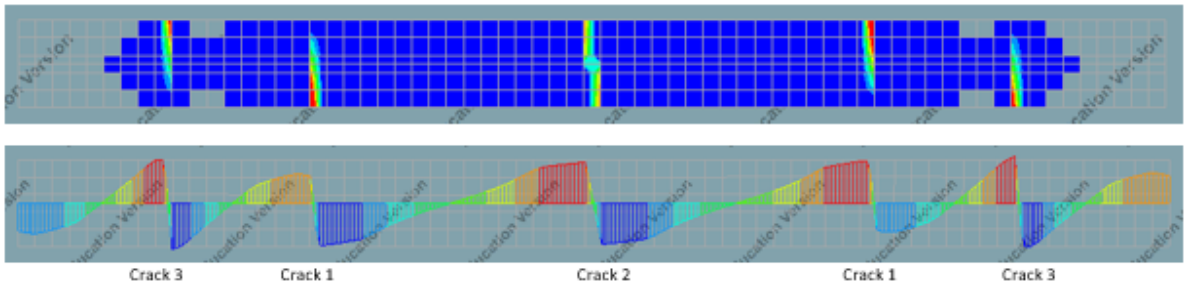

Figure 3.28: Crack pattern and bond stress crack 3 - load step 121 = ΔL = 1.21 mm (Crack Formation Stage)

At a deformation of 1.50 mm two more cracks appeared. This point is assumed to be the end of the crack formation stage, which means that there should be no more space for new cracks to develop and the stabilized cracking stage starts.

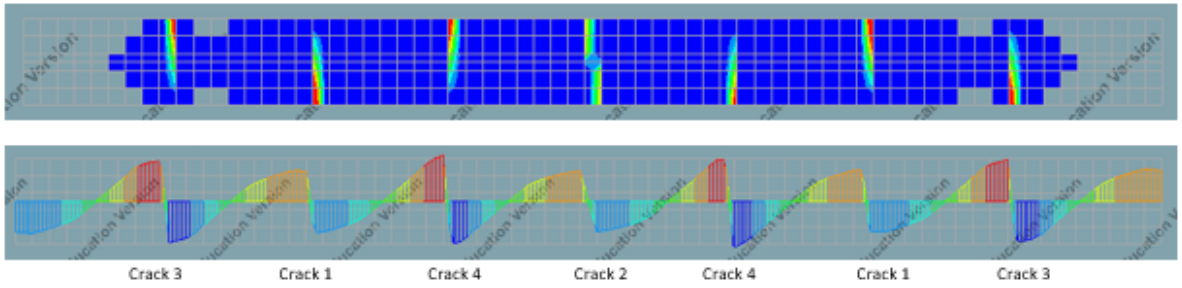

Figure 3.29: Crack pattern and bond stress crack 4 - load step 150 = ΔL = 1.50 mm (Crack Formation Stage)

Figure 3.30 shows the crack pattern and the bond stress gradient at a deformation of 2.45 mm. It can be observed that two new cracks have been developed in what was supposed to be the stabilized cracking stage. According to the cracking theory this was not expected because in the stabilized cracking stage no new cracks should appear and only existing cracks should widen. It is excluded that the development of these two cracks is related to the convergence criteria because all steps of the analysis are fully converged.

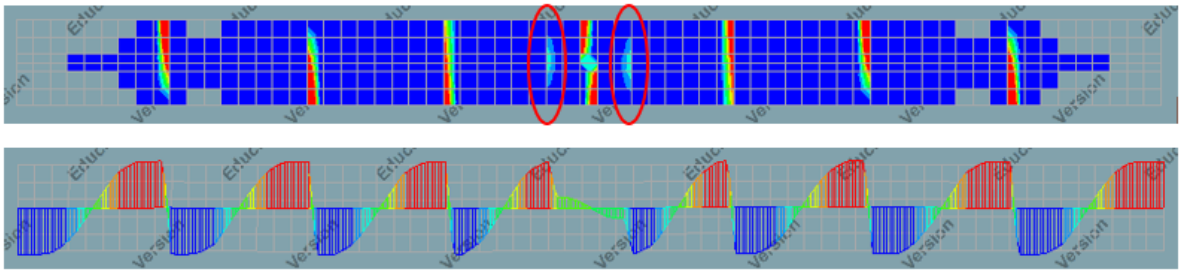

Figure 3.30: Crack pattern and bond stress crack 5 - load step 245 = ΔL = 2.45 mm (Stabilized Cracking Stage)

Figure 3.31 shows the crack pattern and the bond stress gradient at the end of the stabilized cracking stage. It can be observed that no new cracks have been developed and that only existing cracks have been widened. This is in line with the cracking theory as earlier discussed in section 2.2.

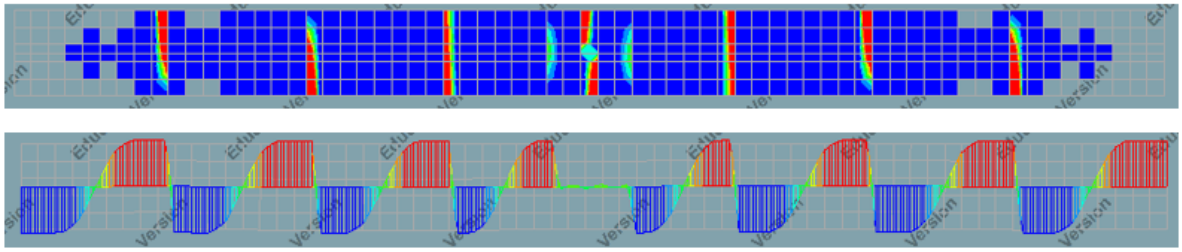

Figure 3.31: Crack pattern and bond stress - load step 450 = ΔL = 4.50 mm (End Stabilized Cracking Stage)

3.4.4. Steel stress development

In figure 3.32 and 3.33 the contour plot and the steel stress development in the cracks are shown. Due to symmetry only half of the contour plot of the tensile bar is presented. It can be observed that due to the fact that the imposed deformation is restrained, this causes initial compressive stresses. When the first crack occurs, the steel stress in crack 1 (yellow line) increases and the steel stress at the support decreases. This is due to the equilibrium of forces in the reinforcement bar. This development was also observed in the other cracks with the exception of crack 5 (black line). From the contour plot of the crack pattern, is can be seen that crack 5 is really close located to crack 2 (green line). Therefore, at the moment that the second crack starts to open there is already some steel stress development at crack 5.

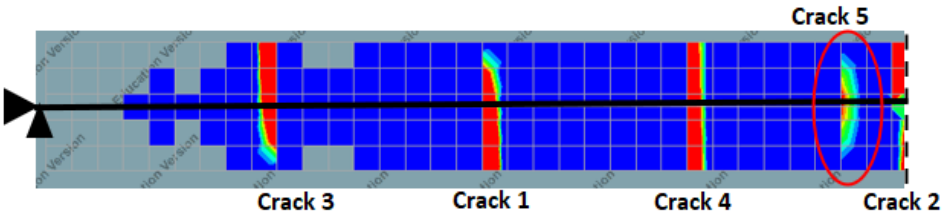

Figure 3.32: Crack width contour plot

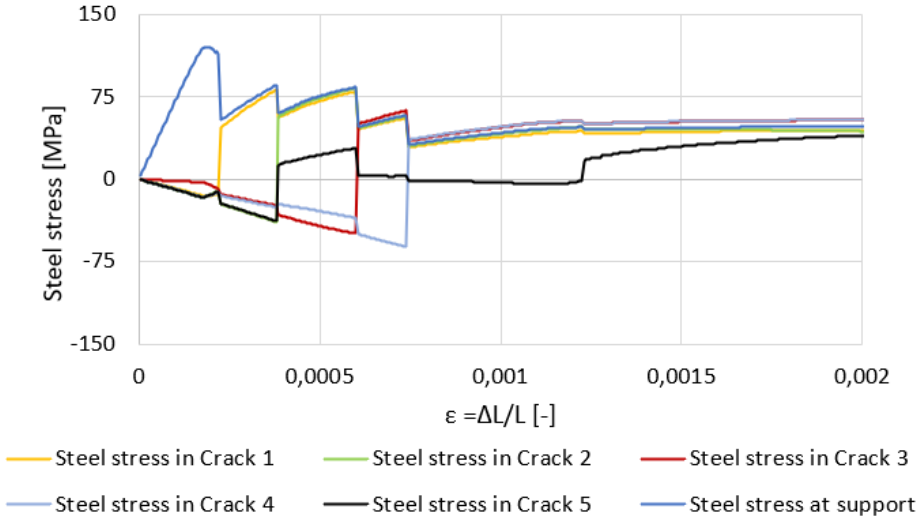

Figure 3.33: Steel stress and its growth at the location of the cracks

3.4.5. Crack width development

In figure 3.34 and 3.35 the contour plot and the maximum crack width development per individual crack (bottom) are presented. It can be observed that when a new crack starts to open, the crack width of the other cracks slightly drops.

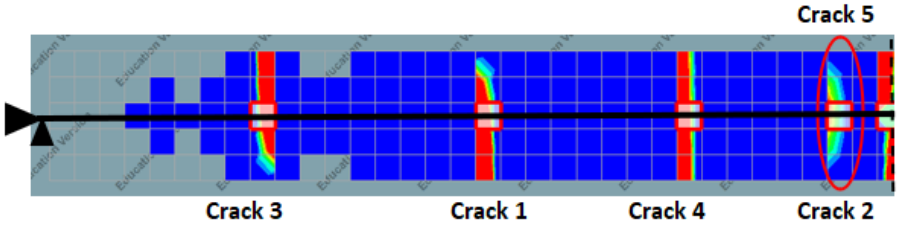

Figure 3.34: Crack width contour plot

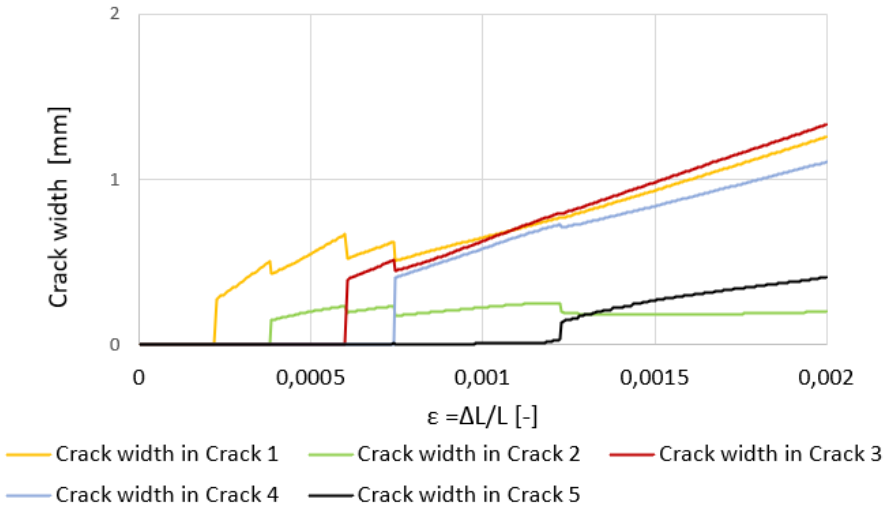

Figure 3.35: Crack width development

3.5. Comparison imposed loading versus imposed deformation

As mentioned before, in practice, when cracks are formed due to imposed loading engineers apply the tensile member model. The theory behind this model is explained in more detail in section 2.2. However, in case that cracks are formed under imposed deformations, it is assumed that under certain conditions and assumptions (section 2.5), the same tensile member model is applicable. From figure 3.36, which compares the numerically calculated steel stress development due to imposed loading and imposed deformations, some important findings can be observed.

First of all, it can be seen that there is a significant difference in the steel stress and its growth when cracking occurs due to imposed loads or under imposed deformations. The most remarkable difference lies in the fact that under imposed loading the cracking load at the formation of each crack increases while under imposed deformations it decreases as the process of crack formation goes on. One of the main reasons for this is that when cracks are formed due to imposed deformations the degree of restraint decreases. The lower the degree of restraint the more imposed strain disappears. The decrease in the peak values is proportional to the stiffness of the reinforcement. It can be seen that the load-displacement curve for the imposed loading case is in good agreement with the analytical curve. In appendix E the analytical calculations regarding the cracking load, the cracking strain and the crack spacing have been elaborated in more detail.

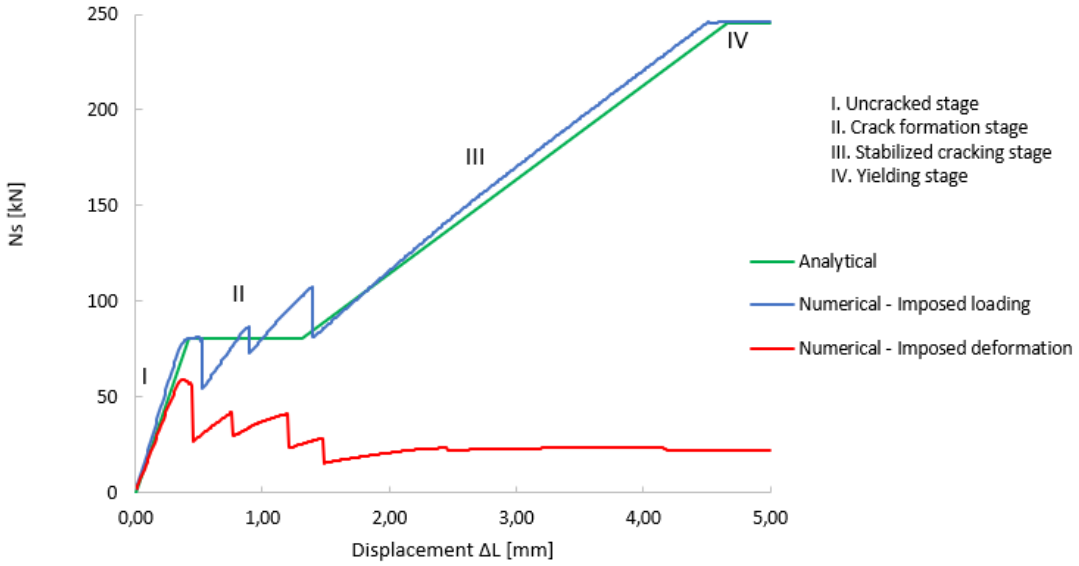

Figure 3.36: Load - deformation diagram under imposed loading or imposed deformation

In figure 3.37 an overview of the numerically calculated results is presented. In case that the tensile member was subjected to an imposed load eight cracks developed. While, in case the imposed deformation was applied, nine cracks developed. Consequently, it can be observed that the mean crack spacing due to the imposed load was slightly larger than under an imposed deformation. However, from this specific numerical analysis, it turned out that the maximum crack spacing is smaller in the imposed loading model in comparison to the imposed deformation model. In addition, the magnitude of the maximum crack width at the end of the stabilized cracking stage due to imposed loading is smaller than under imposed deformation, respectively 2,5 and 2,9 mm.

			Imposed loading	**Imposed deformation**
Number of cracks	n_{cracks}	[-]	8	9
Mean crack spacing	$s_{r,mean}$	[mm]	222	200
Maximum crack spacing	$s_{r,max}$	[mm]	240	270
Maximum crack width **end of Stabilized Cracking Stage**	w_{max}	[mm]	2.5	2.9

Figure 3.37: Comparison numerically calculated results imposed loading versus imposed deformation stabilized cracking stage

3.6. Conclusion

From this finite element analyses it can be concluded that there is a difference between the steel stress development of imposed loading and imposed deformations. This steel stress development is also confirmed by previous NLFEA research conducted by Camara and Luis [8]. The reason for this is that when cracks are formed due to imposed deformations the degree of restraint decreases. The lower the degree of restraint the more imposed strain disappears which results in a reduction of the stress development. In addition, a difference was observed between the maximum crack width of reinforced concrete tensile members subjected to imposed loading and imposed deformations. According to the numerical analyses, imposed loading resulted in fewer cracks, but the maximum crack spacing was smaller, so the corresponding maximum crack width was also smaller. This result confirms the assumption mentioned earlier by Van Breugel and the Model Code, that cracking due to imposed deformations, causes bond degradation and could result in an increase of the maximum crack width.

It should be taken into account that in the numerical models and analytical approach a very large shrinkage strain of $-2 \cdot 10^{-3}$ is applied. According to multiple crack width prediction models such as the Eurocode 2 and the Model Code 2010, the magnitude of this imposed deformation does almost never occur in regular concrete. When looking at more common quantities of imposed deformations, these results confirm that imposed deformations will almost never result in a fully developed crack pattern, or in other words, will almost never reach the stabilized cracking stage.

However, nowadays many new concrete types are being developed, such as for example geopolymers or strain-hardening cementitious composites (SHCC). These species have a much higher magnitude of shrinkage and therefore it may happen more often in the future that imposed deformations cause fully developed crack patterns.

4

Case study: numerical prediction of early age cracking due to hardening of concrete

In this chapter, first the methodology and main findings of the experimental work, carried out during a Ph.D.thesis by M. Sule are highlighted. [16]. Thereafter, a FEA is performed to simulate the hardening process of concrete in combination with autogenous shrinkage as imposed deformations. Finally, the experimental results are used to verify the accuracy of the input parameters of FEA.

4.1. Experimental work by M. Sule

4.1.1. Introduction

This experimental work performed by M. Sule [21] during her PhD, consisted of several reinforced concrete tensile members that were subjected to restrained early-age deformations. The tests were carried out to measure only the thermal and autogenous deformations, therefore the experiments were performed in a laboratory on sealed concrete specimens. Since drying shrinkage plays hardly a role for through-cracking in early-age concrete this is not taken into account. For the determination of the stress development due to restrained early-age deformations the development of the concrete properties has to be known. In all experiments the concrete quality was determined by monitoring the compressive cube strength. In addition, pull-out tests were performed to get more information about the bond strength. Last but not least a Temperature Stress Testing Machine (TSTM) was used to obtain the stress development and the moment of cracking of the reinforced concrete tensile members. In figure 4.1 the experimental test set-up is schematically shown.

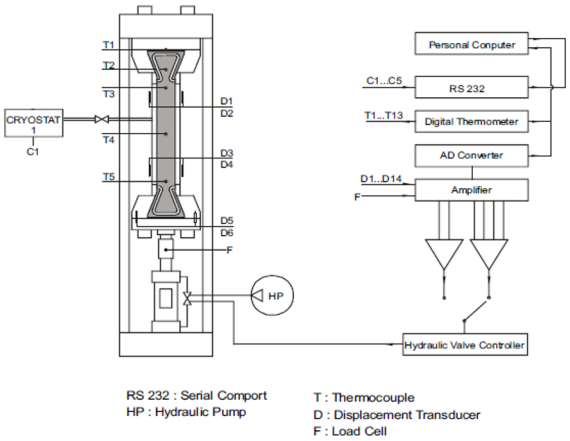

Figure 4.1: Schematic diagram of experimental setup (Sule, 2003)

4.1.2. Geometry and reinforcement arrangement

Figure 4.2 shows an overview of the experiments performed in the TSTM. The concrete cross-sections were 150 x 100 mm^2 due to the limited load capacity of the TSTM. If one reinforcement bar was applied it was located in the centre of the member and if 4 reinforcement bars were applied they were placed in the corners with a concrete cover of 20 mm.

Member notation	Concrete composition	Cross-section [mm^2]	Reinforcement configuration	Reinforcement ratio [%]
TBM-1	HSC	150x100	-	-
TBM-2	HSC	150x100	1ø12	0.76
TBM-3	HSC	150x100	4ø6	0.76
TBM-4	HSC	150x100	1ø16	1.36
TBM-5	HSC	150x100	4ø8	1.36
TBM-6	HSC	150x100	1ø25	3.38
TBM-7	HSC	150x100	4ø12	3.11

Figure 4.2: List of experiments performed in the TSTM (Sule, 2003)

4.1.3. Material properties

4.1.3.1 Concrete properties

In the experiments high strength concrete (HSC) was used. The main differences between normal strength concrete and high strength concrete is the water-cement ratio and the type of cement used. In addition, in practice, superplasticizers were added to HSC. The exact composition of the concrete mixture was as follows:

- 125.4 kg/m^3 water;
- 237.0 kg/m^3 CEM III/B 42.5 LH HS;
- 238.0 kg/m^3 CEM I 52.5 R;
- 50.0 kg/m^3 Slurry micro silica (50/50);
- 1.0 kg/m^3 Superplasticizer BV1 (based on lignosulfanate)
- 9.5 kg/m^3 Superplasticizer FM951 (base on naftaleensulfanate)
- 973.5 kg/m^3 Gravel 4 - 16 mm
- 796.5 kg/m^3 Sand 0 - 4 mm

4.1.3.2 Reinforcement properties

The reinforcement in the experiments was made of hot rolled ribbed steel quality FeB 500. In the research laboratory of Stuttgart the mechanical characteristics were determined. The characteristics are given in figure 4.3 depending on the bar diameter.

Bar diameter $ø_s$ [mm]	Yield strength f_y [MPa]	Ultimate strength f_t [MPa]	Elongation at maximum stress ε_u [%]	Projected rib area f_R [-]
6	557	596	10.4	0.040
8	562	632	20.5	0.076
12	547	672	17.4	0.084
16	568	626	18.0	0.086
25	570	678	15.7	0.066

Figure 4.3: Reinforcement properties (Sule, 2003)

4.1.3.3 Curing temperature

All specimens were cured under the same conditions: semi-adiabatic or isothermal (20°C, 30°C, 40°C). In addition, all specimens were cast in controlled moulds in order to obtain the desired temperature history. The semi-adiabatic curing conditions are often referred to as “realistic” curing conditions. For this curing condition the temperature development was measured in one specimen and afterwards imposed to the other specimen. As a result, the hydration process developed in all specimens at the same rate. This ensured that the properties measured in the experiments involved the same degree of hydration. When the specimens were cast under isothermal conditions, the temperature of the specimens was directly controlled by the computer.

4.1.4. Experimental set-up

4.1.4.1 Autogenous Deformation Testing Machine (ADTM)

In this experimental research, two so called Autogenous Deformation Testing Machines (ADTM) were used. These ADTM’s can determine the load-independent deformation during hardening of the concrete. In the first ADTM test, a plain specimen without any reinforcement was tested and in the second test a reinforced specimen was tested. By using 2 linear variable differential transformers (LVDT’s) at each long side of the ADTM, the deformations were measured. The LVDT’s are electromechanical sensors used to convert mechanical motion or vibrations, into a variable electrical current, voltage or electric signals, and the reverse. From figure 4.4 it can be seen that the LVDT’s were located on the outside of the mould between two steel bars. These steel bars were embedded in concrete and passed through the holes in the mould.

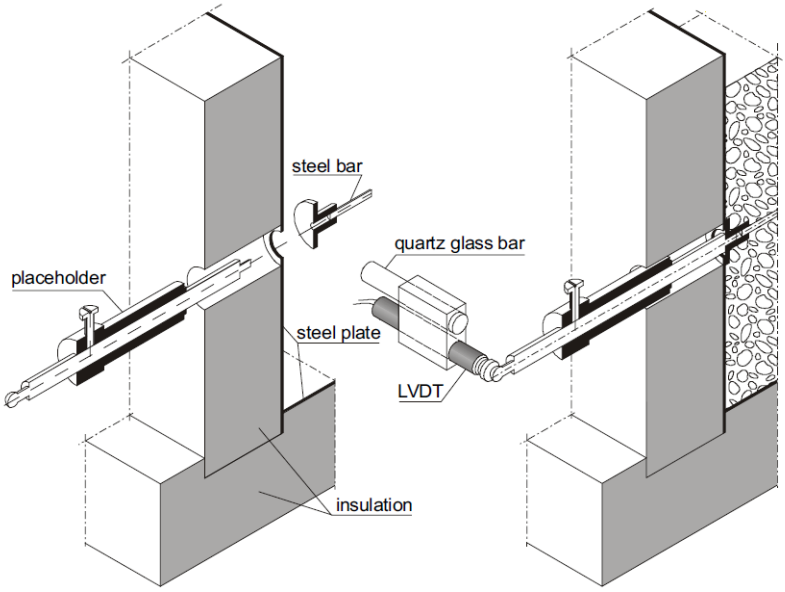

Figure 4.4: Left: installation of measuring bars and right: installation of LVDT’s after casting (Sule, 2003)

The measurements of the deformation could start as soon as the concrete had sufficient stiffness. This could take 5 till 12 hours after the concrete was mixed. The exact time depended on the concrete mixture and hardening temperature. After the mixture had sufficient stiffness, the wooden frame was loosened and the placeholders were removed. Perpendicular to the outer end of the steel bars the LVDT’s were placed . Next, the LVDT’s were attached to a quartz glass bar which was placed on top of the two supports. One of these supports was fixed and the other one was a sliding support. Because quartz glass has a very low coefficient of thermal dilatation, the length changes of the bar due to temperature fluctuations were negligible. For each side, the deformation of the concrete was determined by adding the displacements measured by two LVDT’s. The range of the LVDTs is 400 micrometer with a theoretical resolution of 0.1 micrometer. Since the deformation was measured with 2 LVDT’s per side, the resolution was 0.2 micrometer [21].

4.1.4.2 Temperature Stress Testing Machine (TSTM)

In figure 4.5 the schematic top view of a Temperature Stress Testing Machine (TSTM) is shown. This machine consists of a horizontal frame in which the concrete specimens can be loaded in tension or in compression under various hardening conditions. It is possible to perform both deformation-controlled and load-controlled experiments. Any thermal condition can be realised because of temperature controlled moulds. In this research all specimens were fully restrained.

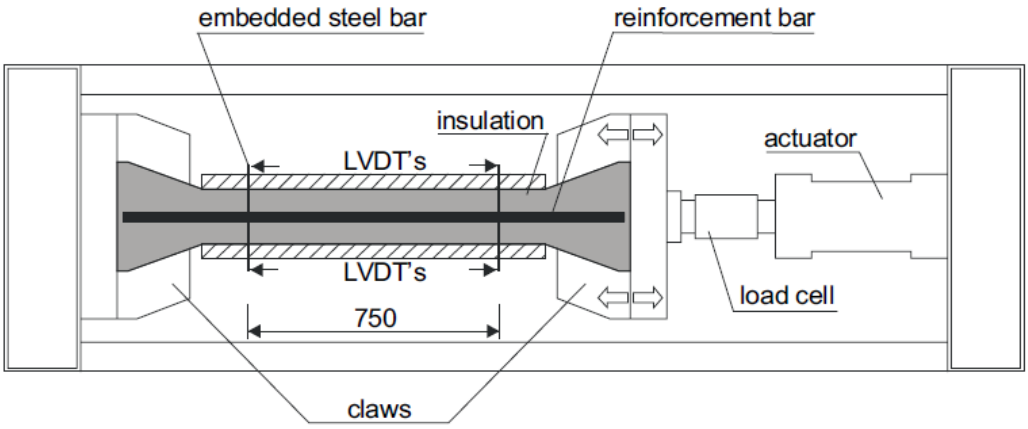

Figure 4.5: Schematic top view of a TSTM (Sule, 2003)

4.2. Finite element analysis

The geometry and concrete properties used in the finite element analysis are corresponding with the experimental results from Sule which are described in section 4.1. In case concrete properties were missing, the Guidelines for Nonlinear Finite Element Analysis for Concrete Structures from Rijkswaterstaat [19] and material characteristics from the Model Code 2010 [10] were applied.

4.2.1. Geometry and time independent concrete properties

An overview of the geometry and time independent material properties of concrete is given in figure 4.6.

		High Strength Concrete
Height [mm]	h	150
Width [mm]	b	100
Length [mm]	L	1000
Area [mm^2]	A	15000
Cement type		CEM I 52.5 R
Poisson ratio	ν	0.2
Mass density [kg/m^3]	ρ	2405
Coefficient of thermal expansion [με/°C]	α_c	11.2

Figure 4.6: Geometry and concrete properties

4.2.2. Time dependent concrete properties

In DIANA, a relatively easy method for modelling time dependent concrete properties is currently not available. DIANA requires analytically determination of the time dependent concrete properties over maturity. Therefore, in the following section the analytical calculations of the numerical input parameters are explained. These input parameters are all based on the degree of hydration. A schematic representation of the degree of hydration concept is given below.

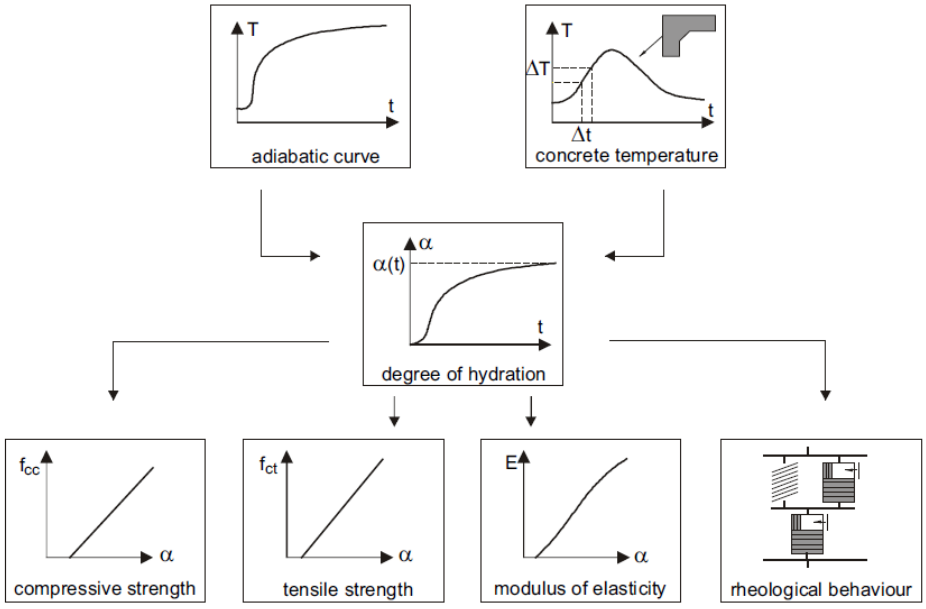

Figure 4.7: Schematic representation of the degree of hydration concept (Lokhorst, 2001)

4.2.2.1 Adiabatic curve

Due to the fact that for the experiments no information is provided regarding the adiabatic heat development, the adiabatic heat curve is determined using FEMMAS. FEMMAS is a software tool that predicts concrete behavior. The course of the curve shown in figure 4.8 depends mainly on the water-cement ratio and the type of cement.

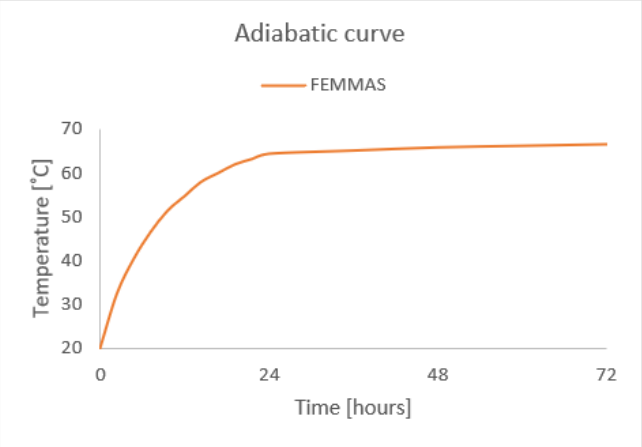

Figure 4.8: Adiabatic heat development (FEMMAS, 2021)

4.2.2.2 Concrete temperature

In figure 4.9 the characteristic semi-adiabatic temperature development measured in the experiments from Sule is shown. Due to the temperature differences in the concrete thermal deformations of the concrete specimens were generated. This temperature development was used to determine the maturity of concrete.

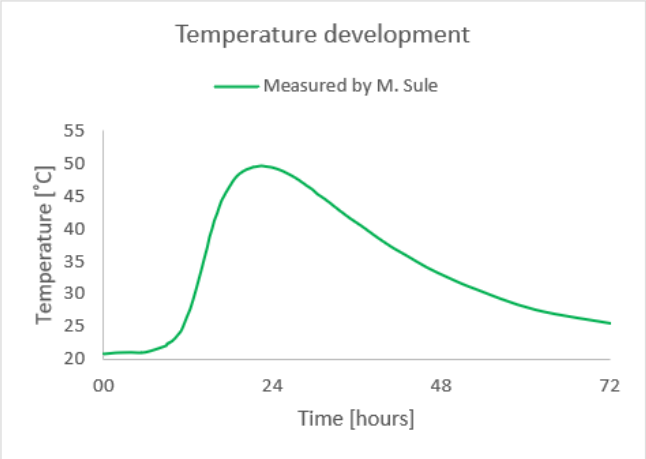

Figure 4.9: Temperature development in the tensile member measured by M. Sule (Sule, 2003)

4.2.2.3 Maturity

As mentioned before, the development of time dependent material properties in concrete can be described by the degree of hydration concept. Instead of the degree of hydration, an equivalent age is calculated which indicates the hydration state of the concrete based on the temperature history, relative to the development at a certain reference temperature. The maturity is therefore also known as the equivalent age at reference curing temperature. For this finite element analysis the maturity of concrete had to be determined, this is done by equation 4.1. This equation was developed by Arrhenius [23] and takes into account the temperature history of the concrete.

$$M(t) = \int_0^t \exp \frac{Q}{R}\left(\frac{1}{273 + T_{ref}} - \frac{1}{T(t) + 273}\right)dt \tag{4.1}$$

Where Q is the activation energy hydration. This factor takes into account the temperature sensitivity of the hydration process. In this case a value of 33.5 kJ/mol was assumed. R is the universal gas constant, 0.0083 kJ/mol K. The time dependent temperature of concrete was given by $T(t)$ and the reference temperature with T_{ref}. For the reference temperature a constant value of 20 °C was used.

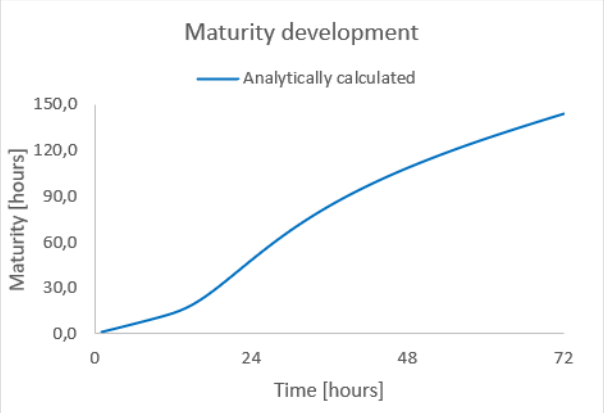

Figure 4.10: Maturity development analytically calculated using equation 4.1

4.2.2.4 Degree of hydration

For this finite element analyses the strength properties such as the young's modulus and the tensile strength of concrete were determined on the base of the degree of hydration. In figure 4.11 the degree of hydration corresponding with the experimental results is shown. In the experiment from Sule [21] the degree of hydration was calculated using the program UCON. UCON is a software tool developed by Van Beek (1995) for the determination of the degree of hydration by using the relative heat production.

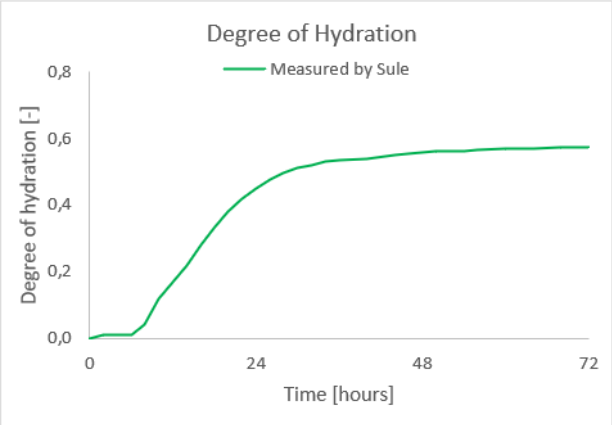

Figure 4.11: Degree of hydration development in tensile member (Sule, 2003)

4.2.2.5 Young's modulus of concrete

In the experiment from Sule, the young's modulus was estimated according to the degree of hydration concept proposed by Rostasy [20]. The equation used for the estimation is as follows:

$$E(\alpha) = E_{max} \cdot \left(\frac{\alpha - 0.1 \cdot \alpha_0}{1 - 0.1 \cdot \alpha_0}\right)^{0.5} \tag{4.2}$$

Where E_{max} is assumed to be the maximum young's modulus of elasticity of concrete (52 GPa). The degree of hydration is named α and for the critical degree of hydration (α_0) a value of 0.1 is used. In figure 4.12 the young's modulus development over time and maturity in the concrete is presented.

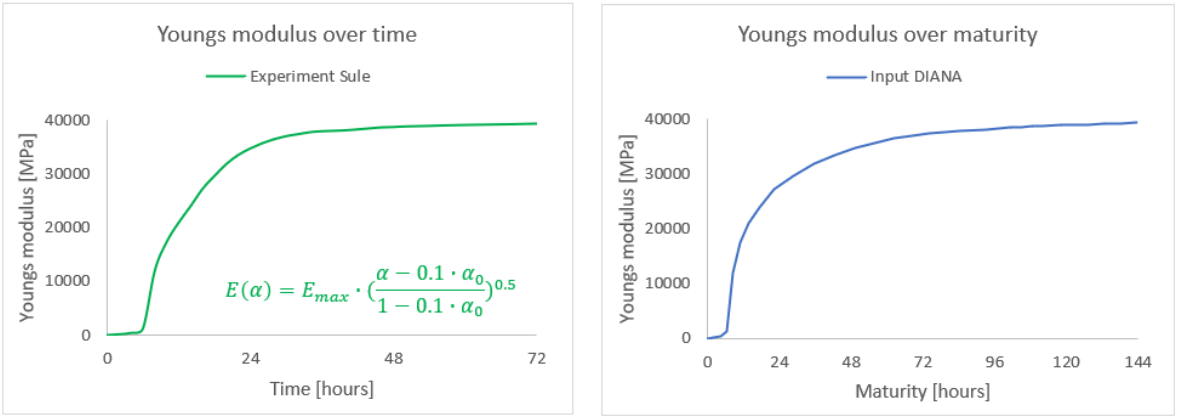

Figure 4.12: Calculated development of young's modulus from experiments (left) and the input for the finite element analysis (right)

4.2.2.6 Tensile behavior

In the experimental work from Sule, the tensile strength development was not given. Due to the fact that the development of degree of hydration α was known (figure 4.11), the tensile strength was determined on the base of equation 4.3, which was proposed by Rostasy [20].

$$f_{ct}(\alpha) = f_{ct,max} \cdot \frac{\alpha - \alpha_0}{1 - \alpha_0} \tag{4.3}$$

Where $f_{ct,max}$ is the fictitious maximum tensile strength. The critical degree of hydration is named α_0 and the degree of hydration is α. In figure 4.13 the tensile strength development versus the time and maturity are given.

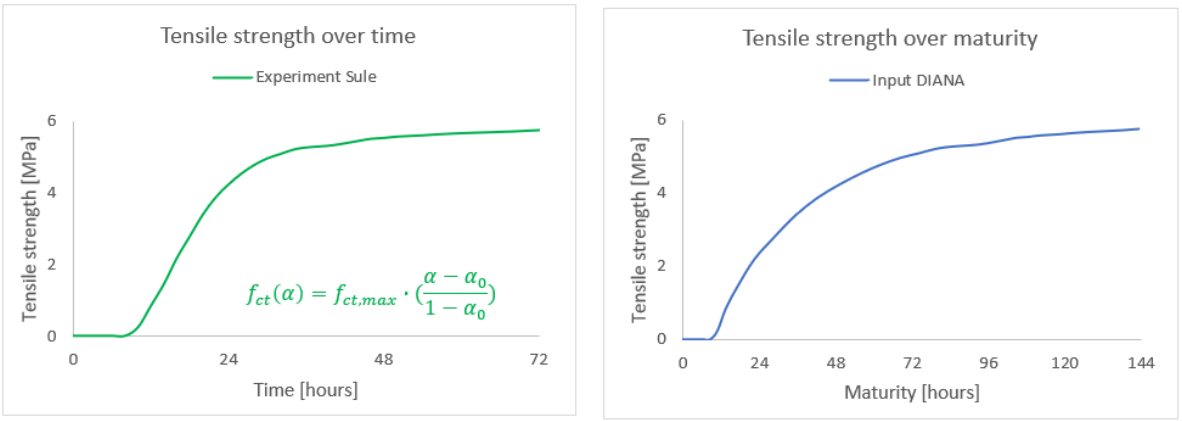

Figure 4.13: Calculated development of tensile strength from experiments (left) and the input for the finite element analysis (right)

4.2.2.7 Fracture energy

In the experiments from Sule the fracture energy was also unknown. For this reason the development of the fracture energy was estimated with equation 4.4, which was based on experiments carried out by Gutsch [11].

$$G_F(\alpha) = G_{F,max} \cdot \frac{\alpha - \alpha_0}{1 - \alpha_0}^{0.5} \tag{4.4}$$

Where $G_{F,max}$ is the fictitious maximum fracture energy in case of complete hydration. The critical degree of hydration is named α_0 and the degree of hydration is α. In figure 4.14 the fracture energy development versus the time and maturity is given.

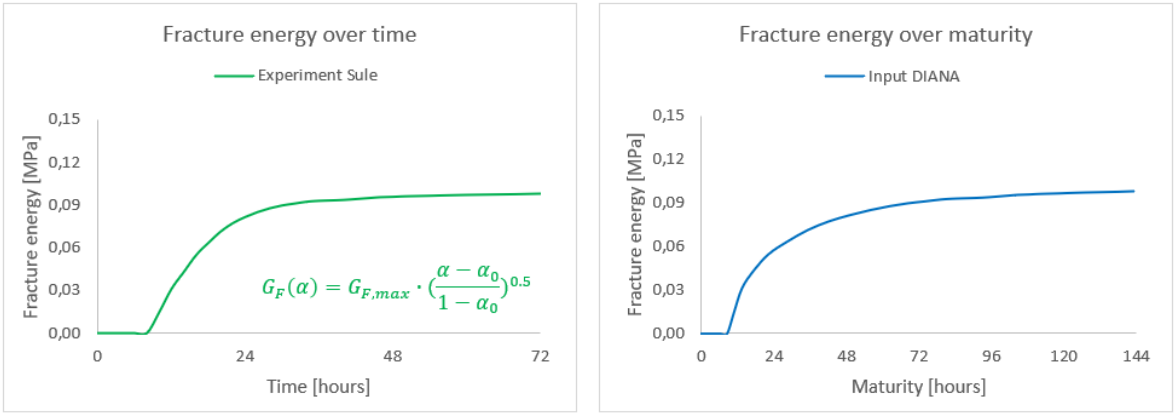

Figure 4.14: Calculated development of fracture energy from experiments (left) and the input for the finite element analysis (right)

4.2.2.8 Compressive behavior

Due to the fact that the compressive behavior, shown in figure 4.15 was not measured in the experiments from Sule, the compressive strength was estimated with equation 4.5. This equation was based on experiments and developed by Rostasy [20].

$$f_{cm}(\alpha) = f_{cm,max} \cdot \frac{\alpha - \alpha_0}{1 - \alpha_0} \tag{4.5}$$

Where $f_{cm,max}$ is the fictitious maximum compressive strength. The critical degree of hydration is named α_0 and the degree of hydration is α. In figure 4.15 the compressive strength development versus the time and maturity is given.

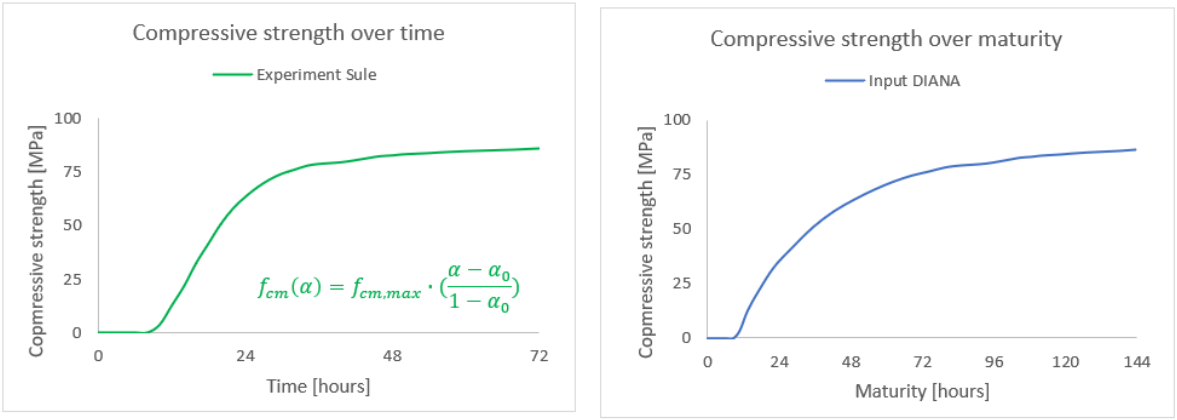

Figure 4.15: Calculated development of compressive strength from experiments (left) and the input for the finite element analysis (right)

4.2.2.9 Autogenous shrinkage

For the estimation of the autogenous shrinkage the Model Code 2010 provides the following equation:

$$\epsilon_{c,as}(t) = \beta_{as}(t) \cdot \epsilon_{c,as}(\infty) \tag{4.6}$$

Where $\epsilon_{c,as}(\infty)$ is the ultimate autogenous shrinkage and $\beta_{as}(t)$ is a function which defines the time dependent development of autogenous shrinkage. The background of this equation is described in more detail in appendix C. For this analysis a concrete class of C70/85 is applied.

However, according to Sule, the autogenous shrinkage should be calculated with equation 4.7. This equation is based on the experimental results and depends mainly on the degree of hydration.

$$\epsilon_{c,as}(\alpha) = -a \cdot (\alpha - b \cdot \frac{T(\alpha)}{20}) \tag{4.7}$$

Where a is assumed as 0.5 and depends on the type of cement. For b a constant value of 0.15 is used. In figure 4.16, the measured autogenous shrinkage (ϵ_{cas}) and the analytically estimations are shown. It can be observed that equation 4.7 gives a much better approximation than the Model Code 2010. Consequently, in the finite element models this autogenous shrinkage was applied as input in the model.

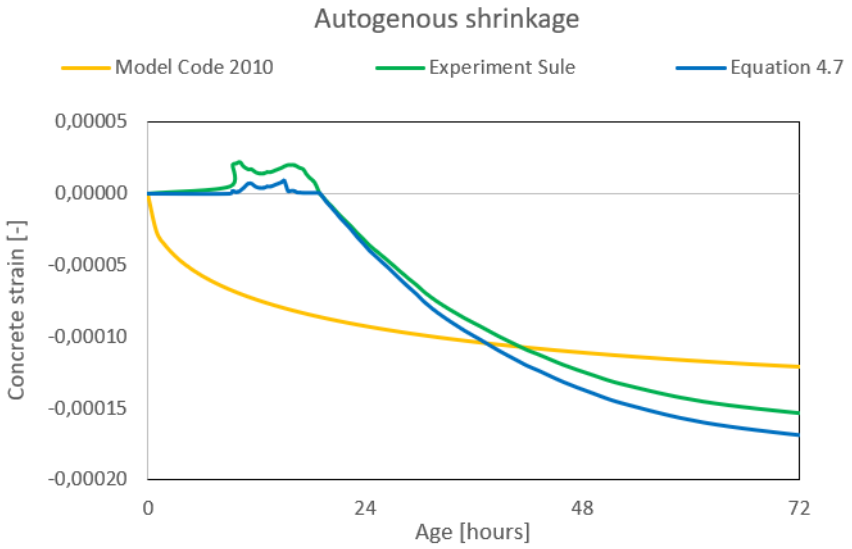

Figure 4.16: Autogenous shrinkage

4.2.3. Mesh size and element types

According to the guideline for non-linear finite element analysis (NLFEA) from Rijkswaterstaat the maximum size of a 3D model is limited by the following rule: maximum element size = $min(\frac{L}{50}; \frac{b}{6}; \frac{h}{6}) \approx 20$ mm. The applied elements in this numerical model were mainly solid isoparametric quadrilateral elements. In DIANA, this type of element is named CHX60 (figure 4.17). This element is a twenty-node isoparametric solid brick and it has three degrees of freedom. It is based on quadratic interpolation and Gauss integration.

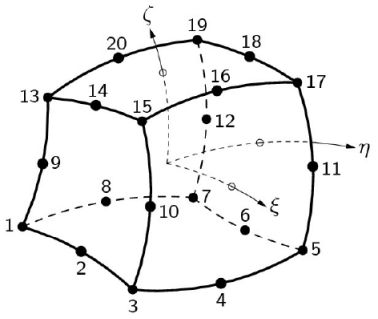

Figure 4.17: CHX60

In addition, BQ4HT elements were applied (figure 4.18). This is a four-node isoparametric quadrilateral element. This element was applied to describe boundaries in three-dimensional general potential flow analysis. It is based on linear interpolation and Gauss integration.

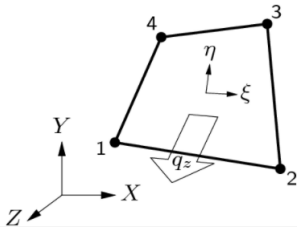

Figure 4.18: BQ4HT

4.2.4. Modelling approach

For the finite element analysis a staggered thermo-structural analysis was performed. This analysis type should, according to DIANA FEA, result in a good approximation of the concrete strains and stresses to simulate the cracking at early age due to hardening of concrete in combination with autogenous shrinkage. In this analysis the following aspects were considered:

- 3D plain concrete tensile member which is fully restrained at both ends.
- Interface boundary elements were used to model convection. Due to different phases (with and without formwork) two time dependent interfaces were considered.
- As part of the heat flow analysis, an adiabatic heat curve was specified to simulate the hardening of concrete.
- The external temperature was assumed equal to 20 °C.
- The initial temperature of the concrete was set equal to 20 °C.
- A transient staggered thermo-structural analysis was performed in order to investigate the hydration (i.e. degree of reaction and equivalent age), temperature variation in time, concrete strains and stresses and the formation of cracks in the concrete.

4.2.5. Analysis set up

For the staggered thermo-structural analysis, all iterations were done with a full Newton-Raphson, meaning the stiffness matrix is updated with each iteration. The load steps and different values for the convergence criteria are given in the following section.

4.2.5.1 Transient heat analysis

The temperature development and hydration process in the young concrete were studied with a transient nonlinear heat flow analysis. In this analysis, 72 load steps of one hour were executed and a convergence tolerance (recommended by the RTD [19]) of 1e-06 was applied.

Time steps [hours]	Method	Type	Max number of iterations	First tangent	Convergence criteria	Convergence tolerance
1(72)	Newton-Raphson	Regular	25	N.A.	N.A.	1e-06

Figure 4.19: Analysis set-up transient heat

4.2.5.2 Non-linear structural analysis

Thereafter, a non-linear structural analysis was performed to study the strain and stress developments. It was often difficult to reach convergence for this type of analysis because of the formation of dominant cracks. In case that a concrete tensile member cracks, this leads to the loss of energy within the structure. For this reason it was difficult for the program to find an equilibrium.

Regarding the equilibrium iteration, the maximum number of iterations is set to 500 and the convergence criterion are chosen according to the RTD [19], which states that both energy and force norms should be satisfied within a tolerance of 0.0001 and 0.01 respectively. The chosen tolerances are presented in figure 4.20.

Time steps [hours]	Method	Type	Max number of iterations	First tangent	Convergence criteria	Convergence tolerance
1(72)	Newton-Raphson	Regular	500	Tangential	Energy	1e-04
					Force	1e-02

Figure 4.20: Analysis set-up non-linear structural

4.3. Results finite element analysis

In this section the finite element results are presented and verified using the experimental work from Sule [21]. The specimen that was used for the verification was semi-adiabatically cured. Under semi-adiabatic curing stresses develop due to autogenous shrinkage and thermal effects. In the experiments from Sule, moulds were applied that were fully temperature controlled. While in the finite element analysis the temperature development was modelled using boundary interfaces. Consequently, the temperature development in the finite element analysis depended mainly on the convection coefficients and the adiabatic heat curve. For the verification, first of all, the temperature development was examined. Second, the maturity was verified. Finally, the results from the structural non-linear analysis were given and compared with the analytically calculations and the experimental results.

4.3.1. Temperature development

Figure 4.21 shows the temperature development which generates thermal deformations of the concrete tensile bar members. It can be seen that in the experiment the starting temperature was about 20°C. Due to hydration the temperature rose until it reached about 50°C after 22 hours. Afterwards it dropped until it reached again 25°C after about 72 hours. A difference can be observed between the temperature development in the experiments and in the finite element model. In the experiments the maximum temperature is 50°C while according to the finite element model it is 53°C. In addition, it can be seen that in the finite element model the maximum peak hydration temperature is reached after 24 hours while in the experiments it is after 21 hours.

Although it should be taken into account that these differences may have consequences for the subsequent results, they were now considered as acceptable. In Appendix G, an attempt was made to optimize the temperature development by increasing the convection coefficient. However, the adjustments (G.1) did not result in a more realistic temperature development. Consequently, it can be concluded that the difference was caused by the adiabatic temperature development. As mentioned before in section 2.5.2.1, the adiabatic temperature development was unknown. Using a software tool called FEMMAS a development that is as realistic as possible was used.

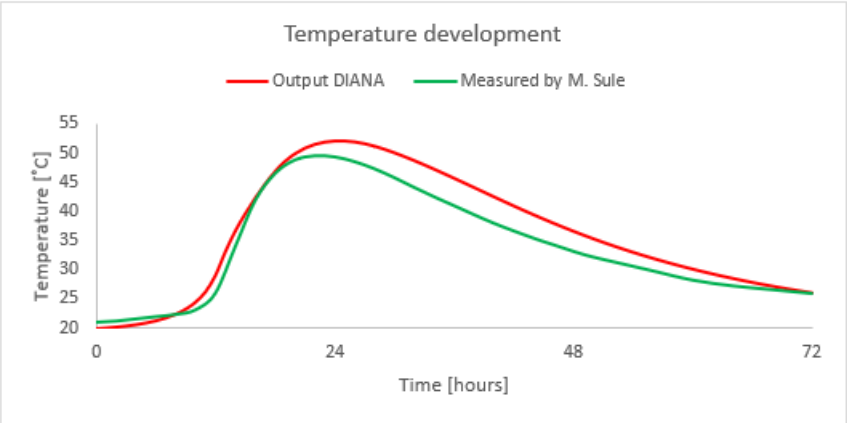

Figure 4.21: Verification temperature development

4.3.2. Maturity development

According to the DIANA FEA manual, for the determination of the maturity of concrete the following expression is applied:

$$t_{eq} = \int_0^t \exp\left(c_A\left(\frac{1}{T_{ref}} - \frac{1}{T(t)}\right)\right)dt \tag{4.8}$$

Where c_A is the Arrhenius constant and T_{ref} is the reference temperature (T_{ref} = 293 K). In DIANA it is possible to specify the Arrhenius constant as a fixed value or as a value which depends on temperature and/or degree of hydration.

From figure 4.22 it can be observed that the maturity in the finite element model is based on the exact same Arrhenius function as is given and described earlier in section 5.2.2.3 (equation 4.1). It turned out that the assumptions in the analytical calculation regarding the activation energy hydration and the universal gas constant were correct.

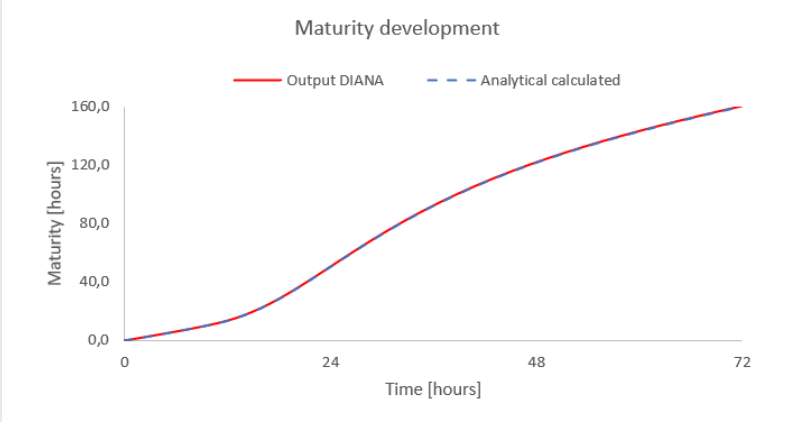

Figure 4.22: Maturity development

4.3.3. Verification concrete strain development

During the hardening process of concrete, the cementitious materials undergo various deformations. These deformations ϵ_{cs} are load independent. Due to the fact that concrete specimens in the experiments were sealed, no drying shrinkage was taken into account. Consequently, the load independent deformations can be divided into thermal deformations ϵ_{cT} caused by the hydration heat and autogenous shrinkage ϵ_{cas}. The concrete strains due to thermal deformation ϵ_{cT} were estimated analytically with the following expression:

$$\epsilon_{cT} = \Delta T(t) \cdot \alpha_{cT}(t) \tag{4.9}$$

Where ΔT is the temperature development in the concrete and α_{cT} is the coefficient of thermal expansion. Depending on the type of cement, the heat of hydration develops and the temperature in the material rises, causing an expansion. After the concrete has reached the maximum temperature it cools down which causes contraction. In figure 4.23 the concrete strains due to thermal deformation are presented. It can be seen that the analytically calculated concrete strain corresponds exactly with the results from the finite element model. In this case no experimental results were available to verify the strain caused by thermal effects only.

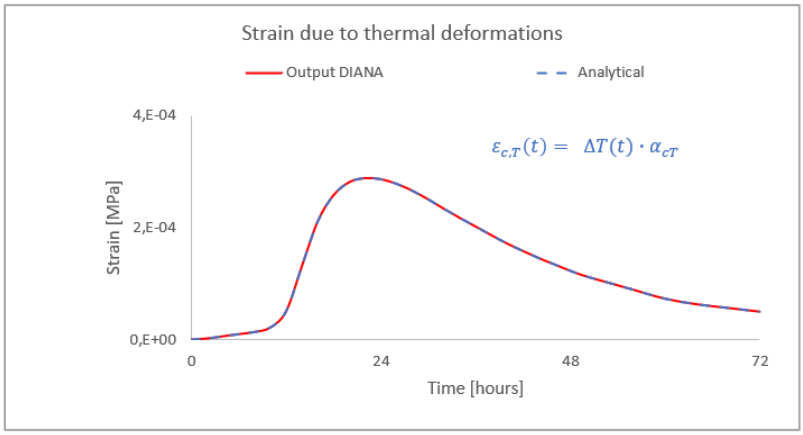

Figure 4.23: Concrete strain due to thermal deformation

4.3.4. Verification concrete stress development (without visco-elastic effects)

The total concrete stress due to the thermal deformations σ_{cT} and autogenous shrinkage σ_{cas} can be estimated analytically by the following expression:

$$\sigma_{c,total} = \sum \sigma_{cT}(t) + \sigma_{cas}(t) \tag{4.10}$$

In figure 4.24 the total concrete stress development is presented. Earlier in figure 4.23 it was shown that in the beginning the temperature rise in the specimen caused thermal expansion. Because this thermal expansion was restrained compressive stresses were generated. These compressive stresses decrease as soon as the maximum temperature was reached. Due to the development of the modulus of elasticity, compressive stresses turn into tensile stresses before the initial temperature is reached. In addition, in this case autogenous deformations also contribute to the development of the tensile stresses in the concrete cross section. The tensile stress in the concrete will increase until the crack criterion was reached.

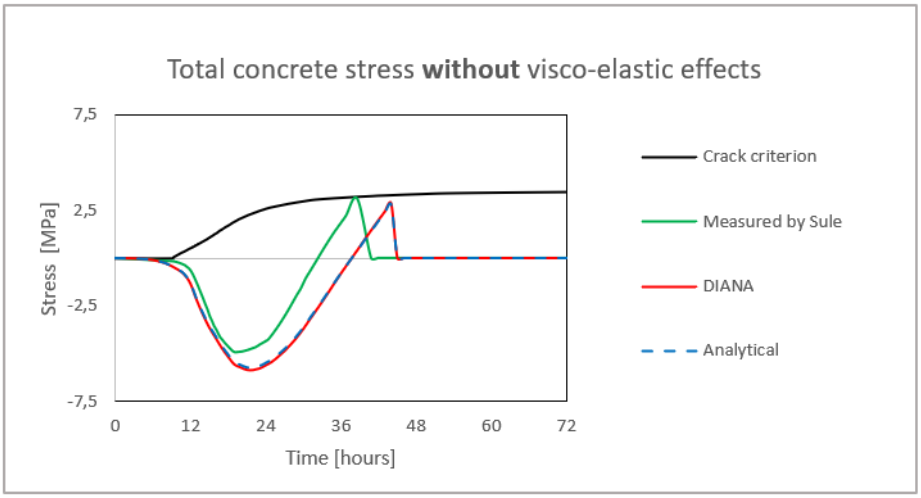

Figure 4.24: Total concrete stress without visco-elastic effects

Figure 4.24 shows that the analytically and numerically determined total concrete stresses are corresponding well. Comparing these calculated total concrete stresses with the concrete stress measured by Sule, a difference can be observed. According to the measurement from Sule, the maximum compressive stresses are approximately 15% smaller than in the analytical and numerical calculations. In addition, regarding the moment of the formation of the first crack, it can be seen that in the in the experiments the first crack already developed after 38 hours, while according to the calculations, this happens after 44 hours.

These differences can be explained by two reasons. First of all, previous results (figure 4.21) have shown that there was a difference between the temperature development in the experiments and the finite element model. Due to the fact that in the experiments the concrete cooled down faster, consequently, the tensile stresses arose earlier and therefore the first cracks developed faster.

Secondly, it has to be taken into account that the visco-elastic behavior such as creep and relaxation is not considered. The visco-elastic effect would reduce the compressive stresses and to a lesser extent the tensile stress development. However, fitting the visco-elastic effects into the finite element model of DIANA is rather complex. Therefore, in the next section an attempt is made to apply a reduction factor to take into account the visco-elastic effects in the analytical calculations.

4.3.5. Modified stress reduction due to creep and relaxation (Lokhorst)

Concrete as a material is subjected to two kinds of visco-elastic effects. The increase in deformation over time under a constant load is defined as **creep** and the decrease in stress over time under a constant deformation is known as **relaxation**. In all types of concrete, creep and relaxation occur.

Nowadays, different models have been applied for calculating the influence of creep and relaxation on the stress development. Most of them are based on experimental data. Due to the fact that most calculation procedures were not practical due to its high computational demands, Lokhorst [13] proposed a fast and simple approach for estimating early-age stress development. The approach is based on the instantaneous reduction of elastic stress increments with so-called stress reduction factors s_h. This reduction factor depends on the degree of hydration and the composition of the concrete.

In the Bar model of Lokhorst (left figure 4.25) a water-cement ratio of 0.5 was assumed. In the experiments from Sule which are used for the verification a water cement ratio of 0.33 was used. Therefore, the Bar model must be modified. In order to determine the stress reduction factors that give the best results, multiple assumptions were made. At the right of figure 4.25, the three different reduction factors are presented.

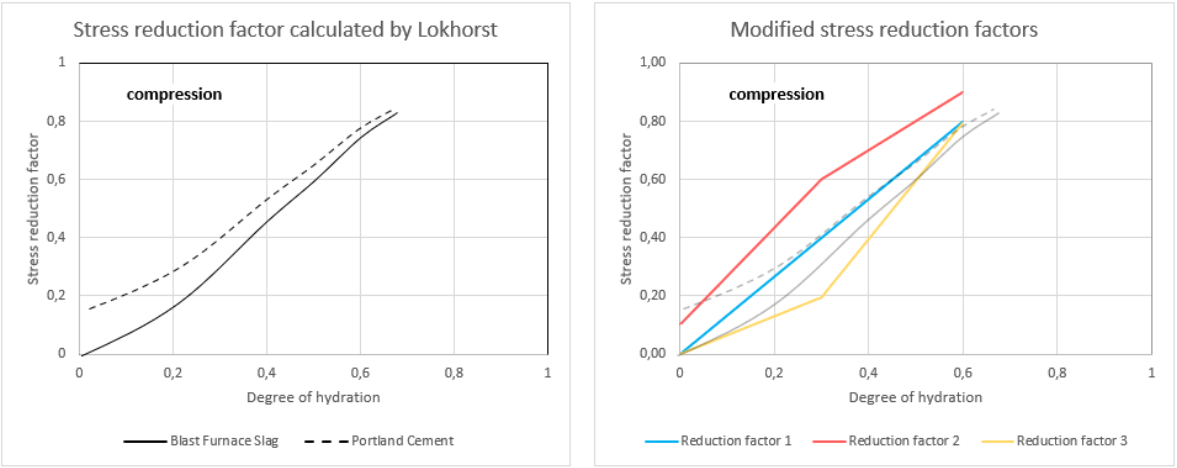

Figure 4.25: Stress reduction factor for w/c ratio = 0.5 (left) and for w/c ratio = 0.33 (right). [21]

The following equations were used when the concrete specimen was under **compression**:

If $0 < \alpha < 0.3$:

For reduction factor 1

$$s_h(\alpha) = \frac{8}{3} \cdot \alpha \tag{4.11}$$

For reduction factor 2

$$s_h(\alpha) = 0.1 + \frac{5}{3} \cdot \alpha \tag{4.12}$$

For reduction factor 3

$$s_h(\alpha) = 0.65 \cdot \alpha \tag{4.13}$$

If $\alpha > 0.3$:

For reduction factor 1

$$s_h(\alpha) = 0.2 + \alpha \tag{4.14}$$

For reduction factor 2

$$s_h(\alpha) = 0.3 + \alpha \tag{4.15}$$

For reduction factor 3

$$s_h(\alpha) = 2 \cdot \alpha - 0.405 \tag{4.16}$$

In figure 4.26 the stress reduction factors according to Lokhorst [13] and the relation used in case that the specimen is in tension for a water cement ratio of 0.33 are given.

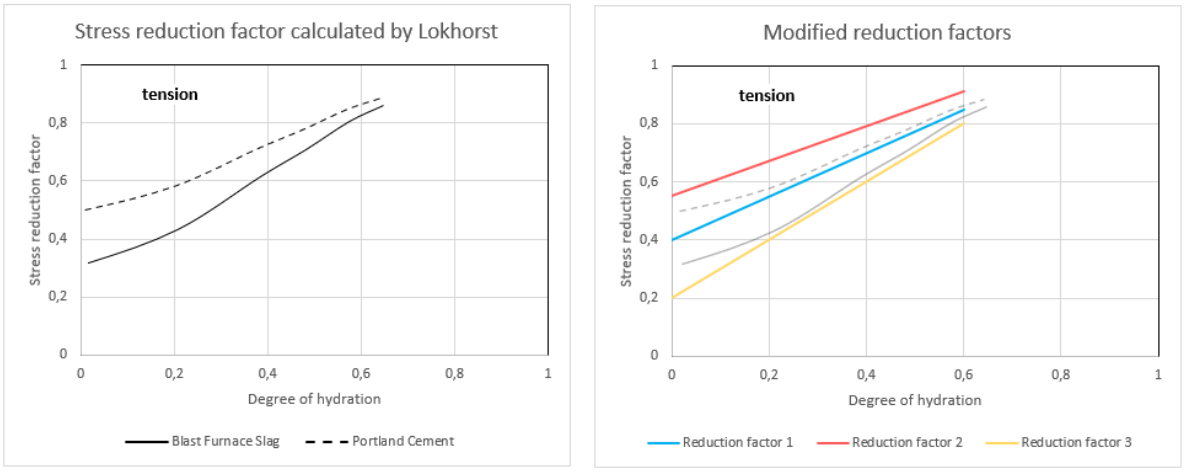

Figure 4.26: Stress reduction factor for w/c ratio = 0.5 (left) and for w/c ratio = 0.33 (right). [21]

In case that the specimen is under **tension**, the following equations were used:

If $0 < \alpha < 0.6$:

For reduction factor 1

$$s_h(\alpha) = 0.4 + 0.75 \cdot \alpha \tag{4.17}$$

For reduction factor 2

$$s_h(\alpha) = 0.55 + 0.6 \cdot \alpha \tag{4.18}$$

For reduction factor 3

$$s_h(\alpha) = 0.2 + \alpha \tag{4.19}$$

4.3.6. Verification concrete stress development (with visco-elastic effects)

Taking into account the above mentioned reduction factors s_h the concrete stress can be calculated with the following equation:

$$\sigma_{c,total} = \sum (\sigma_{cT}(t) + \sigma_{cas}(t)) \cdot s_h(\alpha) \tag{4.20}$$

In figure 4.27 the total concrete stress developments including visco-elastic effects such as creep and relaxation are presented. It can be seen that the best results were obtained by applying the reduction factor 2. That this reduction factor 2 gives the best approximation can be explained by the fact that when the water cement ratio decreases, there is less early age relaxation so the reduction factor increases.

It can be seen that in the first 24 hours, the magnitude of the compressive stresses is about the same in the analytical calculation with reduction factor 2 as in the measurements from Sule [21]. In addition, with regard to the moment of the formation of the first crack, in all cases still a difference was observed. In the experiments the first crack already developed after 38 hours, while according to the calculations, this happens after 44 hours. The reason for this has been stated before and is most likely due to the fact that the temperature drops earlier in the experiment than in the calculations.

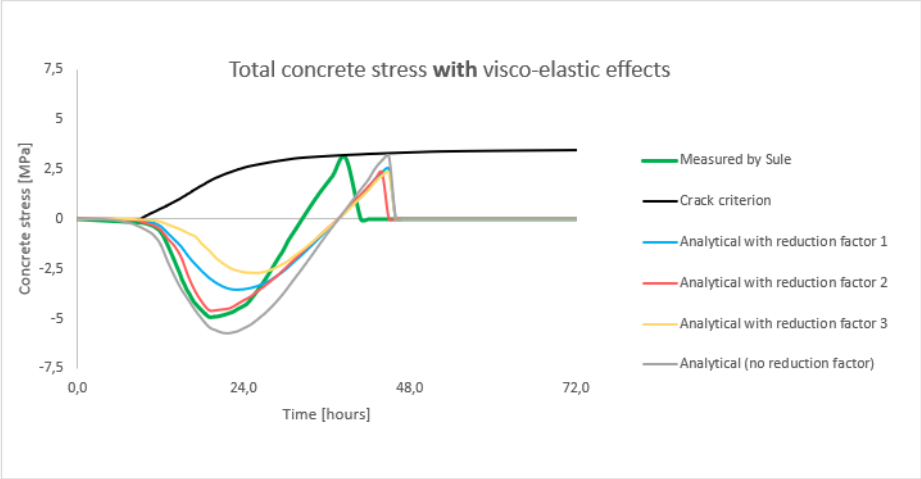

Figure 4.27: Total concrete stress with visco-elastic effects

4.4. Conclusion

Overall, when performing a non-linear finite element analysis for the simulation of the hardening process of concrete in combination with autogenous shrinkage a lot of knowledge was required. It turned out that the analyst's specific choices such as the constitutive model type, the kinematic and equilibrium condition have a major impact on the outcome of the analysis.

Furthermore, it turned out that it was essential to determine the time dependent material properties very accurately. A small difference in the development of for example the elastic modulus of concrete would cause a significant difference in the stress development. In addition, the temperature development was of great importance. In the experiments the concrete cooled down faster than in the numerical analysis. Consequently, the tensile stresses arose earlier and therefore the first cracks developed faster.

In addition, to perform a more adequate calculation the visco-elastic effects should be taken into account. Fitting the visco-elastic effects into the finite element model of DIANA is rather complex therefore an analytical approach was applied. It turned out that using the modified Bar model of Lokhorst in combination with the numerical approach was in close agreement with the experimental findings.

5

Parameter study

This parameter study is carried out to determine which parameters influence the crack width the most. The maximal characteristic crack widths and corresponding parameters are processed in spreadsheet models in Excel. In Appendix A an overview of the different prediction models and corresponding formulas is given. The spreadsheets are given in Appendix B and these models will also contribute to the comparison between the analytical and the numerical models.

5.1. Input parameters

To determine the most important parameters, the impact of the various input parameters is investigated. In order to do this, initial values are defined. For this analysis a concrete tensile member is used with a single eccentrically placed reinforcement bar. In all prediction models one parameter is changed within a range of +/- 20% from the initial value while the values of the other parameters are kept constant. In the results of the parameter study the influence of each parameter will be quantified and the different models are compared. The parameters and initial values used for the analysis are:

Concrete cube strength	f_{ck}	=	30	MPa
Height	h	=	200	mm
Width	b	=	200	mm
Length	L	=	2000	mm
Bar diameter	∅	=	20	mm
Concrete cover	c	=	80	mm
Degree of restraint	R	=	0,5	
Early age of cracking	t_0	=	3	days
Long term age of cracking	t	=	28	days
Temperature drop	T_1	=	40	°C
Long term temperature change	T_2	=	20	°C

For some parameters it may be not realistic that the deviations are in the range of -20% to $+20\%$ of the initial values. However, the aim of the parameter study is only to compare the influence of the different input parameters on the crack width. Therefore, it is more important to use the same range instead of applying realistic deviations. The coefficients for the design codes were determined using the following quite conservative assumptions. The influence of these assumptions is discussed in more detail in chapter 6.

Cement type	=	Normal cement
Load duration	=	Long term loading
Bond properties	=	Smooth bars
Strain distribution	=	Tension

5.2. Results with varying input parameters

In this section the results from the parameter study are presented and discussed. A distinction is made between end restrained tension bar models (TBM's) and continuous base restrained models (CM's). It is important to note, that in the CIRIA (I) a similar method is applied as in the EN 1992-3 (I), therefore the CIRIA (I) is not shown in the results. For the non-linear finite element analysis (NLFEA) the modelling choices described in chapter 3 are applied.

5.2.1. Concrete cube strength

5.2.1.1 Tension bar models

First of all, the influence of the concrete cube strength on the crack width is considered. In figures 5.1 and 5.2 , it is shown that according to all end restrained tension bar models, an increase in the concrete cube strength also results in an increase in the crack width. This can be explained by the fact that an increase in the concrete cube strength results in a increase in the concrete tensile strength, which means that the crack strain increases. The larger the crack strain the larger the crack width.

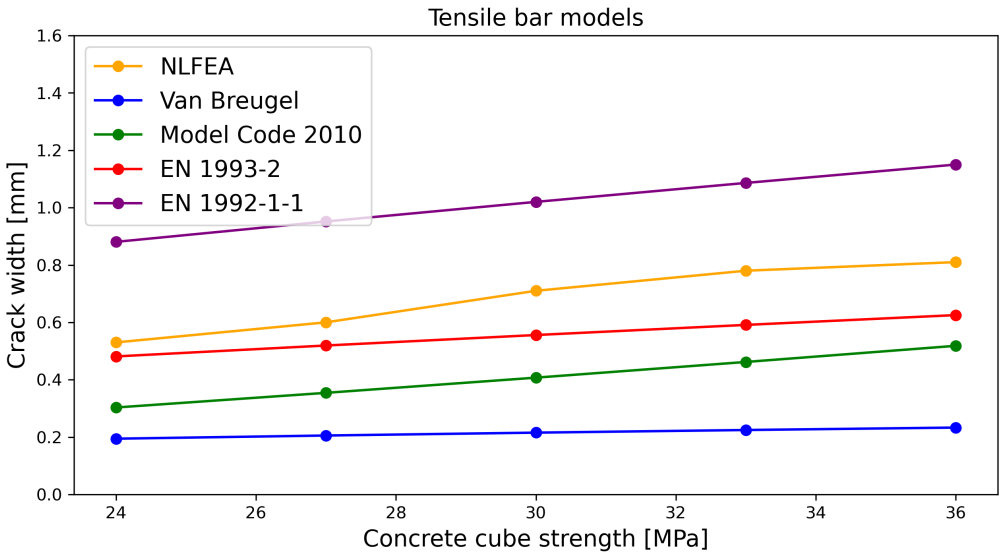

Figure 5.1: Concrete cube strength versus crack width according to tensile bar models

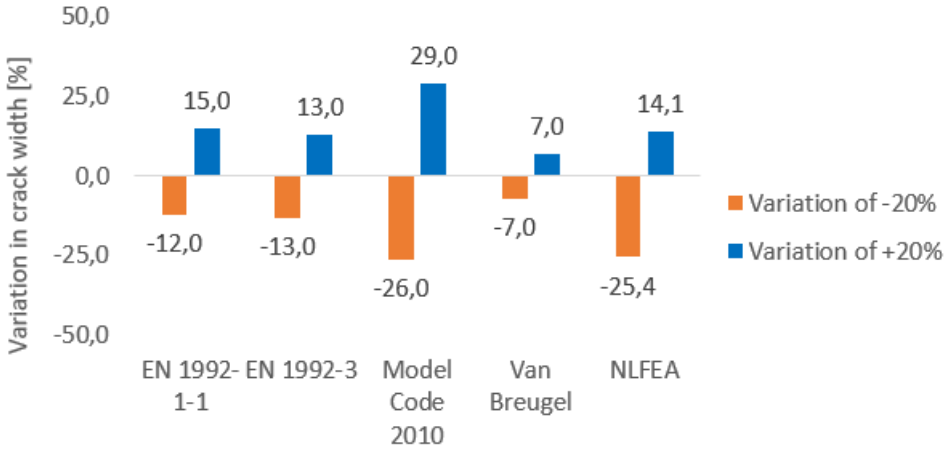

Figure 5.2: Bar chart of the influence of concrete cube strength according to tensile bar models

5.2.1.2 Continuous restraining models

In figures 5.3 and 5.4 the results of the continuous base restrained models are presented. It can be seen that an increase in the concrete cube strength has almost no effect on the crack width. This is because these models take into account two factors that have a contradicting effect on the crack width. First, an increase in concrete cube strength results in an increase in concrete tensile strength, which increases the crack strain. Second, the continuous restraining models take into account that an increase in the concrete strength causes a decrease of the total shrinkage strain. Which means that the autogenous and drying shrinkage are less. The lower the shrinkage strain the smaller the crack width. From figure 5.4 it can be observed that the shrinkage is governing and therefore an increase in the concrete cube strength results in a small decrease in crack width.

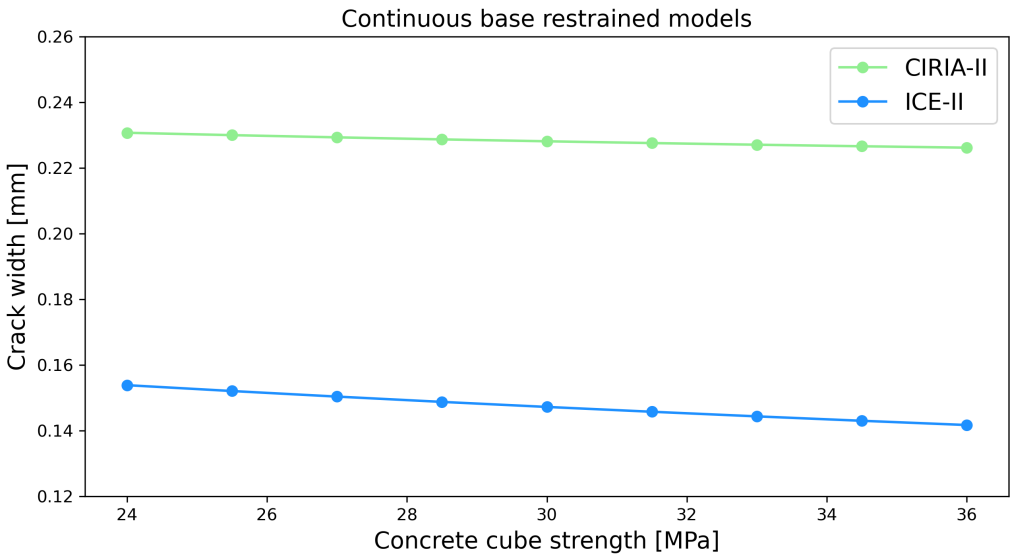

Figure 5.3: Concrete cube strength versus crack width according to continuous base restrained models

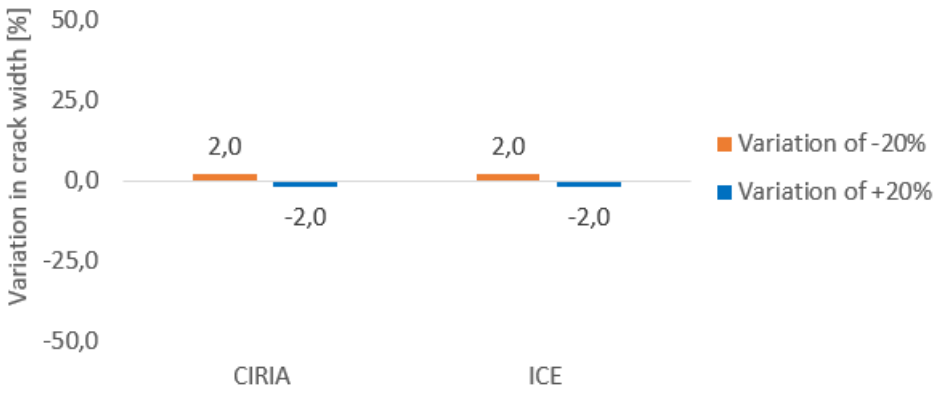

Figure 5.4: Bar chart of the influence of concrete cube strength according to continuous base restrained models

5.2.2. Height

5.2.2.1 Tension bar models

From figures 5.5 and 5.6 it can be seen that the influence of the height h on the crack width w_k is significant. According to all prediction models, an increase in height causes a larger crack width. All models state that in case of full tension, an increase in height results in a larger effective tension area $A_{c,eff}$. Consequently, the reinforcement ratio ρ_s decreases, which causes an increase of the transfer length l_t as shown by equation 5.2. From equation 5.1 it can be seen that with the increase of the transfer length, the crack width will increase proportionally.

$$w_k = l_t \cdot (\epsilon_{sm} - \epsilon_{cm}), \tag{5.1}$$

$$l_t = \frac{1}{4} \frac{f_{ctm}}{\tau_{bm}} \frac{\emptyset}{\rho_s} \tag{5.2}$$

It must be taken into account that in this parametric study, the amount of reinforcement A_s is kept constant. While, in general, if the height increases significantly the amount of reinforcement will increase so that the reinforcement percentage is kept constant. As a result, the effect of height on crack width will probably be smaller in practice than the results suggest.

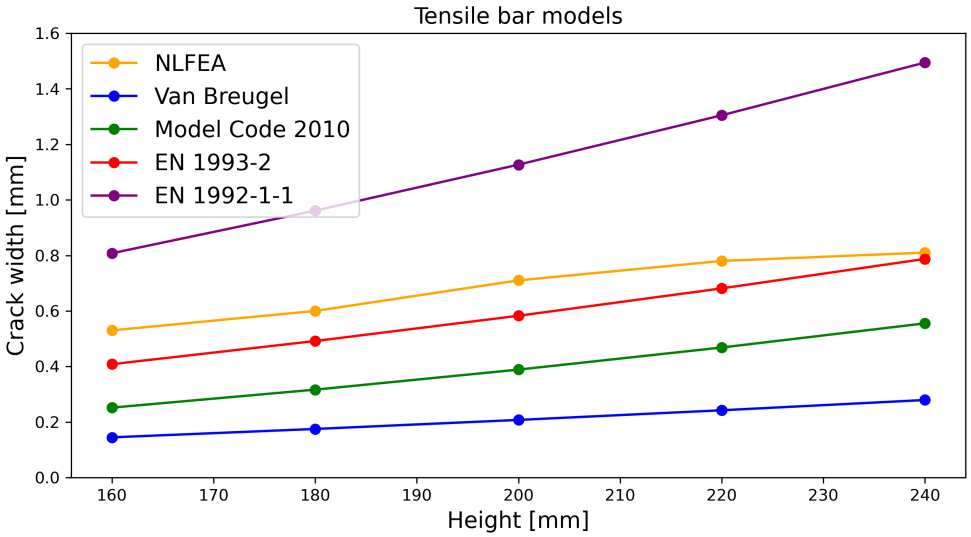

Figure 5.5: Height versus crack width according to tensile bar models

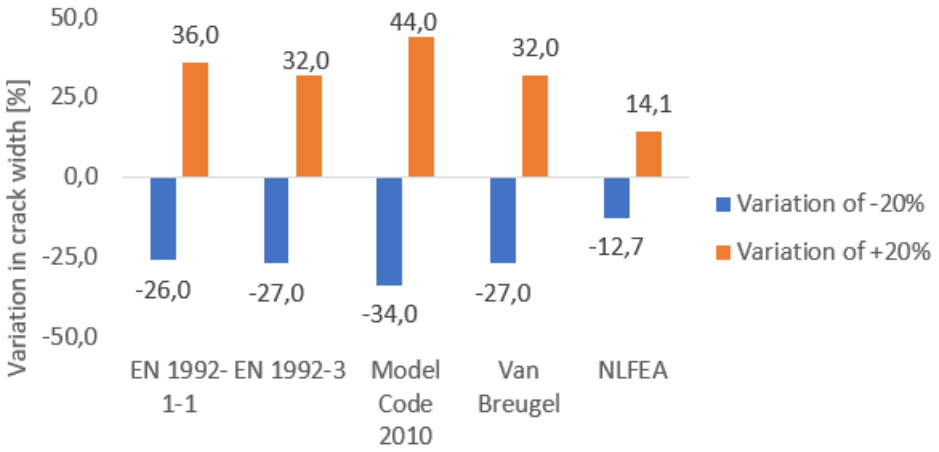

Figure 5.6: Bar chart of the influence of height according to tensile bar models

5.2.2.2 Continuous restraining models

Figures 5.7 and 5.8 display the results of the continuous models. It turned out that, according to the continuous models an increase of the height causes a larger crack width. The reason for this is mentioned before in section 5.2.2.1 and is confirmed by equation 5.3 and 5.4. This shows that also in the continuous restrained model the transfer length plays a crucial role in determining the crack width.

$$w_k = l_t \cdot \epsilon_{cr} \tag{5.3}$$

$$l_t = \frac{1}{4}\frac{f_{ctm}}{\tau_{bm}}\frac{\emptyset}{\rho_s} \tag{5.4}$$

$$\epsilon_{cr} = K_1(\alpha_c T_1 + \epsilon_{ca})R_1 + \alpha_c T_2 R_2 + \epsilon_{cd} R_3 \tag{5.5}$$

In addition, from equation 5.5 it can be seen that in the continuous base restrained models the degree of restraint influences the crack strain ϵ_{cr}. Therefore, it is important to note that previous research, (appendix C.5), has shown that increasing the height causes a reduction of the degree of restraint which influences the crack width. In section 5.2.7 the effect of the degree of restraint on the crack width is investigated in more detail.

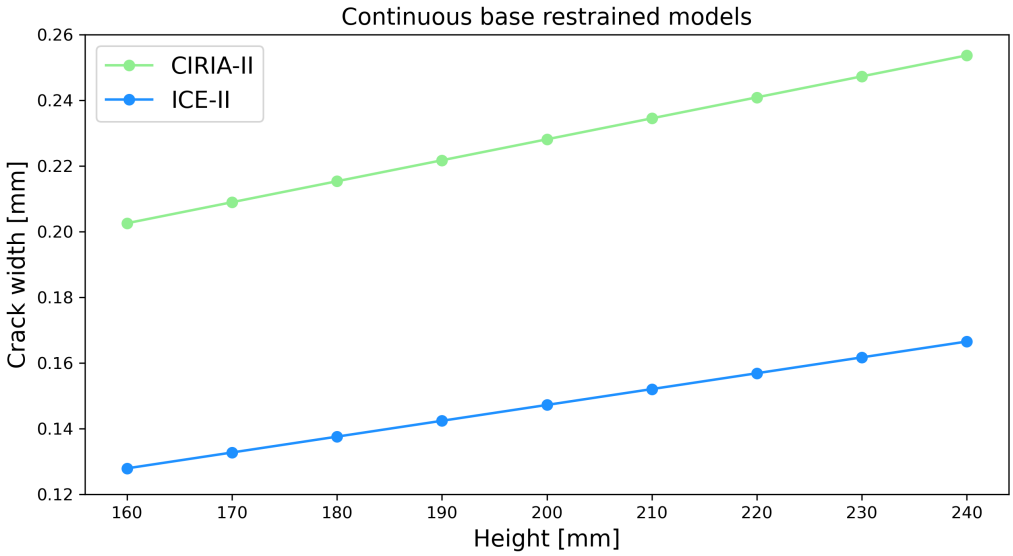

Figure 5.7: Height versus crack width according to continuous base restrained models

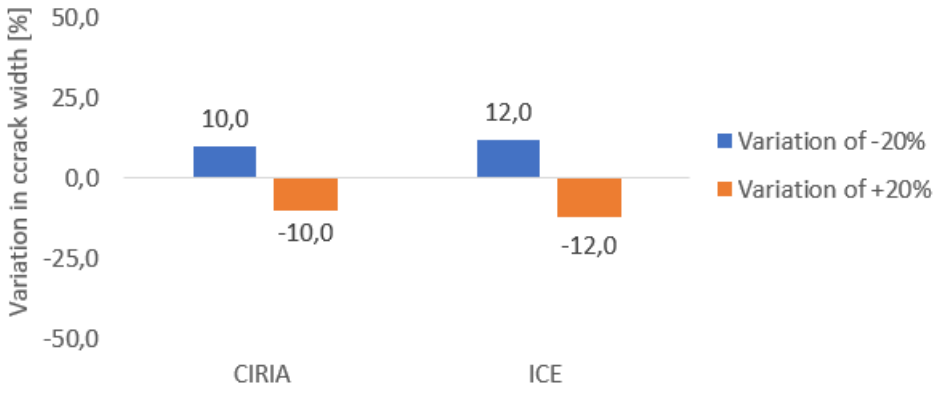

Figure 5.8: Bar chart of the influence of height according to continuous base restrained models

5.2.3. Width

5.2.3.1 Tension bar models

From the literature study [2] it turned out that all tension bar models determine the effective concrete area $A_{c,eff}$ by multiplying the effective height $h_{c,eff}$ with the width b of the member (equation 5.6). This means that if all parameters are kept constant, an increase in width will result in a larger effective area and thus a lower effective reinforcement percentage (equation 5.7). The lower the reinforcement percentage, the larger the crack spacing, crack strain and the crack width.

$$A_{c,eff} = h_{c,eff} \cdot b \tag{5.6}$$

$$\rho_{s,eff} = \frac{A_s}{A_{c,eff}} \tag{5.7}$$

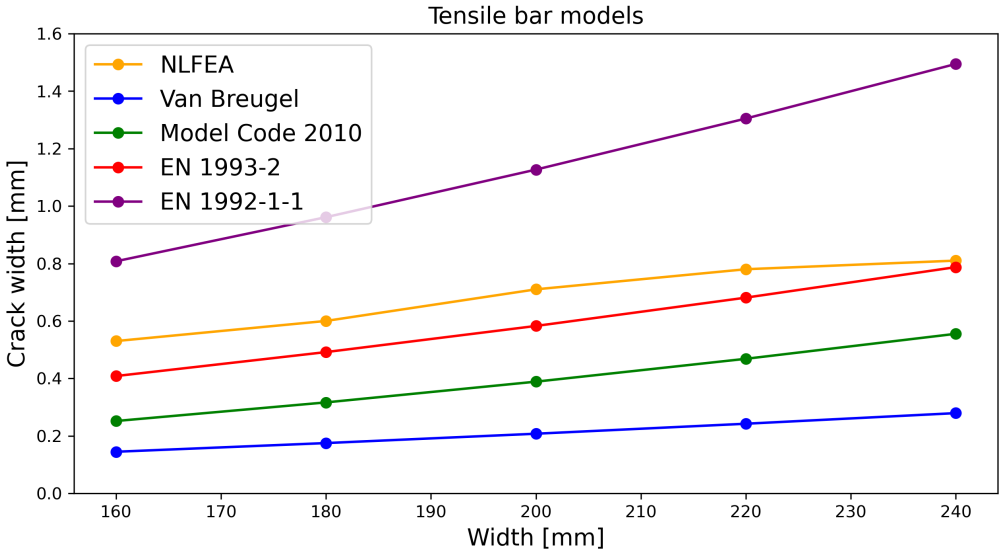

Figure 5.9: Width versus crack width according to tensile bar models

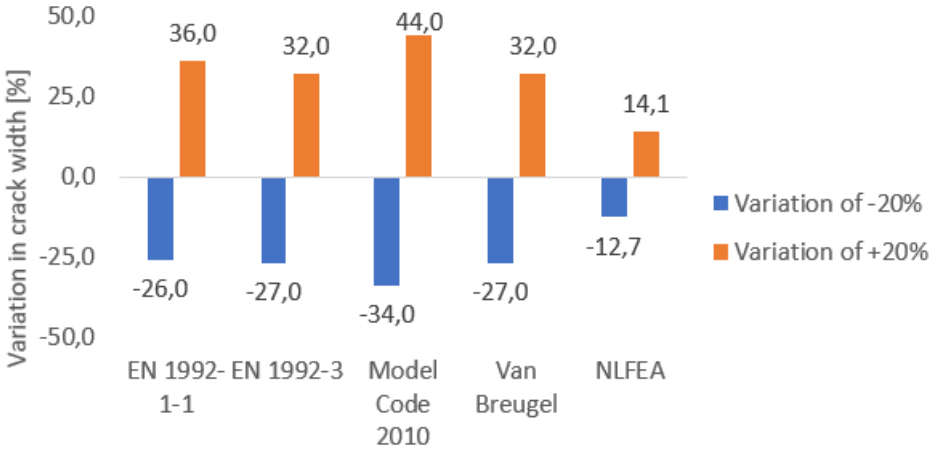

Figure 5.10: Bar chart of the influence of width according to tensile bar models

5.2.3.2 Continuous restraining models

In figures 5.11 and 5.12 the influence of the width for the continuous base restrained models is shown. It can be observed that an increase in the width causes a larger crack width. As mentioned before, increasing the width causes a lower reinforcement percentage, and therefore a larger crack width. It is important to emphasize that changing the width will affect the degree of restraint as is shown in appendix C.5 and hence the crack width but this is not taken into account because all other parameters are kept constant.

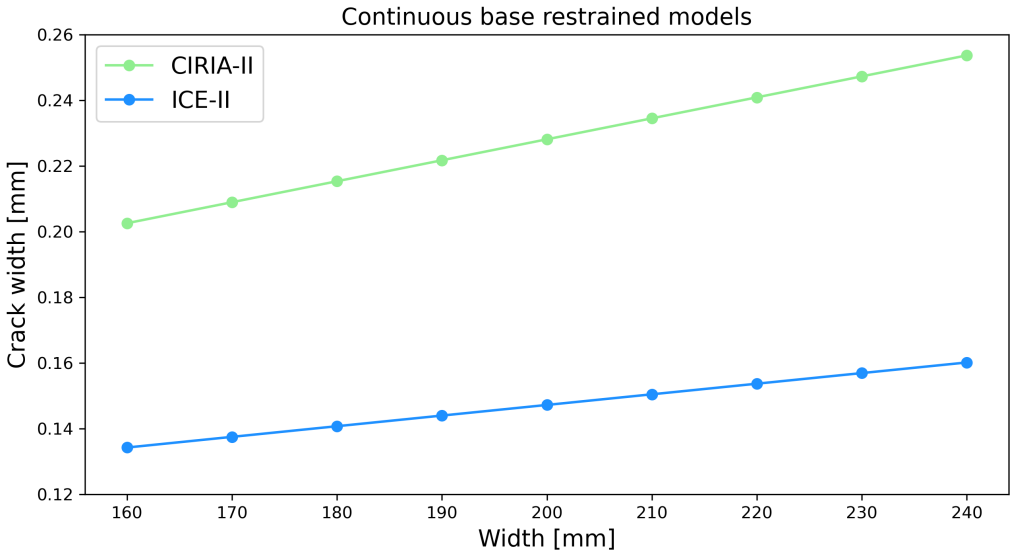

Figure 5.11: Width versus crack width according to continuous base restrained models

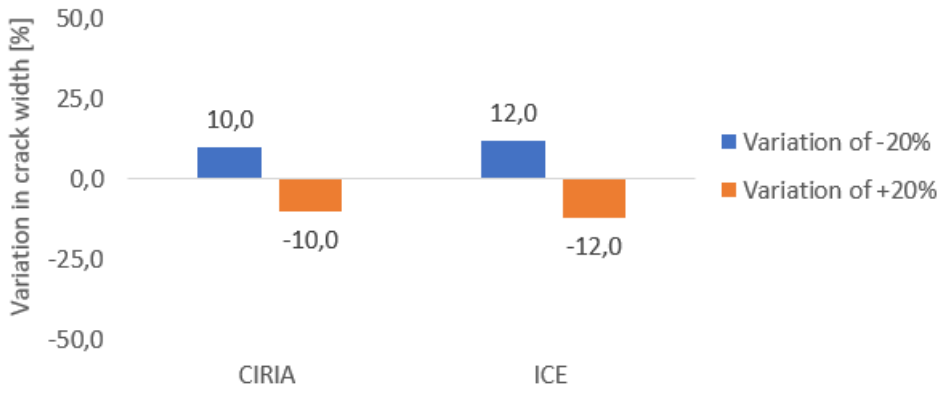

Figure 5.12: Bar chart of the influence of width according to continuous base restrained models

5.2.4. Length

5.2.4.1 Tension bar models

In the tension bar models, the length is not taken into account in the crack width formulas at all.

5.2.4.2 Continuous restraining models

From figures 5.13 and 5.14 it can be concluded that in the continuous base restrained models, the length has also no influence on crack width. However, the ICE-II takes into account the influence of the length because this code applies a length coefficient k_L which is always between 1 and 2. The ICE states that if the degree of restraint is high, the length over which strain relaxation occurs (i.e. zone of influence of the crack) will be less than if the degree of restraint is very low. Because in the parameter study the degree of restraint has been assumed to be constant, the length coefficient k_L is also assumed as a constant of 1.5. For this reason, the influence of the length is not reflected in the results.

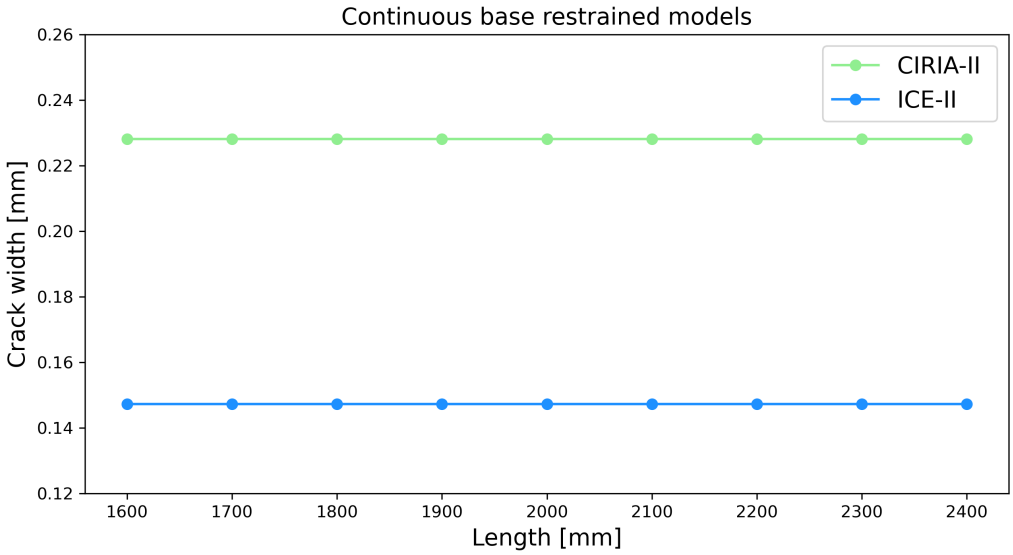

Figure 5.13: Length versus crack width according to continuous base restrained models

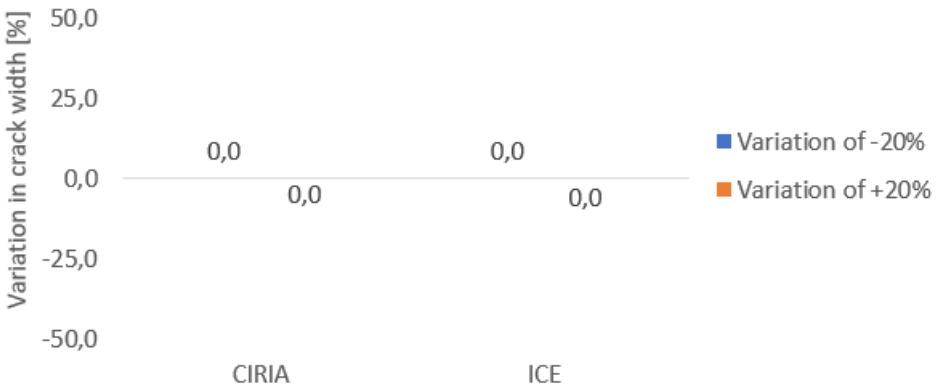

Figure 5.14: Bar chart of the influence of length according to continuous base restrained models

5.2.5. Reinforcement bar diameter

5.2.5.1 Tension bar models

The results in figure 5.15 and 5.16 show that the reinforcement bar diameter has a very large effect on the size of the crack width. This can be explained by the fact that when the bar diameter increases this results in a reduction of the average steel stress in the cracked sections because there is more steel in the cross-section. In the tension bar models a larger bar diameter causes a decrease of crack strain and crack spacing and therefore a lower characteristic crack width.

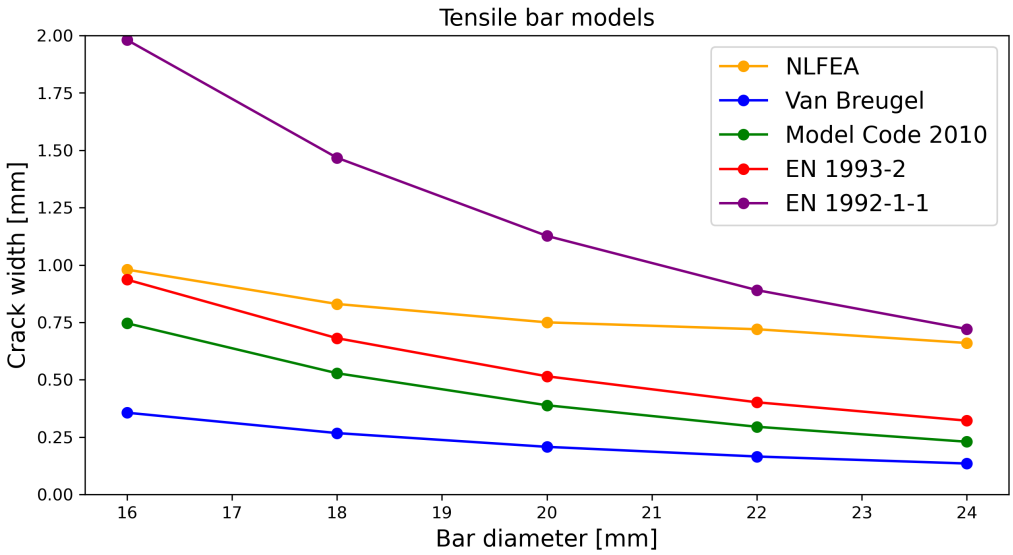

Figure 5.15: Bar diameter versus crack width according to tensile bar models

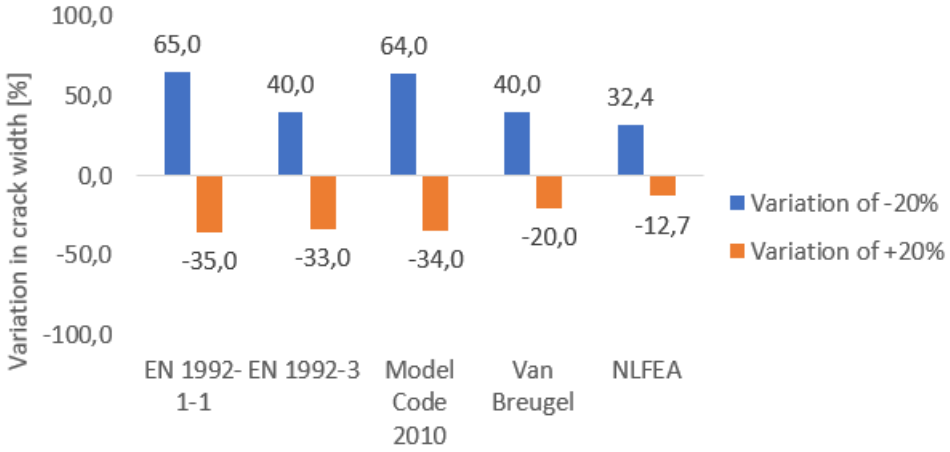

Figure 5.16: Bar chart of the influence of bar diameter according to tensile bar models

5.2.5.2 Continuous restraining models

In the continuous models (figure 5.17 and 5.17) the influence is smaller because the reinforcement bar diameter does not influence the restrained strain but only affects the crack spacing and therefore the crack width.

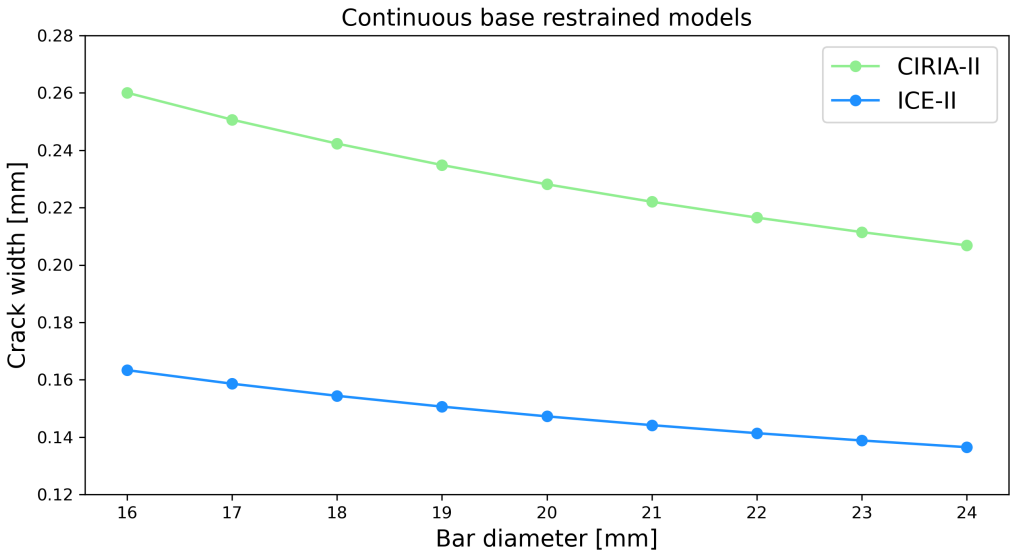

Figure 5.17: Bar diameter versus crack width according to continuous base restrained models

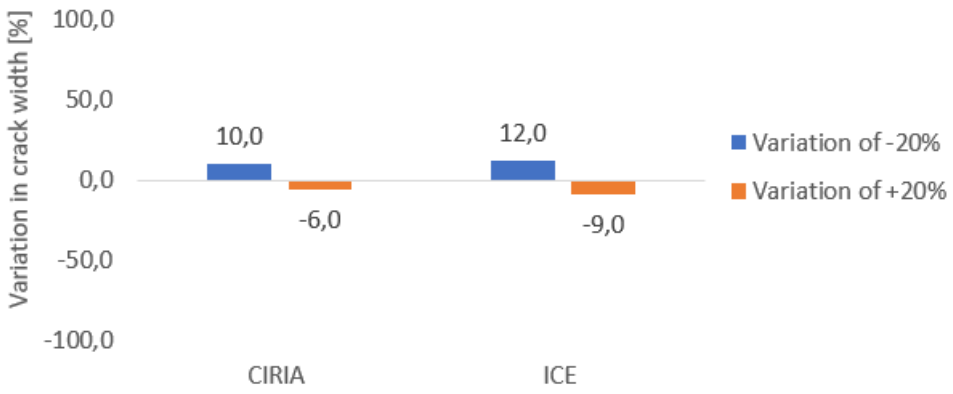

Figure 5.18: Bar chart of the influence of bar diameter according to continuous base restrained models

5.2.6. Concrete cover

5.6.2.1 Tension bar models

From figures 5.19 and 5.20 it can be seen that according to the Eurocode 2 (EN 1992-1-1 and EN 1992-3), increasing the concrete cover results in a larger crack width. While Van Breugel and the Model Code 2010 state that the concrete cover does not have any influence on the crack width. The reason for this is because these codes assume that at each crack, bond failure occurs and that plane sections within the concrete remain plane. This means that cracks are formed parallel throughout the section thickness and the concrete cover does not influence the crack width. This theory is also known as the ”slip” theory and is described in more detail in section 2.4.3. Overall, it can be observed that the NLFEA is less sensitive to the change of a single parameter. One reason for this is that the crack width prediction depends on many more parameters than in the analytical models.

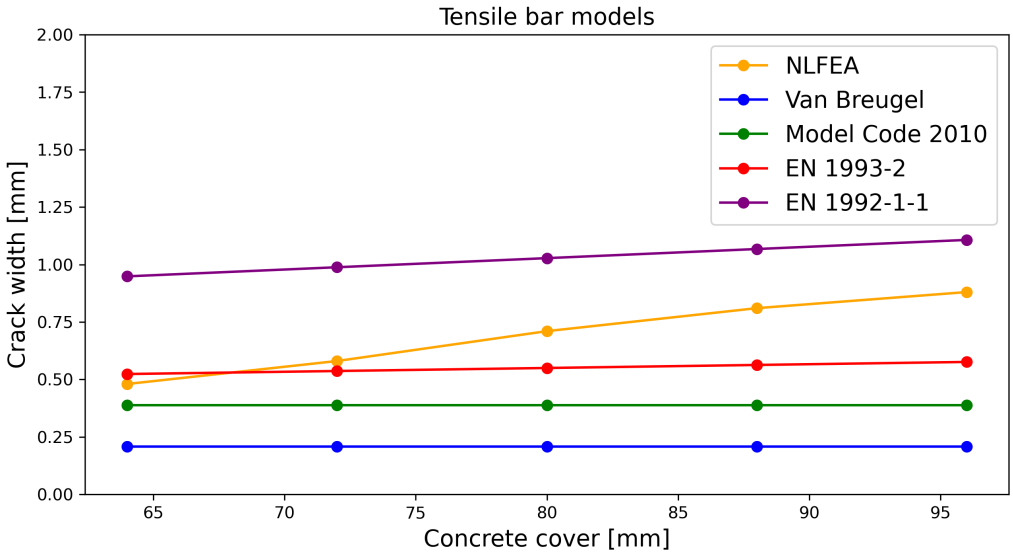

Figure 5.19: Concrete cover versus crack width according to tensile bar models

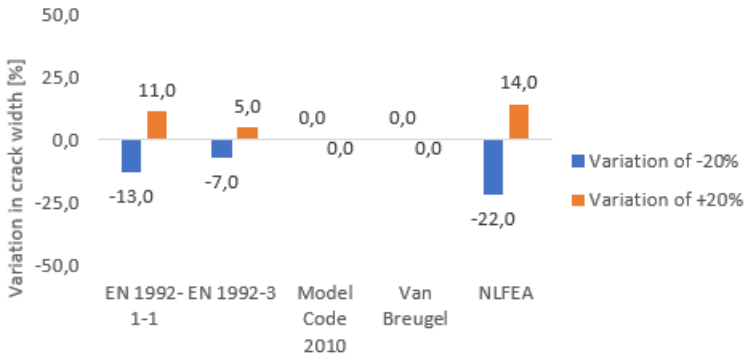

Figure 5.20: Bar chart of the influence of concrete cover according to tensile bar models

5.6.2.2 Continuous restraining models

Figure 5.21 and 5.22 present the influence of the concrete cover according to the continuous restraining models. It can be seen that according to CIRIA-II and ICE-II the crack width increases in case that the concrete cover increases. This is because these models apply a combination of the ”slip” and ”no slip” cracking theory. This means that the transfer length depends on the ratio between the bar diameter and reinforcement percentage and the concrete cover.

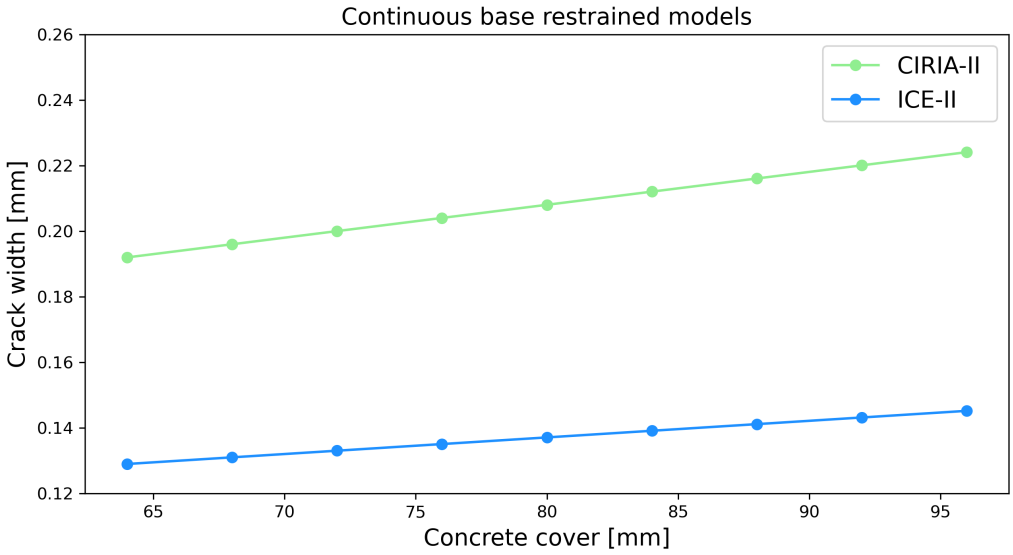

Figure 5.21: Concrete cover strength versus crack width according to continuous base restrained models

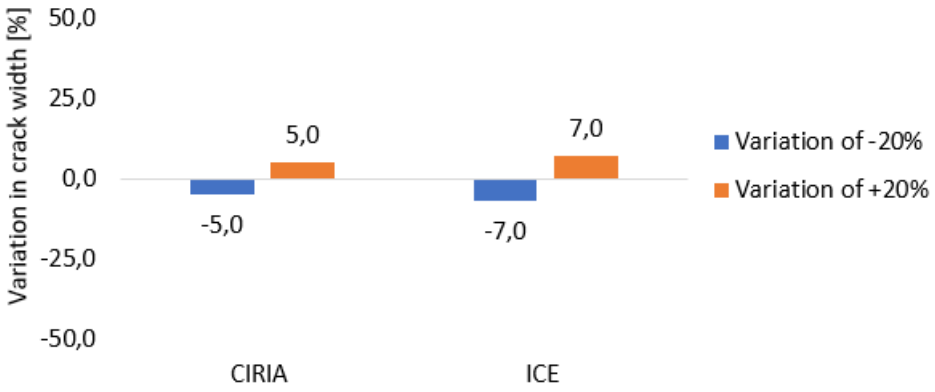

Figure 5.22: Bar chart of the influence of Cconcrete cover according to continuous base restrained models

5.2.7. Degree of restraint

5.2.7.1 Tension bar models

The literature study (chapter 2) showed that in the tension bar models, the degree of restraint is not taken into account and therefore will not affect the crack width prediction.

3.2.7.2 Continuous restraining models

However, according to the continuous models the degree of restraint does have effect. The results in figure 5.23 and 5.24 emphasize the remarkable contrast between the two prediction models. According to CIRIA-II the crack width increases substantially when the the degree of restraint becomes larger. While ICE-II assumes that an increase in the degree of restraint does not by definition lead to an increase in the crack width. The explanation for this is because the ICE states that the higher the degree of restraint the more force the restraining element will take and this will inhibit the growth of cracks.

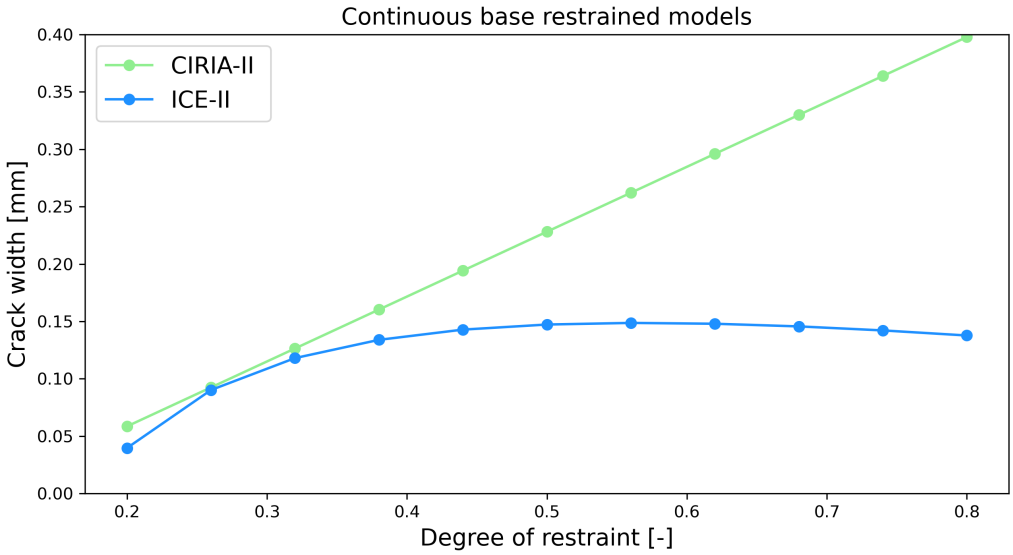

Figure 5.23: Degree of restraint versus crack width according to continuous base restrained models

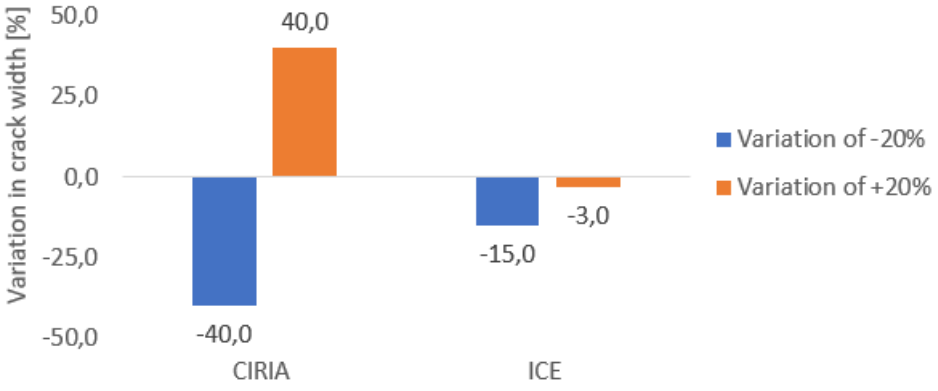

Figure 5.24: Bar chart of the influence of degree of restraint according to continuous base restrained models

5.3. Conclusion

5.3.1. Tension bar models

In figure 5.25 the percentage of change in predicted crack width for 20% decrease or increase in the input parameter is given. A parameter is marked red if the change in predicted crack width is larger than the change of the parameter.

It can be concluded that in all the prediction models which are based on the tensile member theory, the bar diameter influences the crack width the most. Thereafter, the dimensions of the tension bar are crucial for determining the crack width. The fact that the bar diameter has the most influence on the crack width is easily explained by the fact that when the bar diameter increases this results in a reduction of the average steel stress in the cracked sections because there is more steel in the cross-section. The importance of the dimensions of the tension bar was also expected in advance. For larger dimensions, not only the cracking force will increase but also the reinforcement ratio will decrease and this will have a significant influence on the crack width. It has to be noted that in practice, when the dimensions of the tension bar changes, the reinforcement ratio will be kept constant. If the reinforcement ratio is kept constant, the influence of this parameter will be considerably smaller than the results suggest.

	Cube strength		Height		Width		Length		Bar diameter		Concrete cover		Degree of straint	
Prediction method	**-20%**	**+20%**	**-20%**	**+20%**	**-20%**	**+20%**	**-20%**	**+20%**	**-20%**	**+20%**	**-20%**	**+20%**	**-20%**	**+20%**
EN 1992-1-1	-12	15	-26	36	-26	36	0	0	65	-35	-13	11	0	0
EN 1992-3	-13	13	-27	32	-27	32	0	0	40	-33	-21	36	0	0
MC 2010	-26	29	-34	44	-34	44	0	0	64	-34	0	0	0	0
Van Breugel	-7	7	-27	32	-27	32	0	0	40	-20	0	0	0	0
NLFEA	-19	14	12	14	12	14	0	0	32	-13	20	28	0	0

Figure 5.25: Percentage of change in predicted crack width for 20% decrease or increase in input parameter

5.3.2. Continuous restraining models

From figure 5.26 it can be seen that the influence of the degree of restraint remarkably varies between the two prediction methods. According to CIRIA-II the crack width increases substantial when the degree of restraint becomes larger. While ICE-II assumes that an increase in the degree of restraint does not by definition lead to an increase in the crack width. The explanation for this is mentioned before and is because the ICE-II states that the higher the degree of restraint, the more force the restraining element will take and this will inhibit the growth of cracks.

	Cube strength		Height		Width		Length		Bar diameter		Concrete cover		Degree of straint	
Prediction method	**-20%**	**+20%**	**-20%**	**+20%**	**-20%**	**+20%**	**-20%**	**+20%**	**-20%**	**+20%**	**-20%**	**+20%**	**-20%**	**+20%**
CIRIA	2	-2	10	-10	10	-10	0	0	10	-6	-5	5	-40	+40
ICE	2	-2	12	-12	12	-12	0	0	12	-9	-7	-7	-15	-3

Figure 5.26: Percentage of change in predicted crack width for 20% decrease or increase in input parameter

6

Comparison between numerical crack width prediction and crack width prediction using design codes

After the parameter study was performed, a number of findings were made that may relate to the fact that certain 'conservative' assumptions were made. In this chapter the influence of those assumptions has been studied. Therefore, once again a comparison is made between the numerical calculated crack width prediction and the crack width prediction according to various design codes. The model choices described in chapter 3 were applied for the numerical calculations. The design codes included in the comparison are all based on the tension bar model theory and have been discussed earlier in chapter 2.

6.1. Introduction

In this comparison, two reinforced concrete tensile members were used. The difference between the tensile members is the number of rebars and the reinforcement diameter as shown in figure 6.1. If one reinforcement bar was applied it was located in the centre of the tensile member and if 4 reinforcement bars were applied they were modelled in the corners with a concrete cover of 20 mm. In order to make the most reliable comparison, only an autogenous shrinkage strain as an imposed deformation is applied. The material properties are as follows:

Concrete cube strength	f_{ck}	=	30	MPa
Height	h	=	150	mm
Width	b	=	100	mm
Length	L	=	1000	mm
Bar diameter	∅	=	variable	mm
Concrete cover	c	=	variable	mm
Steel stress	σ_s	=	300	MPa
Autogenous shrinkage strain	ϵ_{as}	=	500	$\mu\epsilon$

Member	Number of bars	Diameter [mm]	Reinforcement ratio [%]	Cover [mm]
TBM-1	1	12	0.76	69
TBM-2	4	6	0.76	20

Figure 6.1: Overview amount of reinforcement and reinforcement configuration tensile members

6.1.1. Coefficients Eurocode 2

For the comparison of both parts of the Eurocode 2 (EN 1992-1-1 and EN 1992-3) two cases were considered, one with *normal assumptions* and one with *conservative assumptions*. The input values for the Eurocode 2 [2] coefficients are given in figure 6.2

Coefficient	Normal assumptions	Description	Conservative assumptions	Description
k_1	0.8	For high bond bars	1.6	For smooth bars
k_2	1.0	For pure tension	1.0	For pure tension
k_3 c	7ø	National annex	3.4 c	National annex
k_4	0.425	National annex	0.425	National annex
k	1.0	For webs with h < 800 mm	1.0	For webs with h < 800 mm
k_c	1.0	For pure tension	1.0	For pure tension
k_t	0.4	Long term load	0.4	Long term load

Figure 6.2: Input values normal and conservative assumptions for Eurocode 2 coefficients

6.1.2. Coefficients Model Code 2010

In figure 6.3 the input values used for the crack width calculation according to the Model Code 2010 are presented.

Coefficient		Description
τ_{bm}	1.8 f_{ctm}	Bond stress
β	0.4	Long term load
η_r	1	Including shrinkage

Figure 6.3: Input values for Model Code 2010 coefficients

6.1.3. Coefficients Van Breugel

Figure 6.4 shows two factors which are taken into account in the crack width calculation according to Van Breugel.

Coefficient		Description
γ_s	1.5	Factor for scatter
γ_{--}	1.3	Long term load

Figure 6.4: Input values for Van Breugel coefficients

6.2. Tension bar model 1

In figure 6.5 the cross-section and reinforcement configuration of tension bar model 1 (TBM-1) are presented. In this model a centrically placed single reinforced bar with a diameter of 12 mm is applied. In the contour plot of the crack width from DIANA it can be observed that after the applied shrinkage strain 3 through cracks were developed. The maximum crack width and crack spacing are 0.71 and 420 mm respectively.

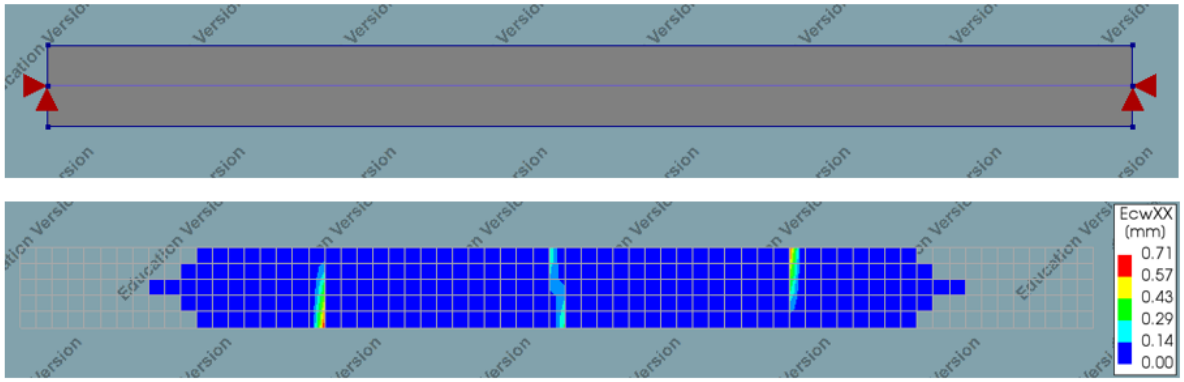

Figure 6.5: Cross-section TBM-1 (top) and contour plot of crack width (DIANA 10.5)

6.2.1. Eurocode 2

From figure 6.6 it can be seen that in case normal coefficients were applied the crack width according to both parts of the Eurocode 2 were smaller than numerically was predicted. If the conservative assumptions were used the crack width according to the EN 1992-1-1 is 63% larger than numerically predicted. While according to the EN 1992-3 the predicted crack width is only 9% larger.

Prediction model	Normal assumptions		Conservative assumptions	
	Crack width [mm]	Difference	Crack width [mm]	Difference
Numerical (FEA)	0.71	n/a		n/a
EN 1992-1-1	0.53	-25% ↓	1.16	+63% ↑
EN 1992-3	0.36	-49% ↓	0.78	+9% ↑

Figure 6.6: Comparison numerical crack width prediction versus Eurocode 2

In figure 6.7 an overview of the predicted crack spacing's are given. It can be observed that the crack spacing in both parts of the Eurocode 2 were the same and that if normal assumptions were made the crack spacing's are 16% smaller than numerically predicted. In addition, it can be seen that when conservative assumptions were made the crack spacing is 85% larger. One of the explanations for these large differences is that in the Eurocode 2 no upper limit value is applied for the maximum crack spacing. If an upper limit would be applied, this will cause a better agreement with the numerical predictions.

Prediction model	Normal assumptions		Conservative assumptions	
	Crack spacing [mm]	Difference	Crack spacing [mm]	Difference
Numerical (FEA)	420	n/a	420	n/a
EN 1992-1-1	353	-16% ↓	776	+85% ↑
EN 1992-3	353	-16% ↓	776	+85% ↑

Figure 6.7: Comparison numerical crack spacing prediction versus Eurocode 2

6.2.2. Model Code 2010 and Van Breugel

In figure 6.8 the comparison between the numerical prediction and the Model Code 2010 and Van Breugel is presented. It can be seen that the crack width according to the Model Code 2010 is 25% smaller than numerically predicted. The reasons for this difference can be explained by the fact the crack spacing is also much smaller. The main expression for calculating the crack width according to Model Code 2010 is based on the crack spacing and the differential mean strain between concrete and reinforcement. Furthermore, it can be seen that for this specific case the crack with prediction according to Van Breugel is in better agreement with the numerical result. Although the predicted crack spacing is 36% lower, the crack width differs only 15% with the numerical result.

Prediction model	Crack width [mm]	Difference	Crack spacing [mm]	Difference
Numerical (FEA)	0.71	n/a	420	n/a
Model Code 2010	0.54	-25% ↓	240	-43% ↓
Van Breugel	0.61	-15% ↓	270	-36% ↓

Figure 6.8: Comparison numerical prediction versus Model Code 2010 and Van Breugel

6.3. Tension bar model 2

In figure 6.9 the cross-section and reinforcement configuration of tension bar model 2 (TBM-2) are presented. In this model four rebars with a diameter of 6 mm were applied. In the contour plot of the crack width from DIANA it can be observed that due to autogenous shrinkage four through cracks were developed.

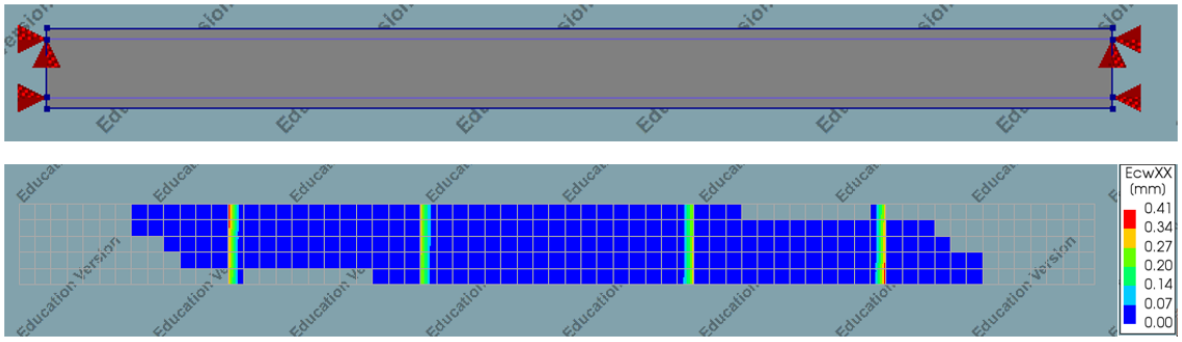

Figure 6.9: Cross-section TBM-2 (top) and contour plot of crack width (DIANA 10.5)

6.3.1. Eurocode 2

From figure 6.10 it can be seen that in case normal coefficients were applied the crack width according to both parts of the Eurocode 2 were much smaller than numerically was predicted. If the conservative assumptions were used the crack width according to the EN 1992-1-1 is 34% larger than numerically predicted. While, even with conservative assumption the EN1992-3 states that the predicted crack width is 36% smaller than numerically predicted.

Prediction model	**Normal assumptions**		**Conservative assumption**	
	Crack width [mm]	Difference	Crack width [mm]	Difference
Numerical (FEA)	0.41	n/a	0.41	n/a
EN 1992-1-1	0.26	-37% ↓	0.55	+34% ↑
EN 1992-3	0.12	-70% ↓	0.26	-36% ↓

Figure 6.10: Comparison numerical crack width prediction versus Eurocode 2

In figure 6.11 an overview of the predicted crack spacing's are given. It can be observed that the crack spacing in both parts of the Eurocode 2 were the same and that if normal assumptions were made the crack spacing's are 64% smaller than numerically predicted. In addition, it can be seen that even when the conservative assumptions were made the crack spacing is 23% smaller than numerically predicted.

Prediction model	Normal assumptions		Conservative assumptions	
	Crack spacing [mm]	Difference	Crack spacing [mm]	Difference
Numerical (FEA)	360	n/a	360	n/a
EN 1992-1-1	128	-64% ↓	275	-23% ↓
EN 1992-3	128	-64% ↓	275	-23% ↓

Figure 6.11: Comparison numerical crack spacing prediction versus Eurocode 2

6.3.2. Model Code 2010 and Van Breugel

In figure 6.12 the comparison between the numerical prediction and the Model Code 2010 and Van Breugel is presented. It can be seen that the crack width according to the Model Code 2010 and Van Breugel are smaller than numerically predicted, respectively 17 and 22%. An explanation for these differences is related to the crack spacing. Important to note is that from earlier research (section 2.4.3.4) it turned out that for the calculation of the crack spacing, the Model Code 2010 and Van Breugel were the only codes that applies the "slip" theory. This theory states that the concrete cover will not influence the crack spacing.

Prediction model	Crack width [mm]	Deviation	Crack spacing [mm]	Deviation
Numerical (FEA)	0.41	n/a	360	n/a
Model Code 2010	0.34	-17% ↓	221	-39% ↓
Van Breugel	0.32	-22% ↓	185	-49% ↓

Figure 6.12: Comparison numerical prediction versus Model Code 2010 and Van Breugel

6.4. Conclusion

Visualizing the results from the design codes in figure 6.13 and 6.14 and disregarding the numerical results for a moment, it becomes clear that there is a large discrepancy between the crack width prediction of the codes. Between the largest and smallest predicted crack width there is a difference up to a factor 3.

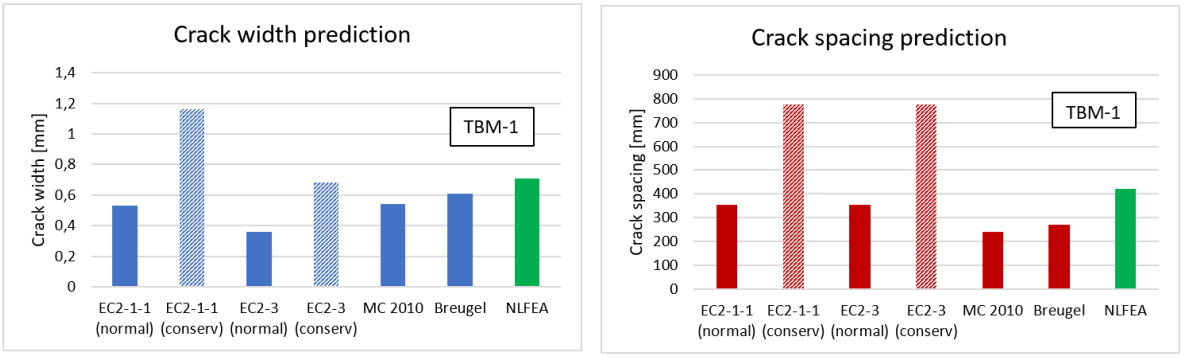

Figure 6.13: Comparison crack width prediction FEM versus design codes

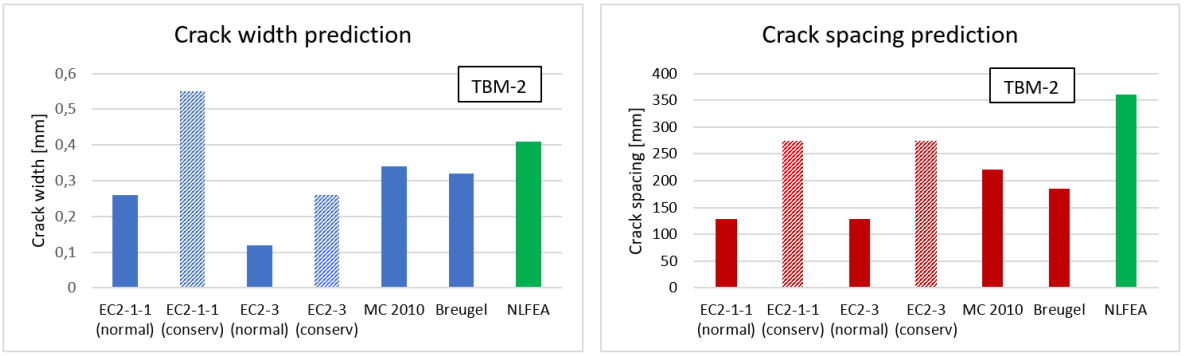

Figure 6.14: Comparison crack width prediction FEM versus design codes

Previous research conducted by Brattstrom and Hagman [7] stated that with respect to end-restrained tensile members under imposed deformations the predicted crack width according to the EC2-3 is a factor 1.4 lower than is predicted numerically using a non-linear finite element analysis. In addition, from the PhD research on continuous base restrained walls from Micallef [14] it also turned out that there was a large under estimation of the crack width due to imposed deformations up to 50%.

Overall, this indicates that there is an unreliability of these design codes and this makes the comparison between the codes and finite element models even more difficult. The differences between the design codes are explained in more detail in paragraph 2.4 but occur mainly due to the fact that all models use different cracking approaches and are applying different empirical parameters.

It immediately stands out that in this research the crack widths that follow from the numerical analyses are in general larger than predicted by the codes. One of the explanations for this difference may lie in the way the crack width is determined in the finite element model. In the finite element model the strains are first determined for all integration points, then these are converted into stresses, which are then converted into internal forces. All internal and external forces together should result in an equilibrium across the entire tensile member as long as the tensile strength is not exceeded. Since an equilibrium of forces must be present everywhere, the finite element model is able to determine peak stress concentrations at for instance local disturbances. Analytically this is not possible, which may result in an underestimation of the real crack width by the codes when assessing disturbed areas.

The only exceptions are the calculations according the Eurocode in which very conservative assumptions were made. Due to these conservative assumptions the crack width turned out to be larger than numerically was predicted. In addition, in the finite element analysis, a very important parameter in the crack width prediction is the bond between the reinforcement and concrete. In the design codes this effect is taken into account in a limited way by using a reduction coefficient which might cause less accurate predictions.

7

Discussion

In this chapter, the results presented throughout this thesis, as well as the way they were obtained, are critically analysed and discussed. Per chapter, the calculations of the crack width prediction are discussed, focusing on the consequence of the assumptions made on the accuracy and certainty of the magnitude of cracking

7.1. Analytical crack width prediction model (design codes)

7.1.1. Codes based on the tension bar model theory

After the literature study had been performed it became clear that there were large differences between the crack width prediction of the concerned design codes. The impact of imposed deformation on reinforced concrete structures was described in a limited scope in both parts of the Eurocode 2 (EN 1992-1-1 and EN 1992-3). In these codes only a general factor of 0,65 was assumed to account for relaxation effects on stresses caused by imposed deformations. In addition, both parts of the Eurocode 2 were vague and inconsistent in the determination of the effective tensile zone for cross-sections with multiple layers or varying reinforcement. Another point of discussion is that both codes state that the crack width prediction according to the stabilize cracking stage is also applicable for the crack formation stage. This assumption will cause the crack width to be overestimated more quickly.

In the Model Code 2010 and Van Breugel which are the more comprehensive crack width prediction design codes, a clear distinction is made between the cracking stage that applies and the type of loading. In both codes it is stated that the effect of an imposed deformation in the crack formation stage was different form that in the stabilized cracking stage. If in the crack formation stage an imposed deformation occurs while simultaneously the external imposed strain remains constant, the crack number tends to increase. Since the external force can not exceed the cracking load in the crack formation stage, the existing crack width will not increase. The result is that only additional cracks will develop and the maximum crack width does not change. While in the stabilized cracking stage, it is assumed that imposed deformations do influence the maximum crack width. Because in the stabilized cracking stage no new cracks are formed, and if imposed deformations are present they cause widening of the existing cracks.

In the end, it is important to realize that in case of short-term loading, the Model Code 2010 and Van Breugel assume that the bonding stress between steel and concrete is equal to approximately two times the mean tensile strength of concrete. While under long term loading, when imposed deformations are present, it is stated that the bond stress decreases and that this could result in an increase in the transfer length of approximately 25%. This value has been determined empirically and it is not supported by the results from this thesis. The boundary conditions on which these empirical values are based are unknown. Therefore, it might be that these values only apply under certain circumstances.

7.1.2. Codes based on the continuous restraining model theory

Only the EN 1992-3, CIRIA and ICE deal with the specific condition of a member which is restrained along one edge. These design codes are also known as the codes which are based on the continuous restraining model theory. One of the most remarkable points of criticism is that in the EN 1992-3 and CIRIA it is assumed that in the area beyond the maximum crack spacing there is no strain relief as a result of the crack occurrence which could lead to a different crack width. This may be acceptable with full edge restraint but in reality most of the structures are only partially restrained and strain relief may occur. Only in the ICE the favourable effect of a member's restrained edge on the reduction of crack spacing and crack width is taken into account.

Another important point of discussion relates to the determination of the degree of restraint. In the EN 1992-3 only a few practical restraint factors for common situations are given. The EN 1992-3 states that in many cases it will be clear that no significant curvature could occur and recommends to assume a restraint factor of 1.0. This assumption seems quite conservative and unrealistic. The CIRIA and ICE provide a formula to determine the degree of restraint which is based on the relative size and stiffness of the restraint elements.

7.2. Numerical crack width prediction (imposed loading versus imposed deformations)

A point of criticism in applying NLFEA is that the analyst's specific choices such as the constitutive model type, the kinematic and equilibrium conditions have a major impact on the outcome of the analysis. To ensure a reliable and safe comparison, the boundary conditions and model choices in this chapter have been made according to the Rijkswaterstaat Technical Document.

In addition, it should be taken into account that in the numerical models a very large shrinkage strain of $-2 \cdot 10^{-3}$ is applied as an imposed deformation. The magnitude of the imposed deformation was chosen in such a way that the crack pattern was fully developed. According to multiple crack width prediction models such as the Eurocode 2 and the Model Code 2010, the magnitude of this imposed deformation does almost never occur in regular concrete. When looking at more common quantities of imposed deformations, these results confirm that imposed deformations will almost never result in a fully developed crack pattern, or in other words, will almost never reach the stabilized cracking stage.

However, nowadays many new concrete types are being developed, such as for example geopolymers or strain-hardening cementitious composites (SHCC). These species have a much higher magnitude of shrinkage and therefore it may happen more often in the future that imposed deformations cause fully developed crack patterns.

7.3. Case study: numerical prediction of early age cracking due to hardening of concrete

The results in chapter 4 have shown that the maximum compressive stresses due to the hardening of concrete in combination with the autogenous shrinkage were approximately 15% smaller in the measurements from Sule [21], than in the finite element calculations. Regarding the moment of the formation of the first crack, it was observed that in the experiments the first crack developed a little earlier.

These differences can be explained by the following reasons. First of all, there was a small difference between the temperature development in the tensile member according to the finite element analysis and the temperature development measured in practice. Due to the fact that in the experiments the concrete cooled down faster, consequently, the tensile stresses arose earlier and therefore the first cracks developed faster. It was impossible to simulate the temperature development that was in complete agreement with the experiments. The reason for this was that in the experiments the concrete temperature was prescribed using temperature controlled moulds. While in the finite element analysis the temperature development was depending on interface boundary elements (used to model the convection) and an adiabatic heat curve. Both parameters for the concrete mixture used in the experiments

were unknown. To be able to model the hardening process of a concrete structure even more accurately, the temperature development according to the finite element analysis should correspond exactly to the measured temperature development in practice. To achieve this, changes in the thermal properties of the concrete mixture and the thermal boundary conditions of the cross-section should be made.

In addition, not taking into account the visco-elastic effects such as creep and relaxation in the finite element analysis caused a difference in stress development. Fitting the visco-elastic effects into the finite element model of DIANA is rather complex due to a lack of knowledge regarding the input parameters. An attempt was made to apply the Bar model of Lokhorst to take into account the visco-elastic effects in an analytical way. In the Bar model of Lokhorst a water-cement ratio of 0.5 was assumed. While, in the experiments from Sule, which are used for the verification, a water cement ratio of 0.33 was used. Therefore, the Bar model was modified. In order to determine the stress reduction factors that give the best results, multiple assumptions were made. One of the explanations that the largest reduction factor gave the best results might be that a decrease of the water cement ratio causes less early age relaxation.

7.4. Parameter study

Regarding the tension bar models, the bar diameter has the largest influence on the crack width prediction. This large influence can be explained. First of all, when the bar diameter increases this results in a reduction of the average steel stress in the cracked sections because there is more steel in the cross-section which causes a decrease of crack strain. In addition to the crack strain, the bar diameter is also normative for the determination of the crack spacing. These two aspects form the basis for the determination of the crack width in the tension bar models.

As far as the continuous models are concerned, there is no one-sided answer to this question. In the prediction method of CIRIA the degree of restraint clearly stands out as the most important parameter which influences the crack width prediction. This code even states that there is a linear relation between the degree of restraint and the predicted crack width. While according to the ICE, the parameters that were investigated in this thesis have limited effect on the crack width prediction. Important to conclude is that the ICE assumes that an increase in the degree of restraint does not by definition result to an increase in the crack width. The explanation for this is because the ICE states that the higher the degree of restraint the more force the restraining element will take and this will inhibit the growth of cracks.

An important point of criticism is the approach of the parameter study. In all prediction models only one parameter has been changed within a range of $+/-20\%$ from the initial value while the values of the other parameters have been kept constant. This might have caused unrealistic situations. For example, in practice, when the dimensions of the tension bar significantly increase the reinforcement ratio will probably be kept constant. In this case, the influence of the bar dimensions will be considerably smaller than the results suggest.

Furthermore, the influence of the length on the crack width can be discussed. In the parameter study the degree of restraint has been assumed to be constant. For this reason the length coefficient, only applied in the ICE, was also assumed to be constant. Consequently, the influence of the length is not reflected in the results from this design code. The ICE states that if the degree of restraint is high, the length over which strain relaxation occurs (i.e. zone of influence of the crack) will be less than if the degree of restraint is very low. Consequently, an increase in length, reduces the degree of restraint, causing a smaller crack width.

A third remark is the contradiction regarding the influence of the degree of restraint between CIRIA and ICE. According to CIRIA the crack width increases substantially when the the degree of restraint becomes larger. While ICE assumes that an increase in the degree of restraint does not by definition lead to an increase in the crack width. The ICE states that the higher the degree of restraint the more force the restraining element will take and this will inhibit the growth of cracks.

7.5. Comparison between numerical crack width prediction and crack width prediction using design codes

It immediately stands out that in this research the crack widths that follow from the numerical analyses are in general larger than predicted by the codes. One of the explanations for this difference may lie in the way the crack width is determined in the finite element model. In the finite element model the strains are first determined for all integration points, then these are converted into stresses, which are then converted into internal forces. All internal and external forces together should result in an equilibrium across the entire tensile member as long as the tensile strength is not exceeded. Since an equilibrium of forces must be present everywhere, the finite element model is able to determine peak stress concentrations at for instance local disturbances. Analytically this is not possible, which may result in an underestimation of the real crack width by the codes when assessing disturbed areas.

One of the disadvantages of the advanced and complex finite element approach is that it is time consuming and the input parameters are difficult to quantify. Therefore, the reliability of this approach might be in practice lower than the results suggest.

8

Conclusions and recommendations

8.1. Conclusions

In this chapter first of all, the answers to the sub-questions are described. Thereafter, the main conclusions and the answer on the research question is given. In the end some recommendations on possible future research are presented.

This master thesis addresses the following research questions:

I. **Which design codes are used to predict the maximum crack width under imposed loads and imposed deformations?**

   Worldwide there is a large number of design codes that predict the maximum crack width in reinforced concrete structures. Based on the accessibility and language, in this master's thesis six different codes were considered. According to the CROW those codes are regularly used in the Netherlands and other European countries. It turned out that a distinction was made between design codes which are based on the tension bar model theory and codes based on continuous restraining model theory. The Eurocode 2, Model Code 2010 and Van Breugel are codes which are based on the tension bar model theory. While, CIRIA C660 and ICE 706 are based on the continuous restraining model theory.

II. **Is there a difference in the steel stress and its growth at the location of cracks when cracking occurs due to imposed loading or due to imposed deformations?**

   There is a large difference in the steel stress and its growth when cracking occurs due to imposed loads or under imposed deformations. The most remarkable difference lies in the fact that under imposed loading the cracking load at the formation of each crack increases while under imposed deformations it decreases as the process of crack formation goes on. This decrease in the peak values is proportional to the stiffness of the reinforcement. In addition, when cracks are formed due to imposed deformations the degree of restraint decreases. The lower the degree of restraint the more imposed strain disappears resulting in a lower steel stress.

III. **Which parameters are essential to simulate the hardening process of concrete in combination with autogenous shrinkage as imposed deformations using a finite element program?**

   Specific choices such as the constitutive model type, the kinematic and equilibrium condition have a major impact on the outcome of the analysis. It is essential to determine the time dependent material properties and the temperature development accurately. In addition, to perform a adequate calculation the visco-elastic effects should be taken into account.

IV. **What are the most important parameters that influence crack prediction according to these analytical design codes?**

Regarding the tension bar models, the bar diameter has the largest influence on the crack width prediction. As far as the continuous models are concerned, there is no one-sided answer to this question. In the prediction method of CIRIA the degree of restraint clearly stands out as the most important parameter which influences the crack width prediction. While according to the ICE, the parameters that were investigated in this thesis have limited effect on the crack width prediction.

V. **Is there a difference between the crack width predicted by the design codes and numerically predicted crack width using a finite element program?**

It can be concluded, that the crack widths that follow from the verified finite element analyses in DIANA were larger than predicted by the codes. The only exceptions are the calculations according to the Eurocode in which very conservative assumptions were made. Due to these conservative assumptions the crack width turned out to be larger than numerically was predicted.

Research question: What is the applicability of the design codes regarding the crack width prediction of reinforced concrete structures under imposed deformations?

It turned out that the design codes considered in this master thesis do not yet fully represent the crack width due to the hardening of concrete or due to autogenous shrinkage. The design codes are applicable for the crack width prediction of reinforced concrete structures under imposed deformations if conservative assumptions are taken into account.

8.2. Recommendations

1. Observations in practice
It appeared that the material properties of the applied analyses in the finite element models are very important and have uncertainties that can affect the validity. In order to improve the validation of the finite element analysis and to assess the reliability of the crack width prediction, more crack width measurements in practice should be performed. This will help to improve the analysis and the design.

2. Further analysis of the effect of creep
Attempts to implement creep in the numerical analyses was made rather late in the thesis. Factors such as switching to a new numerical software, introducing time dependency and the overall complexity of the problem have resulted in that no certain conclusions can be drawn. For a future report, it may be a good idea to fully focus on the concept of creep. Further, it may be of interest to investigate the effect of creep under varying climate such as temperature and relative humidity.

3. Investigation of autogenous shrinkage
In the Eurocode 2 and Model Code 2010 it is assumed that the autogenous shrinkage develops instantly after the moment of casting of the concrete. This is however contradicted by the experimental measurement which suggests that the period of autogenous swelling prior to the period of shrinkage should also be taken into account. Taking the period of autogenous swelling into account influences the stress development during hardening.

4. Conducting laboratory tests
In the end it can be concluded that it is the combination of the different material properties and model parameters that determine the stress development during the hardening of concrete. For all parameters the magnitude at early-ages is of high importance. It should therefore be considered to do more laboratory tests on material properties at very early-ages (0-48 hours).

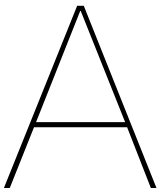

Overview crack width prediction models

A.1. EN 1992-1-1

General information

- Year: 2011
- Type: Code of practice
- Origin: Europe
- Theory: Tension bar model (restraint at both ends)

Effective height

$$h_{c,eff} = min(2,5(h-d); h/2) \tag{A.1}$$

Transfer length and crack spacing

$$l_{st} = s_{r,min} = \frac{s_{r,max}}{1,33 \cdot 1,70} \tag{A.2}$$

$$s_{r,mean} = \frac{s_{r,max}}{1,70} \tag{A.3}$$

$$s_{r,max} = 3,4 \cdot c + 0,34 \cdot \frac{\emptyset}{\rho_{p,eff}} \tag{A.4}$$

Crack width

$$w_k = s_{r,max} \cdot (\epsilon_{sm} - \epsilon_{cm}), \tag{A.5}$$

$$(\epsilon_{sm} - \epsilon_{cm}) = \frac{\sigma_s - k_t \frac{f_{ct,eff}}{\rho_{p,eff}}(1 + \alpha_e \cdot \rho_{p,eff})}{E_s} \geq 0,6\frac{\sigma_s}{E_s}. \tag{A.6}$$

A.2. EN 1992-3 (1)

General information

- Year: 2006
- Type: Code of practice
- Origin: Europe
- Theory: Tension bar model (restraint at both ends)

Effective height

$$h_{c,eff} = min(2,5(h-d); h/2) \tag{A.7}$$

Transfer length and crack spacing

$$l_{st} = s_{r,min} = \frac{s_{r,max}}{1,33 \cdot 1,70} \tag{A.8}$$

$$s_{r,mean} = \frac{s_{r,max}}{1,70} \tag{A.9}$$

$$s_{r,max} = 3,4 \cdot c + 0,34 \cdot \frac{\emptyset}{\rho_{p,eff}} \tag{A.10}$$

Crack width

$$w_k = s_{r,max} \cdot (\epsilon_{sm} - \epsilon_{cm}), \tag{A.11}$$

$$(\epsilon_{sm} - \epsilon_{cm}) = \frac{0.5k \cdot k_c \cdot f_{ct,eff} \cdot \alpha_e}{E_s}((\frac{1}{\alpha_e \rho} + 1). \tag{A.12}$$

A.3. Model Code 2010

General information

- Year: 2010
- Type: Guideline
- Origin: Europe
- Theory: Tension bar model (restraint at both ends)

Effective height

$$h_{c,eff} = min(2,5(h-d); h/2) \tag{A.13}$$

Transfer length and crack spacing

$$l_{st} = s_{r,min} = \frac{s_{r,max}}{2,0} \tag{A.14}$$

$$s_{r,mean} = \frac{s_{r,max}}{1,5} \tag{A.15}$$

$$s_{r,max} = 2c + 0,28 \cdot \frac{\emptyset}{\rho_s} \tag{A.16}$$

Crack width

Crack formation stage

$$w_k = 2 * l_{st} \cdot (\epsilon_{sm} - \epsilon_{cm}), \tag{A.17}$$

$$(\epsilon_{sm} - \epsilon_{cm}) = \frac{\sigma_s - 0,6\frac{f_{ct,eff}}{\rho_{p,eff}}(1 + \alpha_e \rho_{p,eff})}{E_s} \tag{A.18}$$

Stabilized cracking stage

$$w_k = s_{r,max} \cdot (\epsilon_{sm} - \epsilon_{cm}), \tag{A.19}$$

$$(\epsilon_{sm} - \epsilon_{cm}) = \frac{\sigma_s - 0,4\frac{f_{ct,eff}}{\rho_{p,eff}}(1 + \alpha_e \rho_{p,eff})}{E_s} + \epsilon_r \tag{A.20}$$

A.4. Van Breugel

General information

- Year: 2016
- Type: Guideline
- Origin: The Netherlands
- Theory: Tension bar model (restraint at both ends)

Effective height

$$h_{c,eff} = min(c + 2\emptyset + 1, 2l_{st}; h/2) \tag{A.21}$$

Transfer length and crack spacing

$$l_{st} = s_{r,min} = \frac{s_{r,max}}{2,0} \tag{A.22}$$

$$s_{r,mean} = \frac{s_{r,max}}{1,5} \tag{A.23}$$

$$s_{r,max} = 2,4 \cdot w_{mo} \cdot \frac{E_s}{\sigma_{s,cr}} \tag{A.24}$$

Crack width

Crack formation stage

$$w_{mo} = 2 \cdot [\frac{0,4 \cdot \emptyset}{f_{cm,cube} \cdot E_s} \cdot (\frac{\sigma_{cr}}{\rho})^2 \cdot (1 + \alpha_e \cdot \rho)]^{0,85} \tag{A.25}$$

Stabilized cracking stage

$$w_{mv} = 1,8 \cdot w_{mo} \cdot \frac{\sigma_s}{\sigma_{s,cr}} - 0,5 \tag{A.26}$$

A.5. CIRIA C660 II

General information

- Year: 2007
- Type: Guideline
- Origin: United Kingdom
- Theory: Continuous model (restraint along one edge)

Effective height

$$h_{c,eff} = min(2,5(h-d); h/2) \tag{A.27}$$

Transfer length and crack spacing

$$l_{st} = s_{r,min} = \frac{s_{r,max}}{1,33 \cdot 1,70} \tag{A.28}$$

$$s_{r,mean} = \frac{s_{r,max}}{1,70} \tag{A.29}$$

$$s_{r,max} = 3,4 \cdot c + 0,34 \cdot \frac{\emptyset}{\rho_{p,eff}} \tag{A.30}$$

Crack width

$$w_k = s_{r,max} \cdot \epsilon_{cr}, \tag{A.31}$$

$$\epsilon_{cr} = K_1(\alpha_c T_1 + \epsilon_{ca})R_1 + \alpha_c T_2 R_2 + \epsilon_{cd} R_3 \tag{A.32}$$

A.6. ICE 706

General information

- Year: 2010
- Type: Guideline
- Origin: United Kingdom
- Theory: Continuous model (restraint along one edge)

Effective height

$$h_{c,eff} = min(2,5(h-d); h/2) \tag{A.33}$$

Transfer length and crack spacing

$$l_{st} = s_{r,min} = \frac{s_{r,max}}{1,33 \cdot 1,70} \tag{A.34}$$

$$s_{r,mean} = \frac{s_{r,max}}{1,70} \tag{A.35}$$

$$s_{r,max} = 3,4 \cdot c + 0,34 \cdot \frac{\emptyset}{\rho_{p,eff}} \tag{A.36}$$

Crack width

$$w_k = w_{k1} + w_{k2} \tag{A.37}$$

$$w_{k1} = s_{r,max} \cdot \frac{0,5L \cdot \epsilon_{ctu} \cdot (1 - R_{edge})B}{1 - \frac{S \cdot R_{edge}}{k_L \cdot H}[1 - 0,5(B + \frac{1}{1-R_{edge}})]}, \tag{A.38}$$

$$w_{k2} = s_{r,max} \cdot (1 - 0,5R_{edge})K_1(\epsilon_{free} - \frac{\epsilon_{ctu}}{R_{edge} \cdot K_1}) \tag{A.39}$$

B

Spreadsheets prediction models

The spreadsheet models of the following prediction methods are given in this appendix.

Tension bar models

B.1. EN 1992-1-1

B.2. EN 1993-2

B.3. Model Code 2010

B.4. Van Breugel

Continuous restraining models

B.5. CIRIA C660

B.6. ICE 0706

B.1. EN 1992-1-1

Input parameters	Symbol		Value	Unit	
Section details and material properties					
Concrete quality		=	C30/37		
Characteristic concrete cube strength	f_{ck}	=	30	MPa	
Characteristic yield strength	f_{yk}	=	500	MPa	
Width	b	=	200	mm	
Section thickness	h	=	200	mm	
Length of the wall	L	=	1000	mm	
Early age of cracking	t_0	=	3	days	
Long term age of cracking	t	=	28	days	
Cement type		=	R	(S, N or R)	
Load duration		=	L	(S or L)	S = Short term and L = Long term
Bond properties		=	H	(H or L)	H = High bond and L = Low bond
Strain distribution		=	T	(B or T)	B = Bending and T = Tension
Reinforcement details					
Number of bars	n	=	1		
Horizontal bar diameter	$ø_{hor}$	=	20	mm	
Horizontal bar spacing	s_{hor}	=	0	mm	
Vertical bar diameter	$ø_{vert}$	=	0	mm	
Vertical bar spacing	s_{vert}	=	0	mm	
Concrete cover 1	c_1	=	20	mm	
Concrete cover 2	c_2	=	0	mm	
Modulus of elasticity of steel	E_s	=	200000	MPa	
Calculations					
Horizontal steel area per face	$A_{s,hor}$	=	314	mm^2	n*Pi()/4 * $ø_{hor}$^2
Area of concrete	A_c	=	40000	mm^2	(b*h)
Reinforcement ratio	ρ	=	0,79	%	As/Ac
Effective height	$h_{c,eff}$	=	75	mm	Min(2,5*(c1+øhor/2) ; h/2)
Effective tension area	$A_{c,eff}$	=	15000	mm^2	hc,eff* b
Effective reinforcement ratio	$ρ_{p,eff}$	=	2,09	%	As / Ac,eff
Concrete properties					
Mean compressive strength at 28 days	f_{cm}	=	38	MPa	fck+8
Mean concrete compressive strength at an age of t days	f_{cm} (t)	=	38	MPa	βcc(t)*fcm
Mean concrete tensile strength	f_{ctm}	=	2,90	MPa	0,30*fck^(2/3)
Effective concrete tensile strength at an age of t days	$f_{ct,eff}$ (t)	=	2,90	MPa	βcc(t)^α * fctm
Coefficient which depends on the age of concrete	$β_{cc}$(t)	=	1,00		exp(s(1-(28/t)^0,5))
	α	=	0,67		α = 1 for t < 28 and α = 2/3 for t=>28
Coefficient which depends on the type of cement	s	=	0,20		S = 0,38; N = 0,25; R = 0,20
Modulus of elasticity of concrete	E_{cm}	=	32837	MPa	22*(fcm)/10)^0,3 * 10^3
Modulus of elasticity of concrete at an age of t days	E_{cm} (t)	=	32837	MPa	(((βcc(t)*fcm(t))/fcm(t))^0,3)*Ecm
Modular ratio	$α_e$	=	6,1		Es\Ecm(t)
Coëfficients					
Bond properties of reinforcement	k1	=	0,80		high bond = 0,8 ; bars with effective plain surface = 1,6
Strain distribution in cross section	k2	=	1,0		bending = 0,5 and pure tension = 1,0
Takes into account the cover	k3	=	3,4		
Takes into account the cross section of reinforcement	k4	=	0,425		
Effect of the load duration	kt	=	0,40		long term (L) = 0,4 and short term (S) = 0,6
Takes into account stress distribution	kc	=	1,00		pure tension = 1,0
Takes into account the effect of non-uniform equilibrium stresses which lead to a reduction of restraint forces	k	=	1,00		h ≤ 300 = 1,0 and h > 800 = 0,65
Creep factor	K1	=	0,65		
Sustained load factor	K2	=	0,8		
Coefficient of thermal expansion of concrete	αc	=	11,8	με/˚C	
Crack spacing and crack width					
Cracking Force	N_{cr}	=	121	kN	fct,eff * Ac * (1+ρ* αe)
Steel stress directly after cracking	$σ_s = σ_{s,cr}$	=	386	MPa	Ncr/As
Transfer length	$l_{st} = s_{r,min}$	=	174	mm	sr,mean / 1,33
Mean crack spacing	$s_{r,mean}$	=	231	mm	sr,max / 1,7
Max final crack spacing	$s_{r,max}$	=	393	mm	k3 * c + k1 * k2 * k4 * ø / pp,eff
Strain difference	$ε_{sm}$-$ε_{cm}$	=	1932	με	{σs - kt * fct,eff/ρ,eff (1+ αe ρ,eff) }/Es
Long term crack width	w_k	=	0,759	mm	sr,max * (εsm-εcm)

Figure B.1: Spreadsheet EN 1992-1-1

B.2. EN 1992-1-1

Input parameters	Symbol		Value	Unit	
Section details and material properties					
Concrete quality		=	C30/37		
Characteristic concrete cube strength	f_{ck}	=	30	MPa	
Characteristic yield strength	f_{yk}	=	500	MPa	
Width	b	=	200	mm	
Section thickness	h	=	200	mm	
Length of the wall	L	=	1000	mm	
Early age of cracking	t_0	=	3	days	
Long term age of cracking	t	=	28	days	
Cement type		=	R	(S, N or R)	
Load duration		=	L	(S or L)	S = Short term and L = Long term
Bond properties		=	H	(H or L)	H = High bond and L = Low bond
Strain distribution		=	T	(B or T)	B = Bending and T = Tension
Reinforcement details					
Number of bars	n	=	1		
Horizontal bar diameter	$ø_{hor}$	=	20	mm	
Horizontal bar spacing	s_{hor}	=	0	mm	
Vertical bar diameter	$ø_{vert}$	=	0	mm	
Vertical bar spacing	s_{vert}	=	0	mm	
Concrete cover 1	c_1	=	20	mm	
Concrete cover 2	c_2	=	0	mm	
Modulus of elasticity of steel	E_s	=	200000	MPa	
Calculations					
Horizontal steel area per face	$A_{s,hor}$	=	314	mm^2	n*Pi()/4 * $ø_{hor}$^2
Area of concrete	A_c	=	40000	mm^2	(b*h)
Reinforcement ratio	ρ	=	0,79	%	As/Ac
Effective height	$h_{c,eff}$	=	75	mm	Min(2,5*(c1+øhor/2) ; h/2)
Effective tension area	$A_{c,eff}$	=	15000	mm^2	hc,eff* b
Effective reinforcement ratio	$ρ_{p,eff}$	=	2,09	%	As / Ac,eff
Concrete properties					
Mean compressive strength at 28 days	f_{cm}	=	38	MPa	fck+8
Mean concrete compressive strength at an age of t days	f_{cm} (t)	=	38	MPa	βcc(t)*fcm
Mean concrete tensile strength	f_{ctm}	=	2,90	MPa	0,30*fck^(2/3)
Effective concrete tensile strength at an age of t days	$f_{ct,eff}$ (t)	=	2,90	MPa	βcc(t)^α * fctm
Coefficient which depends on the age of concrete	$β_{cc}$(t)	=	1,00		exp(s(1-(28/t)^0,5))
	α	=	0,67		α = 1 for t < 28 and α = 2/3 for t=>28
Coefficient which depends on the type of cement	s	=	0,20		S = 0,38; N = 0,25; R = 0,20
Modulus of elasticity of concrete	E_{cm}	=	32837	MPa	22*(fcm)/10)^0,3 * 10^3
Modulus of elasticity of concrete at an age of t days	E_{cm} (t)	=	32837	MPa	(((βcc(t)*fcm(t))/fcm(t))^0,3)*Ecm
Modular ratio	$α_e$	=	6,1		Es\Ecm(t)
Coëfficients					
Bond properties of reinforcement	k1	=	0,80		high bond = 0,8 ; bars with effective plain surface = 1,6
Strain distribution in cross section	k2	=	1,0		bending = 0,5 and pure tension = 1,0
Takes into account the cover	k3	=	3,4		
Takes into account the cross section of reinforcement	k4	=	0,425		
Effect of the load duration	kt	=	0,40		long term (L) = 0,4 and short term (S) = 0,6
Takes into account stress distribution	kc	=	1,00		pure tension = 1,0
Takes into account the effect of non-uniform equilibrium stresses which lead to a reduction of restraint forces	k	=	1,00		h ≤ 300 = 1,0 and h > 800 = 0,65
Creep factor	K1	=	0,65		
Sustained load factor	K2	=	0,8		
Coefficient of thermal expansion of concrete	αc	=	11,8	με/˚C	
Crack spacing and crack width					
Cracking Force	N_{cr}	=	121	kN	fct,eff * Ac * (1+ρ* αe)
Steel stress directly after cracking	$σ_s = σ_{s,cr}$	=	386	MPa	Ncr/As
Transfer length	$l_{st} = s_{r,min}$	=	174	mm	sr,mean / 1,33
Mean crack spacing	$s_{r,mean}$	=	231	mm	sr,max / 1,7
Max final crack spacing	$s_{r,max}$	=	393	mm	k3 * c + k1 * k2 * k4 * ø / pp,eff
Strain difference	$ε_{sm}$-$ε_{cm}$	=	390	με	{0,5 * αe * k * kc * fct,eff (1+1/ αe *$ρ_{p,eff}$}/Es
Long term crack width	w_k	=	0,153	mm	sr,max * (esm-ecm)

Figure B.2: Spreadsheet EN 1992-3

B.3. Model Code 2010

Input parameters	Symbol		Value	Unit	
Section details and material properties					
Concrete quality		=	C30/37		
Characteristic concrete cube strength	f_{ck}	=	30	MPa	
Characteristic yield strength	f_{yk}	=	500	MPa	
Width	b	=	200	mm	
Section thickness	h	=	200	mm	
Length of the wall	L	=	1000	mm	
Early age of cracking	t_0	=	3	days	
Long term age of cracking	t	=	28	days	
Cement type		=	R	(S, N or R)	
Load duration		=	L	(S or L)	S = Short term and L = Long term
Bond properties		=	H	(H or L)	H = High bond and L = Low bond
Strain distribution		=	T	(B or T)	B = Bending and T = Tension
Reinforcement details					
Number of bars	n	=	1		
Horizontal bar diameter	$\emptyset_{hor}$	=	20	mm	
Horizontal bar spacing	s_{hor}	=	0	mm	
Vertical bar diameter	$\emptyset_{vert}$	=	0	mm	
Vertical bar spacing	s_{vert}	=	0	mm	
Concrete cover 1	c_1	=	20	mm	
Concrete cover 2	c_2	=	0	mm	
Modulus of elasticity of steel	E_s	=	200000	MPa	
Calculations					
Horizontal steel area per face	$A_{s,hor}$	=	314	mm^2	n*Pi()/4 * $\emptyset_{hor}$^2
Area of concrete	A_c	=	40000	mm^2	(b*h)
Reinforcement ratio	ρ	=	0,79	%	As/Ac
Effective height	$h_{c,eff}$	=	75	mm	Min(2,5*(c1+$\emptyset$hor/2) ; h/2)
Effective tension area	$A_{c,eff}$	=	15000	mm^2	hc,eff* b
Effective reinforcement ratio	$\rho_{p,eff}$	=	2,09	%	As / Ac,eff
Concrete properties					
Mean compressive strength at 28 days	f_{cm}	=	38	MPa	fck+8
Mean concrete compressive strength at an age of t days	f_{cm} (t)	=	38	MPa	βcc(t)*fcm
Mean concrete tensile strength	f_{ctm}	=	2,90	MPa	0,30*fck^(2/3)
Effective concrete tensile strength at an age of t days	$f_{ct,eff}$(t)	=	2,90	MPa	βcc(t)^α * fctm
Coefficient which depends on the age of concrete	β_{cc}(t)	=	1,00		exp(s(1-(28/t)^0,5))
	α	=	0,67		α = 1 for t < 28 and α = 2/3 for t=>28
Coefficient which depends on the type of cement	s	=	0,20		S = 0,38; N = 0,25; R = 0,20
Modulus of elasticity of concrete	E_{cm}	=	32837	MPa	22*(fcm)/10)^0,3 * 10^3
Modulus of elasticity of concrete at an age of t days	E_{cm} (t)	=	32837	MPa	(((βcc(t)*fcm(t))/fcm(t))^0,3)*Ecm
Modular ratio	α_e	=	6,1		Es\Ecm(t)
Coëfficients					
Early age			C F S	S C S	
Mean bond strenght between reinforcement and concrete	τ	=	5,2	5,2	
Emperical coefficient to asses the mean strain over sr,max	β	=	0,6	0,6	
Take into account contribution shrinkage	η_r	=	0,0	0,0	
Long-term			C F S	S C S	
Mean bond strenght between reinforcement and concrete	τ	=	3,9	5,2	
Emperical coefficient to asses the mean strain over sr,max	β	=	0,6	0,4	
Take into account contribution shrinkage	η_r	=	0,0	1,0	
Model Code 10					
Cracking force	N_{cr}	=	121	kN	fct,eff * Act * (1+ρ * αe)
Imposed deformation (imposed strain)	ε_{imp}	=	418	με	Next/ (As * Es)
Concrete strain at onset of cracking	ε_{cr}	=	88	με	fctm/Ec
Concrete strain at onset of the fully devevelop crack pattern	ε_{fdc}	=	1195	με	fctm * (0,6 + αe*ρ) / Es * ρ
Steel yielding strain	ε_{sy}	=	2174	με	(fyk/1,15)/Es
Uncracked stage ($\varepsilon_{imp} < \varepsilon_{cr}$)	N/A				
Steel tensile stress	σ_s	=	84	MPa	ε_{imp} * Es
Concrete tensile stress	σ_c	=	14	MPa	ε_{imp} * Ecm
Crack formation stage ($\varepsilon_{cr} < \varepsilon_{imp} < \varepsilon_{fdc}$)	Crack Formation Stage				
Steel tensile stress in the crack/directly after cracking	$\sigma_s = \sigma_{s,cr}$	=	386	MPa	Ncr/As
Transfer length	l_{st}	=	177	mm	0,25 * (fctm/tbm) *(øeq/$\rho_{p,eff}$)
Mean crack spacing	$s_{r,mean}$	=	236	mm	(4/3)*lst
Maximum crack spacing	$s_{r,max}$	=	354	mm	2*lst
Average strain	$\varepsilon_{sm} - \varepsilon_{cm} - \varepsilon_{sh}$	=	773	με	(σs - β * σsr)/Es + η_r * εimp
Mean crack width	w_k	=	0,27	mm	sr,max * (εsm - εcm - εcs)
Stabilzed cracking stage ($\varepsilon_{fdc} < \varepsilon_{imp} < \varepsilon_{sy}$)	N/A				
Steel stress in the crack	σ_s	=	231	MPa	Ncr/As + Es (εimp - εfdcp)
Steel stress directly after cracking	$\sigma_{s,cr}$	=	231	MPa	Ncr/As
Transfer length	l_{st}	=	133	mm	0,25 * (fctm/tbm) *(øeq/$\rho_{p,eff}$)

Figure B.3: Spreadsheet Model Code 2010

B.4. Van Breugel

Input parameters	Symbol		Value	Unit	
Section details and material properties					
Concrete quality		=	C30/37		
Characteristic concrete cube strength	f_{ck}	=	30	MPa	
Characteristic yield strength	f_{yk}	=	500	MPa	
Width	b	=	200	mm	
Section thickness	h	=	200	mm	
Length of the wall	L	=	1000	mm	
Early age of cracking	t_0	=	3	days	
Long term age of cracking	t	=	28	days	
Cement type		=	R	(S, N or R)	
Load duration		=	L	(S or L)	S = Short term and L = Long term
Bond properties		=	H	(H or L)	H = High bond and L = Low bond
Strain distribution		=	T	(B or T)	B = Bending and T = Tension
Reinforcement details					
Number of bars	n	=	1		
Horizontal bar diameter	ϕ_{hor}	=	20	mm	
Horizontal bar spacing	s_{hor}	=	0	mm	
Vertical bar diameter	ϕ_{vert}	=	0	mm	
Vertical bar spacing	s_{vert}	=	0	mm	
Concrete cover 1	c_1	=	20	mm	
Concrete cover 2	c_2	=	0	mm	
Modulus of elasticity of steel	E_s	=	200000	MPa	
Calculations					
Horizontal steel area per face	$A_{s,hor}$	=	314	mm^2	n*PI()/4 * ϕ_{hor}^2
Area of concrete	A_c	=	40000	mm^2	(b*h)
Reinforcement ratio	ρ	=	0,79	%	As/Ac
Effective height	$h_{c,eff}$	=	75	mm	Min(2,5*(c1+ϕ_{hor}/2) ; h/2)
Effective tension area	$A_{c,eff}$	=	15000	mm^2	hc,eff* b
Effective reinforcement ratio	$\rho_{p,eff}$	=	2,09	%	As / Ac,eff
Concrete properties					
Mean compressive strength at 28 days	f_{cm}	=	38	MPa	fck+8
Mean concrete compressive strength at an age of t days	f_{cm} (t)	=	38	MPa	βcc(t)*fcm
Mean concrete tensile strength	f_{ctm}	=	2,90	MPa	0,30*fck^(2/3)
Effective concrete tensile strength at an age of t days	$f_{ct,eff}$(t)	=	2,90	MPa	βcc(t)^α * fctm
Coefficient which depends on the age of concrete	β_{cc}(t)	=	1,00		exp(s(1-(28/t)^0,5))
	α	=	0,67		α = 1 for t < 28 and α = 2/3 for t=>28
Coefficient which depends on the type of cement	s	=	0,20		S = 0,38; N = 0,25; R = 0,20
Modulus of elasticity of concrete	E_{cm}	=	32837	MPa	22*(fcm)/10)^0,3 * 10^3
Modulus of elasticity of concrete at an age of t days	E_{cm} (t)	=	32837	MPa	(((βcc(t)*fcm(t))/fcm(t))^0,3)*Ecm
Modular ratio	α_e	=	6,1		Es\Ecm(t)
Van Breugel					
Cracking force	N_{cr}	=	121	kN	fct,eff * Act * (1+ρ * αe)
Imposed strain	ε_{imp}	=	418	με	Next/ (As * Es)
Concrete strain at onset of cracking	ε_{cr}	=	88	με	fctm/Ec
Concrete strain at onset of the fully devevelop crack pattern	ε_{stc}	=	987	με	(60 + 2,4 * σs,cr) * 10^-6
Steel yielding strain	ε_{sy}	=	2174	με	(fyk/1,15)/Es
Uncracked stage ($\varepsilon_s = \varepsilon_c = \varepsilon_{imp} < \varepsilon_{cr}$)	N/A				
Steel tensile stress	σ_s	=	84	MPa	ε_{imp} * Es
Concrete tensile stress	σ_c	=	14	MPa	ε_{imp} * Ecm
Crack formation stage ($\varepsilon_{cr} < \varepsilon_{imp} < \varepsilon_{stc}$)	Crack Formation Stage				
Steel tensile stress in the crack/directly after cracking	$\sigma_s = \sigma_{s,cr}$	=	386	MPa	Ncr/As
Concrete tensile stress directly after cracking	σ_{cr}	=	2,9	MPa	fctm
Mean crack width not fully developed crack pattern	w_{m0}	=	0,40	mm	2*((0,4*ε_{eq}/fcm*Es)*(σcr/ρ)^2*(1+αe ρ))^0,85
Factor for scatter	γ_s	=	1,3		
Factor for sustained load/alternating load	γ_{∞}	=	1,3		
Max crack width	w_{max}	=	0,67	mm	γs * γ∞ * wm0
Stabilzed cracking stage ($\varepsilon_{imp} > \varepsilon_{stc}$)	N/A				
Steel tensile stress	σ_s	=	273	MPa	Ncr/As + Es (εimp - εfdcp)
Steel tensile stress directly after cracking	$\sigma_{s,cr}$	=	386	MPa	Ncr/As or **fctm/ρ (1+αe * ρ)**
Transfer length	l_{st}	=	248	mm	1,2 * wm0 * Es / σs,cr
Mean crack spacing	$s_{r,mean}$	=	372	mm	1,5 *lst
Maximum crack spacing	$s_{r,max}$	=	495	mm	
Mean crack width fully developed crack pattern	w_{mv}	=	0,15	mm	Sr,mean/Es * (σs - 0,5 * σs,cr)
Mean crack width not fully developed crack pattern	w_{mv}	=	0,36	mm	1,8 * wm0 *((σs/σs,cr) - 0,5)
Factor for scatter	γ_s	=	1,5		Tension = 1.5 and Flexure = 1.7
Factor for sustained load/alternating load	γ_{∞}	=	1,3		
Max crack width	w_{max}	=	0,29		γs * γ∞ * wm0
Steel yielding stage ($\varepsilon_{imp} > \varepsilon_{sy}$)	N/A				

Figure B.4: Spreadsheet Van Breugel

B.5. CIRIA C660 - II

Input parameters	Symbol		Value	Unit	
Section details and material properties					
Concrete quality		=	C30/37		
Characteristic concrete cube strength	f_{ck}	=	30	MPa	
Characteristic yield strength	f_{yk}	=	500	MPa	
Width	b	=	200	mm	
Section thickness	h	=	200	mm	
Length of the wall	L	=	1000	mm	
Early age of cracking	t_0	=	3	days	
Long term age of cracking	t	=	28	days	
Cement type		=	R	(S, N or R)	
Load duration		=	L	(S or L)	S = Short term and L = Long term
Bond properties		=	H	(H or L)	H = High bond and L = Low bond
Strain distribution		=	T	(B or T)	B = Bending and T = Tension
Reinforcement details					
Number of bars	n	=	1		
Horizontal bar diameter	$ø_{hor}$	=	20	mm	
Horizontal bar spacing	s_{hor}	=	0	mm	
Vertical bar diameter	$ø_{vert}$	=	0	mm	
Vertical bar spacing	s_{vert}	=	0	mm	
Concrete cover 1	c_1	=	20	mm	
Concrete cover 2	c_2	=	0	mm	
Modulus of elasticity of steel	E_s	=	200000	MPa	
Calculations					
Horizontal steel area per face	$A_{s,hor}$	=	314	mm^2	n*Pi()/4 * $ø_{hor}$^2
Area of concrete	A_c	=	40000	mm^2	(b*h)
Reinforcement ratio	ρ	=	0,79	%	As/Ac
Effective height	$h_{c,eff}$	=	75	mm	Min(2,5*(c1+øhor/2) ; h/2)
Effective tension area	$A_{c,eff}$	=	15000	mm^2	hc,eff* b
Effective reinforcement ratio	$ρ_{p,eff}$	=	2,09	%	As / Ac,eff
Early age concrete properties					
Mean compressive strength at 28 days	f_{cm}	=	38	MPa	fck+8
Mean concrete compressive strength at an age of t_0 days	f_{cm} (t)	=	25	MPa	βcc(t)*fcm
Mean concrete tensile strength	f_{ctm}	=	2,90	MPa	0,30*fck^(2/3)
Effective concrete tensile strength at an age of t days	$f_{ct,eff}$ (t)	=	1,92	MPa	**βcc(t)^α * fctm**
Coefficient which depends on the age of concrete	$β_{cc}$(t)	=	0,66		exp(s(1-(28/t)^0,5))
	α	=	1,00		α = 1 for t < 28 and α = 2/3 for t=>28
Coefficient which depends on the type of cement	s	=	0,20		S = 0,38; N = 0,25; R = 0,20
Modulus of elasticity of concrete	E_{cm}	=	32837	MPa	22*(fcm)/10)^0,3 * 10^3
Modulus of elasticity of concrete at an age of t days	E_{cm} (t)	=	29027	MPa	(((βcc(t)*fcm(t))/fcm(t))^0,3)*Ecm
Modular ratio	$α_e$	=	6,9		Es\Ecm(t)
Long term concrete properties					
Mean concrete compressive strength at an age of t days	f_{cm} (t)	=	38	MPa	βcc(t)*fcm
Effective concrete tensile strength at an age of t days	$f_{ct,eff}$ (t)	=	2,90	MPa	βcc(t)^α * fctm
Coefficient which depends on the age of concrete	$β_{cc}$(t)	=	1,00		exp(s(1-(28/t)^0,5))
	α	=	0,67		α = 1 for t < 28 and α = 2/3 for t=>28
Coefficient which depends on the type of cement	s	=	0,20		S = 0,38; N = 0,25; R = 0,20
Modulus of elasticity of concrete	E_{cm}	=	32837	MPa	22*(fcm)/10)^0,3 * 10^3
Modulus of elasticity of concrete at an age of t days	E_{cm} (t)	=	32837	MPa	(((βcc(t)*fcm(t))/fcm(t))^0,3)*Ecm
Modular ratio	$α_e$	=	6,1		Es\Ecm(t)
Coëfficients					
Bond properties of reinforcement	k1	=	0,80		high bond = 0,8 ; bars with effective plain surface = 1,6
Strain distribution in cross section	k2	=	1,0		bending = 0,5 and pure tension = 1,0
Takes into account the cover	k3	=	3,4		
Takes into account the cross section of reinforcement	k4	=	0,425		
Effect of the load duration	kt	=	0,40		long term (L) = 0,4 and short term (S) = 0,6
Takes into account stress distribution	kc	=	1,00		pure tension = 1,0
Takes into account the effect of non-uniform equilibrium stresses which lead to a reduction of restraint forces	k	=	1,00		h ≤ 300 = 1,0 and h > 800 = 0,65
Creep factor	K1	=	0,65		
Sustained load factor	K2	=	0,8		
Coefficient of thermal expansion of concrete	αc	=	11,8	με/°C	
Early age strain					
Degree of restraint	R1	=	0,5		
Temperature drop	T1	=	40	°C	T_2 = Peak temperature - mean ambient temperature
Early age tensile strain capacity	εctu(ea)	=	81	με	(fctm(to)/Ecm) * (K2/K1)
Autogenous shrinkage	εca(ea)	=	15	με	2,5(fck-10) * (1-exp(-0,2*to^0,5)
Early age free contraction	εfree(ea)	=	487	με	αc * T1 + εca(ea)
Early age restraind contraction	εr(ea)	=	158	με	R1 * K1 * (T1 * αc + εca(ea))
Early age crack inducing strain	εcr(ea)	=	117	με	R1 * K1 * (T1 * αc + εca(ea)) - 0,5 εctu(ea)
Long term strain (excluding eary age strain)					
Restraint to long term thermal strains	R2	=	0,5		
Restraint to drying shrinkage	R3	=	0,5		
Long term temperature change	T2	=	20	°C	
Drying shrinkage	εcd	=	385	με	

Figure B.5: Spreadsheet CIRIA C660 II

B.6. ICE 0706 - II

Input parameters	Symbol		Value	Unit	
Section details and material properties					
Concrete quality		=	C30/37		
Characteristic concrete cube strength	f_{ck}	=	30	MPa	
Characteristic yield strength	f_{yk}	=	500	MPa	
Width	b	=	200	mm	
Section thickness	h	=	200	mm	
Length of the wall	L	=	1000	mm	
Early age of cracking	t_0	=	3	days	
Long term age of cracking	t	=	28	days	
Cement type		=	R	(S, N or R)	
Load duration		=	L	(S or L)	S = Short term and L = Long term
Bond properties		=	H	(H or L)	H = High bond and L = Low bond
Strain distribution		=	T	(B or T)	B = Bending and T = Tension
Reinforcement details					
Number of bars	n	=	1,0		
Horizontal bar diameter	$Ø_{hor}$	=	20	mm	
Horizontal bar spacing	s_{hor}	=	0	mm	
Vertical bar diameter	$Ø_{vert}$	=	0	mm	
Vertical bar spacing	s_{vert}	=	0	mm	
Concrete cover 1	c_1	=	20	mm	
Concrete cover 2	c_2	=	0	mm	
Modulus of elasticity of steel	E_s	=	200000	MPa	
Calculations					
Horizontal steel area per face	$A_{s,hor}$	=	314	mm^2	n*Pi()/4 * ØhorA2
Area of concrete	A_c	=	40000	mm^2	(b*h)
Reinforcement ratio	ρ	=	0,79	%	As/Ac
Effective height	$h_{c,eff}$	=	75	mm	Min(2,5*(c1+Øhor/2) ; h/2)
Effective tension area	$A_{c,eff}$	=	15000	mm^2	hc,eff* b
Effective reinforcement ratio	$ρ_{p,eff}$	=	2,09	%	As / Ac,eff
Early age concrete properties					
Mean compressive strength at 28 days	f_{cm}	=	38	MPa	fck+8
Mean concrete compressive strength at an age of t_0 days	f_{cm} (t)	=	25	MPa	βcc(t)*fcm
Mean concrete tensile strength	f_{ctm}	=	2,90	MPa	0,30*fckA(2/3)
Effective concrete tensile strength at an age of t days	$f_{ct,eff}$ (t)	=	1,92	MPa	**βcc(t)*α * fctm**
Coefficient which depends on the age of concrete	$β_{cc}$(t)	=	0,66		exp(s(1-(28/t)^0,5))
	α	=	1,00		α = 1 for t < 28 and α = 2/3 for t=>28
Coefficient which depends on the type of cement	s	=	0,20		S = 0,38; N = 0,25; R = 0,20
Modulus of elasticity of concrete	E_{cm}	=	32837	MPa	22*(fcm)/10)^0,3 * 10^3
Modulus of elasticity of concrete at an age of t days	E_{cm} (t)	=	29027	MPa	(((βcc(t)*fcm(t))/fcm(t))^0,3)*Ecm
Modular ratio	$α_e$	=	6,9		Es\Ecm(t)
Strain relief	B	=	7,9		((k*kc)/(αe*p,eff)) + 1
Long term concrete properties					
Mean concrete compressive strength at an age of t days	f_{cm} (t)	=	38	MPa	βcc(t)*fcm
Effective concrete tensile strength at an age of t days	$f_{ct,eff}$ (t)	=	2,90	MPa	βcc(t)*α * fctm
Coefficient which depends on the age of concrete	$β_{cc}$(t)	=	1,00		exp(s(1-(28/t)^0,5))
	α	=	0,67		α = 1 for t < 28 and α = 2/3 for t=>28
Coefficient which depends on the type of cement	s	=	0,20		S = 0,38; N = 0,25; R = 0,20
Modulus of elasticity of concrete	E_{cm}	=	32837	MPa	22*(fcm)/10)^0,3 * 10^3
Modulus of elasticity of concrete at an age of t days	E_{cm} (t)	=	32837	MPa	(((βcc(t)*fcm(t))/fcm(t))^0,3)*Ecm
Modular ratio	$α_e$	=	6,1		Es\Ecm(t)
Strain relief	B	=	8,8		((k*kc)/(αe*p,eff)) + 1
Coëfficients					
Bond properties of reinforcement	k1	=	0,80		high bond = 0,8 ; bars with effective plain surface = 1,6
Strain distribution in cross section	k2	=	1,0		bending = 0,5 and pure tension = 1,0
Takes into account the cover	k3	=	3,4		
Takes into account the cross section of reinforcement	k4	=	0,425		
Effect of the load duration	kt	=	0,40		long term (L) = 0,4 and short term (S) = 0,6
Takes into account stress distribution	kc	=	1,00		pure tension = 1,0
Takes into account the effect of non-uniform equilibrium stresses which lead to a reduction of restraint forces	k	=	1,00		h ≤ 300 = 1,0 and h > 800 = 0,65
Lenght coefficient	k_L	=	1,50		1 < kL < 2
Creep factor	K1	=	0,7		
Sustained load factor	K2	=	0,8		
Coefficient of thermal expansion of concrete	αc	=	11,8	με/°C	
Early age strain					
Degree of restraint	R1	=	0,5		
Temperature drop	T1	=	40	°C	T_1 = Peak temperature - mean ambient temperature
Early age tensile strain capacity	εctu(ea)	=	81	με	(fctm(to)/Ecm) * (K2/K1)
Autogenous shrinkage	εca(ea)	=	15	με	2,5(fck-10) * (1-exp(-0,2*to^0,5)
Early age free contraction	εfree(ea)	=	487	με	αc * T1 + εca(ea)
Early age restraind contraction	εr(ea)	=	158	με	R1 * K1 * (T1 * αc + εca(ea))
Early age crack inducing strain	εcr(ea)	=	117	με	R1 * K1 * (T1 * αc + εca(ea)) - 0,5 εctu(ea)
Long term strain (excluding eary age strain)					
Restraint to long term thermal strains	R2	=	0,5		
Restraint to drying shrinkage	R3	=	0,5		
Long term temperature change	T2	=	20	°C	
Drying shrinkage	εcd	=	385	με	
Long term tensile strain capacity	εctu(lt)	=	109	με	(fctm(t1)/Ecm) * (K2/K1)
Increase in tensile strain capacity	δεctu	=	27	με	εctu(lt) - εctu(ea)
Autogenous shrinkage (residual up to 28 days)	δεca(lt)	=	18	με	2,5(fck-10) * (1-exp(-0,2*to^0,5) - εca(ea)
Long term free contraction	εfree(lt)	=	639	με	δεca(lt) + αc * T2 + εca(lt)
Long term restraind contraction	εr(lt)	=	208	με	K1 * (R2 * T2 * αc + R3 (δεca + εcd))
Long term crack inducing strain	εcr(lt)	=	181	με	K1 * (R2 * T2 * αc + R3 (δεca + εcd)) - δεca(lt)
Total strain (early-age + long term)					
Free contraction	$ε_{free}$(total)	=	1126	με	εfree(ea) + εfree(lt)
Restrained contraction	εr(total)	=	366	με	εr(ea) + εr(lt)
Crack inducing strain	εcr(total)	=	298	με	εcr(ea) + εcr(lt)
Crack spacing and crack width					
Transfer length	l_{st} = $S_{r,max}$	=	174	mm	sr,mean / 1,33
Mean crack spacing	$S_{r,mean}$	=	231	mm	sr,max / 1,7
Max final crack spacing	$S_{r,max}$	=	393	mm	k3 * c + k1 * k2 * k4 * ø / ρp,eff
Early age crack width stage 1	$w_{k1(ea)}$	=	0,018	mm	[0,5 * sr,max * εctu(ea)(1-Redge)B] / [1- sr,max Redge / kL * H (1-0,5 (B+1/(1-Redge)))]
Early age crack width stage 2	$w_{k2(ea)}$	=	0,045	mm	sr,max (1-0,5 R) *K1 * (εfree - εctu/Redge*K1)
Early age crack width	$w_{k(ea)}$	=	0,063	mm	wk1(ea) + wk2(ea)
Long term crack width stage 1	$w_{k1(lt)}$	=	0,024	mm	[0,5 * sr,max * εctu(ea)(1-Redge)B] / [1- sr,max Redge / kL * H (1-0,5 (B+1/(1-Redge)))]
Long term crack width stage 2	$w_{k2(lt)}$	=	0,152	mm	sr,max (1-0,5 R) *K1 * (εfree - εctu/Redge*K1)
Long term crack width stage 2	$w_{k(lt)}$	=	0,176	mm	wk1(lt) + wk2(lt)

Figure B.6: Spreadsheet ICE 706

C

Data required for design

During the design stage, there might be limited knowledge of the concrete to be used or the construction process and therefore conservative assumptions should be made that may not be reflected in practice. In addition, many aspects of performance such as usability, durability and structural integrity has to be taken into account. The designer should be aware of implications such as minimizing the cement content for durability reasons, because this may increase the risk of thermal cracking.

In this section the most important data which is required for the predictions of cracking is explained.

C.1. Estimating drying shrinkage

For the estimation of the drying shrinkage the Eurocode 2 provides a method which is based on the strength class, the average ambient RH and the dimensions of the element. This estimation start with the calculation of the nominal unrestrained drying shrinkage $\epsilon_{cd,0}$. This value is based on the ambient humidity and the strength class of the concrete.

$$\epsilon_{cd,0} = 0,85[(220 + 110 \cdot \alpha_{ds1}) \cdot exp(-\alpha_{ds2} \cdot \frac{f_{cm}}{f_{cmo}}] \cdot 10^{-6} \cdot \beta_{RH}, \quad \text{(C.1)}$$

where:

α_{ds1} coefficient which depends on the type of cement

= 3 for cement class S

= 4 for cement class N

= 6 for cement class R

α_{ds2} coefficient which depends on the type of cement

= 0,13 for cement class S

= 0,12 for cement class N

= 0,11 for cement class R

f_{cm} mean compressive strength

f_{cmo} 10 MPa

RH ambient relative humidity (%)

RH_0 100 %

β_{RH} = $1,55[1 - (\frac{RH}{RH_0})^3]$

The codes takes into account the fact that the ultimate shrinkage will be lower in larger section by implementing a coefficient k_h. This coefficient depends on the notional size of the cross-section h_0 according to the following equation:

$$h_0 = \frac{2 \cdot A_c}{u}, \tag{C.2}$$

where

A_c concrete cross-sectional area

u perimeter of the part of the cross section which is exposed to drying

For walls that drying from two faces, it is assumed that h_0 is approximately equal to the wall thickness h. For walls or slabs drying from one face only, $h_0 = 2 \cdot h$. The relationship between the coefficient k_h and the notional size h_0 is shown in figure X.

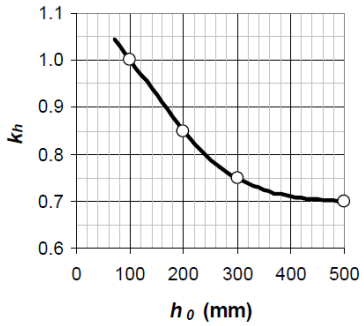

Figure C.1: Relationship between coefficient kh and notional size h0

The rate at which the shrinkage occur can be calculated with the following equation:

$$\epsilon_{cd}(t) = \beta_{ds}(t, t_s) \cdot k_h \cdot \epsilon_{cd,0}, \tag{C.3}$$

where:

$$\beta_{ds}(t, t_s) = \frac{(t - t_s}{(t - t_s) + 0.04 * \sqrt{(h_0)^3}}$$

t age of the concrete at time (in days)

t_s age of concrete at beginning of drying (in days)

Estimation of drying shrinkage				
Input parameters	**Symbol**		**Value**	**Unit**
Number of drying faces	n	=	2	
Age of concrete at time	t	=	42	days
Age of concrete at begin drying	t_s	=	2	days
	α_{ds1}	=	4	-
	α_{ds2}	=	0,12	-
Mean compressive strength	f_{cm}	=	63	MPa
	f_{cm0}	=	10	MPa
Relative humidity	RH	=	60	%
	RH_0	=	100	%
	β_{RH}	=	1,215	-
Unrestraint drying shrinkage	$\epsilon_{cd,0}$	=	310	µm
Notional size	h_0	=	750	mm
Coefficient	k_h	=	0,70	
	$\beta_{ds}(t,t_s)$	=	0,571	
Drying shrinkage	$\epsilon_{cd}(t)$	=	**124,2**	µm

Values for factor kh for calculation of finale value of drying shrinkage strain	
h_0 [mm]	k_h
100	1,00
200	0,85
300	0,75
≥ 500	0,70

Figure C.2: Estimation of drying shrinkage implemented in spreadsheet

C.2. Estimation of the autogenous shrinkage

For the estimation of the autogenous shrinkage does the Model Code 2010 also provide a method. This method is only based on the strength class of the concrete.

$$\epsilon_{ca}(t) = \beta_{as}(t) \cdot \epsilon_{ca}(\infty), \tag{C.4}$$

where:

$\epsilon_{ca}(t)$ autogenous shrinkage at time t days

$\epsilon_{ca}(\infty)$ ultimate autogenous shrinkage = $2.5(f_{ck} - 10) \cdot 10^{-6}$

$\beta_{ds}(t)$ function which defines the time dependent development of autogenous shrinkage
$=1 - exp(-0,2 \cdot t^{0,5})$

Estimation of autogenous shrinkage				
Input parameters	**Symbol**		**Value**	**Unit**
	$\beta_{as}(t)$	=	0,726	-
	$\epsilon_{ca}(\infty)$	=	112,5	µm
Autogenous shrinkage	**$\epsilon_{ca}(t)$**	**=**	**81,72**	**µm**

Figure C.3: Estimation of autogenous shrinkage implemented in spreadsheet

C.3. Estimating temperature drop T1

For the prediction of the temperature drop T_1 the cement content is required. Values for T_1 for CEM I are given in Figure X for walls cooling from both sides.

C.4. Annual temperature drop T2

Over the long-term the concrete will respond to changing environmental conditions. This is taken into account by applying T_2. Before realistic assumption can be made the following has to be taken into account:

- In general, is concrete cast during the day when the actual temperature is higher than the average temperature.
- Changes in temperature within each month will result in periods when the ambient temperature is significantly higher or lower than the monthly average temperature.
- The time of the year when the concrete is cast.

For the annual temperature changes the Eurocode recommend to assume for T_2 a value of 10 C for concrete cast in the winter and a value of 20 C for concrete cast in the summer.

C.5. Estimation degree of restraint

Determine degree of restraint				
Input parameters	**Symbol**		**Value**	**Unit**
			Wall	
Length	L	=	1	m
Height	H	=	0,2	m
L/H	L/H	=	5	
Thickness	t	=	0,2	m
Area of concrete	An	=	0,04	m^2
			Base	
Width	b	=	1	m
Thickness	t	=	0,2	m
Area of concrete	Ao	=	0,2	m^2
Ratio of areas	A_n/A_o	=	0,20	
Ratio of moduli	E_n/E_o	=	5,00	
Restraint factor at joint	**Rj**	**=**	0,50	

Figure C.4: Estimation degree of restraint

D

Mechanics of composite structures

In the following sections, the equations are given needed for the determination of stresses in composite structures subjected to imposed deformations.

D.1. Theory

D.1.1. Cross-sectional properties

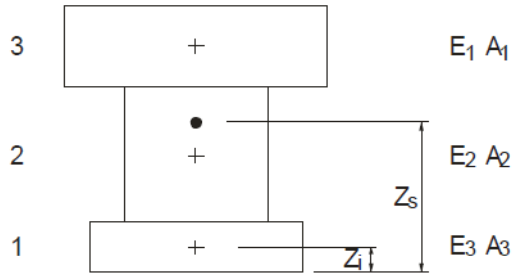

Figure D.1: Composite cross-section

The axial stiffness of one single layer i:

$$K_i = E_i \cdot A_i \tag{D.1}$$

The axial stiffness of a structure which consisting of n layers:

$$(EA)_s = \sum_{i=1}^{n} z_i \cdot E_i \cdot A_i \tag{D.2}$$

The position of the elastic centre of gravity of the composite structure:

$$z_s = \frac{\sum_{i=1}^{n} z_i \cdot E_i \cdot A_i}{(EA)_s} \tag{D.3}$$

The distance of the centre of gravity of an individual layer to that of the composite structure is:

$$a_i = z_s - z_i \tag{D.4}$$

The flexural stiffness of an single layer i is:

$$S_i = E_i \cdot I_i \tag{D.5}$$

The flexural stiffness of a structure which consisting of n layers:

$$(EI)_s = \sum_{i=1}^{n} E_i \cdot I_i + \sum_{i=1}^{n} (z_i - z_s)^2 \cdot E_i A_i \tag{D.6}$$

D.1.2. Response under external loading

In figure D.2 a composite cross-section which is subjected to a external axial force is shown. The axial force acts in the elastic centre of gravity.

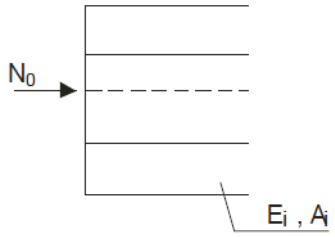

Figure D.2: Composite cross-section

The force in the individual layer is:

$$N_i = N_0 \cdot \frac{E_i A_i}{(EA)_s} \tag{D.7}$$

In figure D.3 a composite cross section which is subjected to a flexural moment is shown.

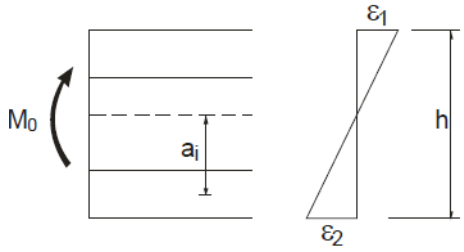

Figure D.3: Composite cross-section

Curvature of composite structure:

$$\kappa_s = \frac{|\epsilon_1| + \epsilon_2}{h} = \frac{M_o}{(EI)_s} \tag{D.8}$$

Strain ϵ_i and axial force N_i in individual layer i

$$\epsilon_i = a_i \cdot \kappa_s = a_i \cdot \frac{M_o}{(EI)_s} \tag{D.9}$$

$$N_i = \epsilon \cdot E_i \cdot A_i = M_o \cdot \frac{a_i \cdot (E_i A_i)}{(EI)_s} \tag{D.10}$$

Curvature κ_i and flexural moment M_i in individual layer i

$$\kappa_i = \frac{M_i}{(E_i I_i)} = \frac{M_o}{(EI)_s} \tag{D.11}$$

$$M_i = M_o \cdot \frac{(EI)_i}{(EI)_s} \tag{D.12}$$

D.1.3. Response under imposed deformation

This paragraph explains the calculation procedure of stresses in case structures are subjected to imposed deformations. The imposed deformation is in this case a temperature drop of one single layer as is shown in figure D.4a.

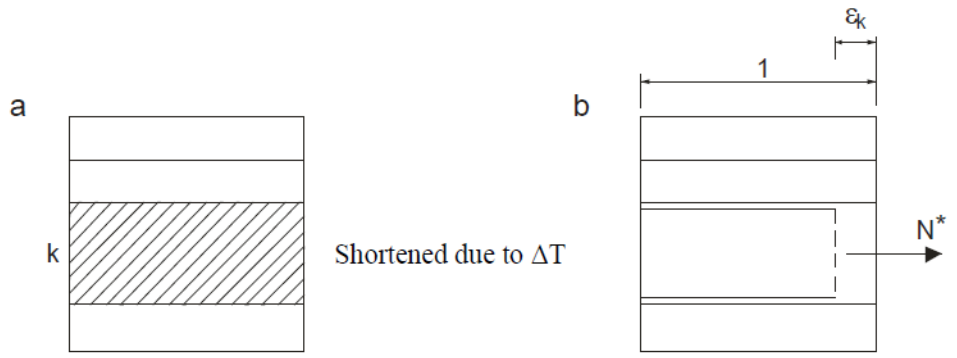

Figure D.4: Schematic overview of response under an imposed deformation (part 1)

For the determination of the stresses in the cross-section, the following procedure applies:

- First of all, it is assumed that the layer of which the temperature changes is able to deform freely. The shortening of the layer is ϵ_k. Then an axial force N^* is applied to eliminate the temperature induced deformation. This force is:

$$N^* = \epsilon_k \cdot (E_k A_k) \tag{D.13}$$

  After this force is applied, the layers are connected to each other again.

- Now the force N^* is applied to the composite cross-section, it has to be noted that this force is applied in the other direction (reverse sign) as is shown in figure D.5c.

- The force N^* should moved to the elastic centre of gravity. This will cause a compensating moment M^* as is illustrated in figure D.5d. This compensating moment can be determined by:

$$M^* = N^* \cdot e, \tag{D.14}$$

  where e is the distance of the axis along which the axial force $N*$ works to the centre of gravity of the composite cross section.

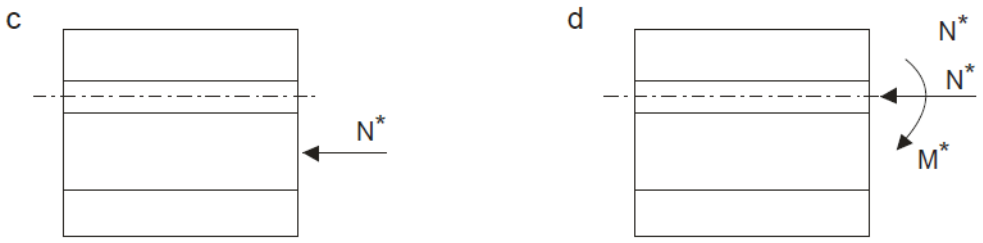

Figure D.5: Schematic overview of response under an imposed deformation (part 2)

Now it is possible to determine the forces and moments in all layers. A distinction can be made between the axial forces and bending moments in the layer which is subjected to the temperature drop (layer k) and the other layers.

Axial force in layer i due to force N^*

$$N_i = \frac{E_i A_i}{(EA)_s} \cdot N^* \tag{D.15}$$

Axial force in layer i due to moment M^*

$$N_i = \frac{M^*}{(EI)_s} \cdot (EA)_i \cdot a_i \tag{D.16}$$

Bending moment in layer i

$$M_i = M^* \cdot \frac{E_i I_i}{(EI)_s} \tag{D.17}$$

Axial force in layer k

$$N_k = N^* - \frac{(EA)_k}{(EA)_s} \cdot N^* + M * \cdot \frac{(EA)_k}{(EI)_s} \cdot a_k \tag{D.18}$$

Bending moment in layer k

$$M_k = \frac{M^*}{(EI)_s} \cdot E_k \cdot I_k \tag{D.19}$$

D.2. Case study - RC wall base restrained by steel section

D.2.1. Introduction

To apply the theory from section D.1 a case study of a reinforced concrete wall which is base restrained by a steel UC section is considered. The height of the wall is 500 mm and the wall thickness is 180 mm. The steel section is a 254x254x73 UC profile. In the following, a more general, straightforward calculation procedure is shown. In this calculation, a lot of non-linearities that play an role in the stress development in hardening concrete are not taken into account. As a result of this, the predicted stresses are less accurate. However, the advantages of this method are its simplicity and speed of execution.

First of all, the situation short after casting of the concrete wall is considered. In this stage, because of the liberation of the heat of hydration, the temperature of the wall increases. The stiffness and strength of the wall also increases. After a while, the elastic modulus and the tensile strength have significantly increase and the wall starts to cool down. In this case is the wall in axial direction restrained by a steel section and as a result the tensile stresses starts to develop in the wall. In order to determine the stresses in the wall, some simplification are required.

It is assumed that the elastic modulus of the wall one week after casting is 31882 MPa and its mean tensile strength is 3.8 MPa. The elastic modulus of the steel is assumed to be 227000 MPa. Furthermore, the temperature drop due to cooling of the wall is estimated at 40 °C. The following quantities apply to the structure:

D.2.2. Calculation

Axial stiffness

Concrete wall

$$E_c \cdot A_c = 31882 \cdot 90000 = 2.87 \cdot 10^9 N \tag{D.20}$$

Steel section

$$E_s \cdot A_s = 227000 \cdot 9310 = 2.11 \cdot 10^9 N \tag{D.21}$$

Flexural stiffness

Concrete wall

$$E_c \cdot I_c = 31882 \cdot \frac{1}{12} \cdot 180 \cdot 500^3 = 5.98 \cdot 10^{13} Nmm^2 \tag{D.22}$$

Steel section

$$E_s \cdot I_s = 22700 \cdot \frac{1}{12} \cdot 180 \cdot 500^3 = 5.98 \cdot 10^{13} Nmm^2 \tag{D.23}$$

Position of the centre of gravity, measured from the top side of the wall.

$$z = \frac{A_c \cdot E_c \cdot z_2 + A_s \cdot E_s \cdot z_1}{K_1 + K_2} = \frac{90000 \cdot 31882 \cdot 250 + 9310 \cdot 227000 \cdot 627}{(2.11 + 2.87) \cdot 10^9} = 410mm \tag{D.24}$$

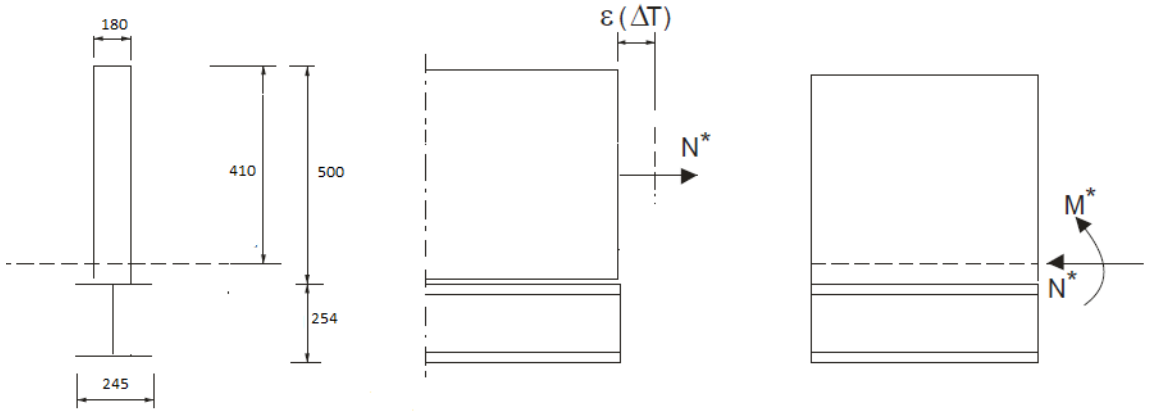

Figure D.6: Concrete wall cast on steel UC section

In first instance there is assumed that the wall is not connected to the steel section. The wall will then shorten due to a temperature-induced shrinkage strain. This shrinkage strain is:

$$\epsilon(\Delta T) = \Delta T \cdot \alpha_c = 40 \cdot 1.18 \cdot 10^{-5} = 0.472 mm/m \tag{D.25}$$

A force N^* is required to restore its original length:

$$N^* = \epsilon(\Delta T) \cdot E_c \cdot A_c = 0.472 * 10^{-3} \cdot 31882 \cdot 90000 = 1.35 \cdot 10^6 N \tag{D.26}$$

Now, the wall is connected to the steel section again. The axial force N^* is applied at the same height but with opposite sign. In order to simplify calculation, the axial force is replaced by a combination of a flexural moment M^* and a axial force N^* which acts in the centre of gravity of the composite structure.

$$M^* = N * \cdot e = 1.35 \cdot 10^6 \cdot (410 - 250) = 2.16 \cdot 10^8 Nmm \tag{D.27}$$

E

Comparison between analytical theory and numerical models

In this section, a comparison is made between the analytical theory and the numerical results. The comparison concerns the cracking load, the cracking strain and the crack spacing which are calculated analytically.

3.2.6.1 Input parameters analytical calculations

Concrete properties

Concrete tensile strength	f_{ctm}	=	2.9	MPa
Elastic modulus of concrete	E_c	=	32836	MPa
Area of concrete	A_c	=	22500	mm^2
Stiffness of concrete	$(EA)_c$	=	738810	kN

Steel properties

Steel yield strength	f_{sy}	=	500	MPa
Elastic modulus of steel	E_s	=	200	GPa
Area of steel	A_s	=	491	mm^2
Stiffness of steel	$(EA)_s$	=	98175	kN

Composite properties

Composite elastic modulus	$(E)_{cs}$	=	$\frac{E_s \cdot A_s + E_s \cdot A_s}{A_s + A_c}$	=	36405	MPa
Composite area	$(A)_{cs}$	=	$\frac{E_s \cdot A_s + E_s \cdot A_s}{E_s + E_c}$	=	3595	MPa
Composite stiffness	$(EA)_{cs}$	=	130867	kN		

3.2.6.1 Cracking load

For the analytical calculation of the cracking load which is described in more detail in section 2.3, the following equation is applied:

$$N_{cr} = \epsilon_{cr} \cdot E_c \cdot A_c \cdot (1 + \alpha_e \cdot \rho) = 8.8 \cdot 10^{-5} \cdot 32836MPa \cdot 22500mm^2 \cdot (1 + 6.1 \cdot 0.022) = 73.74kN \quad \text{(E.1)}$$

According to the numerical model, the cracking load at the beginning of the crack formation stage is 74.06 kN. This is in good agreement with the analytically calculated cracking load.

3.2.6.2 Cracking strain

For the analytical calculation of the cracking strain of the concrete the following equation is applied:

$$\epsilon_{cr} = \frac{f_{ct}}{E_c} = \frac{2.9MPa}{32836MPa} = 8.8 \cdot 10^{-5}[-] \quad \text{(E.2)}$$

In figure E.1 it can be observed that at a prescribed deformation of 0.34 mm, a strain of 8.86e-05 is present in the concrete. At this deformation the first micro cracks occurred. This is in good agreement with the analytical approximation. Important to mention is that the first through cracks developed at a prescribed deformation of 0.53 mm.

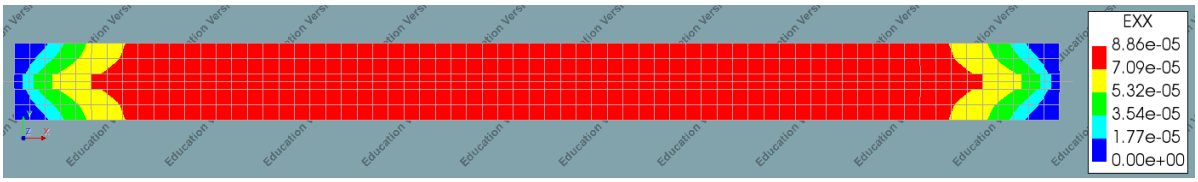

Figure E.1: Cracking strain of concrete at prescribed deformation 0.34 mm according to DIANA

3.2.6.3 Crack spacing

The maximum crack spacing at the end of the crack formation stage can be determined analytically with the following expression:

$$s_{r,max} = 2\dot{l}_t = 2 \cdot \frac{1}{4} \cdot \frac{f_{ctm}}{\tau_{bm}} \cdot \frac{\emptyset}{\rho} = 2 \cdot \frac{1}{4} \cdot \frac{2.9MPa}{5.8MPa} \cdot \frac{25mm}{0.022} = 284mm \quad \text{(E.3)}$$

From figure E.2 it can be observed that according to the numerical models the mean crack spacing is approximately 225 mm. From this it can be concluded that the maximum crack spacing according to the analytical theory is larger than numerically predicted.

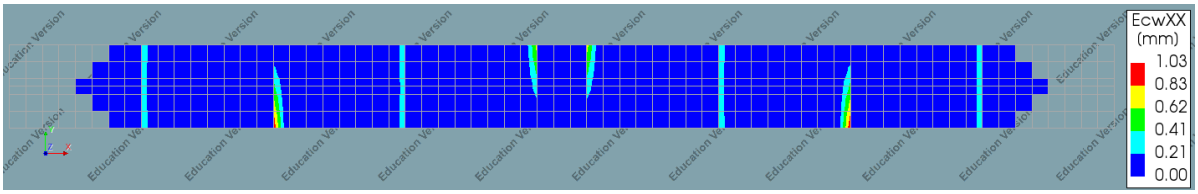

Figure E.2: Crack spacing and crack width at the end of the crack formation stage

F

Results NLFEA using ATENA from J. Camara and R. Luis

In figures F.1 and F.2 the response of a tensile member due to imposed loading and imposed deformations according to the NLFEA using ATENA performed by J. Camara and R. Luis are presented.

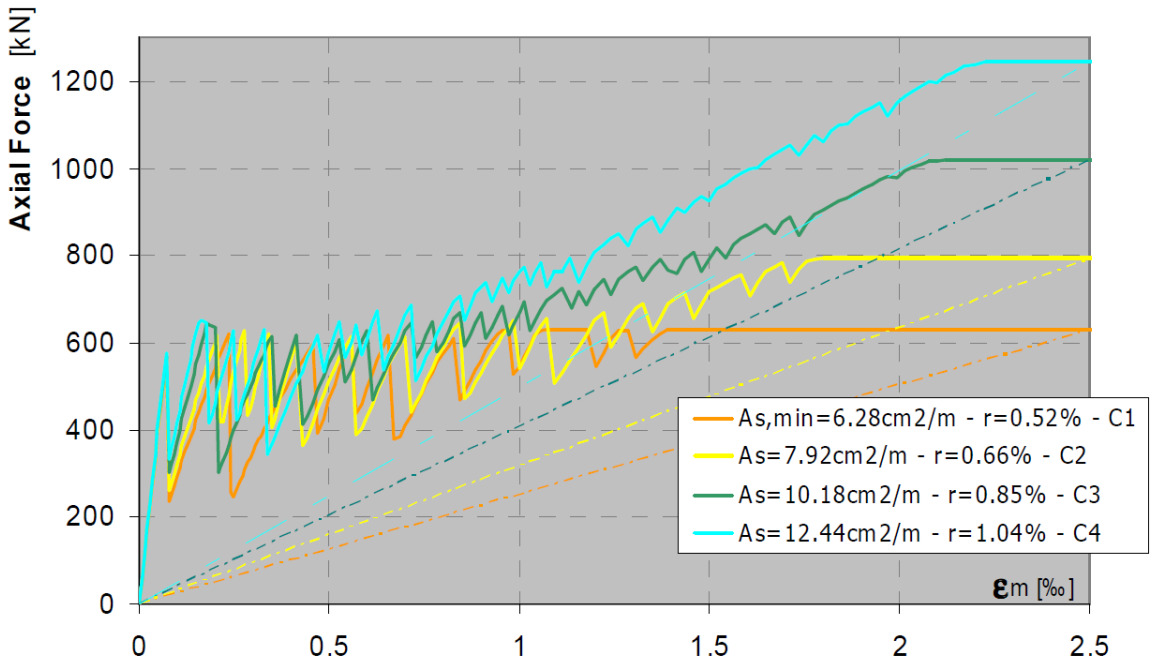

Figure F.1: NLFEA result from J. Camara and R. Luis

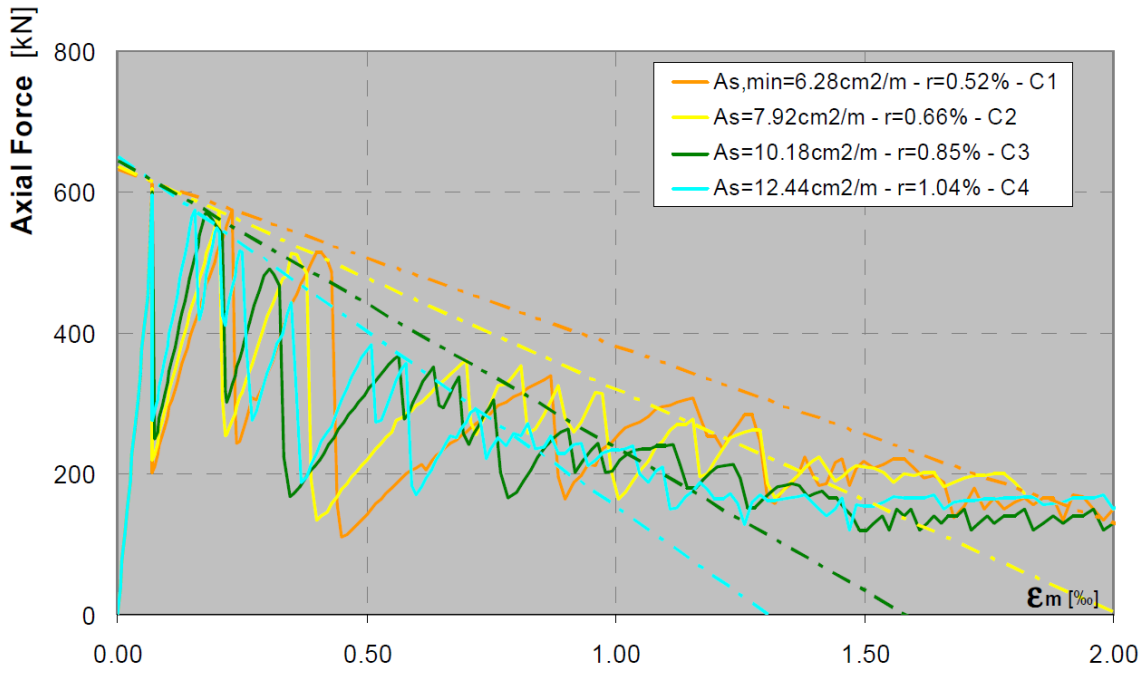

Figure F.2: NLFEA result from J. Camara and R. Luis

G

Influence of convection coefficient in DIANA FEA

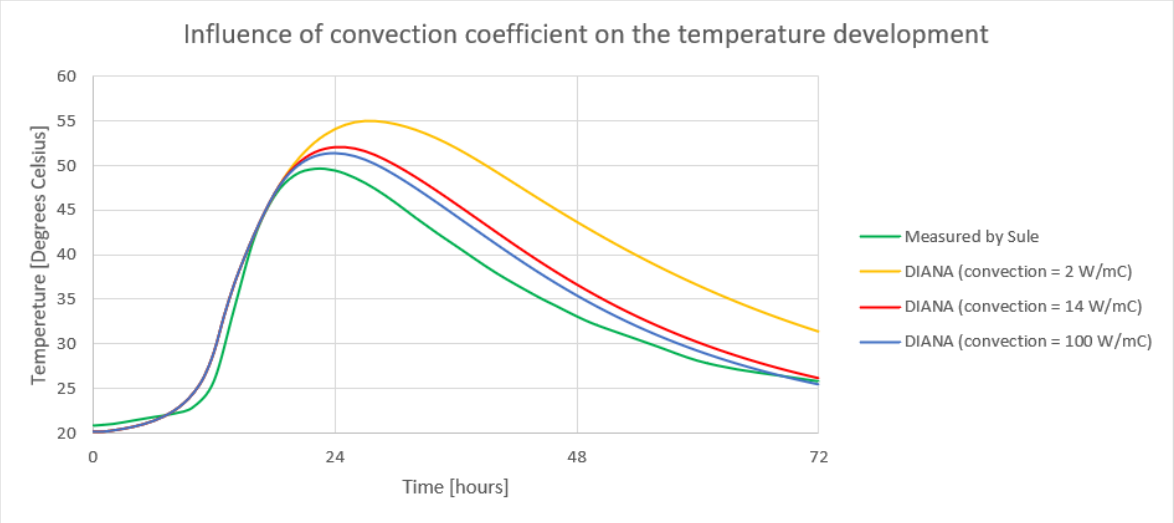

Figure G.1: Influence convection coefficient in DIANA FEA

H

Input files DIANA FEA

Performing a non-linear analysis of a reinforced concrete structure can be a very effective tool to investigate the structural behavior. However, despite the fact that reinforced concrete structures have been widely studied and modelled, modelling of these structures are still very complex and presents a lot of challenges. To make the NLFEA reproducible, in this appendix the main challenges and the python script which has been used to perform a non-linear finite element analysis, simulating the hardening process of concrete in combination with autogenous shrinkage as imposed deformations are given.

H.1. Main challenges

- Modelling the concrete tensile behavior, tension stiffening and cracking in concrete (3.1.1)
- Modelling the bond-slip between the reinforcement and the concrete (3.1.4)
- Modelling the time dependent concrete material properties (4.2.2)
- Numerical convergence problems at cracking (4.2.5)

H.2. Python script

newProject(”name”, 1000,)

Project settings

```
setModelAnalysisAspects( [ ”STRUCT”, ”HEATFL” ] )
setModelDimension( ”3D” )
setDefaultMeshOrder( ”QUADRATIC” )
setDefaultMesherType( ”HEXQUAD” )
setDefaultMidSideNodeLocation( ”LINEAR” )
```

Units

```
setUnit( ”LENGTH”, ”MM” )
setUnit( ”FORCE”, ”N” )
setUnit( ”TIME”, ”HOUR” )
setUnit( ”TEMPER”, ”CELSIU” )
```

Geometry concrete tensile member

```
createBlock( ”Concrete”, [ 0, 0, 0 ], [ 1000, 100, 150 ] )
```

Concrete material properties

```
addMaterial( ”Concrete”, ”CONCR”, ”TSCR”, [ ”HEATFL”, ”MATURI”, ”THERMA” ] )
setParameter( ”MATERIAL”, ”Concrete”, ”LINEAR/ELASTI/YOUNG”, 39283 )
setParameter( ”MATERIAL”, ”Concrete”, ”LINEAR/ELASTI/POISON”, 0.2 )
```

setParameter(”MATERIAL”, ”Concrete”, ”LINEAR/MASS/DENSIT”, 1.93e-16)
setParameter(”MATERIAL”, ”Concrete”, ”LINEAR/THERMA/THERMX”, 1e-05)

Young’s modulus
setParameter(”MATERIAL”, ”Concrete”, ”LINEAR/MATURI/MATYOU”, [0, 0, 2.01733, 150, 4.06923, 400, 6.17812, 1200, 8.38563, 12000, 10.7804, 17333.3, 13.6179, 20904.8, 17.4992, 23949.4, 22.4795, 27156.1, 28.5123, 29563.8, 35.4129, 31789.7, 42.8417, 33464, 50.5018, 34666.7, 58.1664, 35637.9, 65.6606, 36396.2, 72.8638, 36954.8, 79.7183, 37322.5, 86.2011, 37686.6, 92.3078, 37867.4, 103.435, 38047.3, 113.246, 38404.5, 117.722, 38581.9, 121.948, 38652.7, 125.949, 38758.5, 133.371, 38864.1, 136.832, 38934.3, 143.343, 39039.4, 149.395, 39109.3, 155.08, 39179.1, 160.468, 39283.5])

Poisson ratio
setParameter(”MATERIAL”, ”Concrete”, ”LINEAR/MATURI/MATPOI”, [0, 0.2, 2.01733, 0.2, 4.06923, 0.2, 6.17812, 0.2, 8.38563, 0.2, 10.7804, 0.2, 13.6179, 0.2, 17.4992, 0.2, 22.4795, 0.2, 28.5123, 0.2, 35.4129, 0.2, 42.8417, 0.2, 50.5018, 0.2, 58.1664, 0.2, 65.6606, 0.2, 72.8638, 0.2, 79.7183, 0.2, 86.2011, 0.2, 92.3078, 0.2, 103.435, 0.2, 113.246, 0.2, 117.722, 0.2, 121.948, 0.2, 125.949, 0.2, 133.371, 0.2, 136.832, 0.2, 143.343, 0.2, 149.395, 0.2, 155.08, 0.2, 160.468, 0.2])

Thermal expansion coefficient
setParameter(”MATERIAL”, ”Concrete”, ”LINEAR/MATURI/MATALP”, [0, 1e-05, 2.01733, 1e-05, 4.06923, 1e-05, 6.17812, 1e-05, 8.38563, 1e-05, 10.7804, 1e-05, 13.6179, 1e-05, 17.4992, 1e-05, 22.4795, 1e-05, 28.5123, 1e-05, 35.4129, 1e-05, 42.8417, 1e-05, 50.5018, 1e-05, 58.1664, 1e-05, 65.6606, 1e-05, 72.8638, 1e-05, 79.7183, 1e-05, 86.2011, 1e-05, 92.3078, 1e-05, 103.435, 1e-05, 113.246, 1e-05, 117.722, 1e-05, 121.948, 1e-05, 125.949, 1e-05, 133.371, 1e-05, 136.832, 1e-05, 143.343, 1e-05, 149.395, 1e-05, 155.08, 1e-05, 160.468, 1e-05])

Concrete tensile behavior
setParameter(”MATERIAL”, ”Concrete”, ”MODTYP/TOTCRK”, ”ROTATE”)
setParameter(”MATERIAL”, ”Concrete”, ”TENSIL/TENCRV”, ”HORDYK”)
setParameter(”MATERIAL”, ”Concrete”, ”TENSIL/TENSTR”, 5.8)
setParameter(”MATERIAL”, ”Concrete”, ”TENSIL/GF1”, 0.09)
setParameter(”MATERIAL”, ”Concrete”, ”TENSIL/GF1”, 0.09)

Tensile strength
setParameter(”MATERIAL”, ”Concrete”, ”TENSIL/MATURI/MATTST”, [0, 0, 2.01733, 0, 4.06923, 0, 6.17812, 0, 8.38563, 0, 10.7804, 0.2422, 13.6179, 0.8478, 17.4992, 1.4533, 22.4795, 2.18, 28.5123, 2.7856, 35.4129, 3.3911, 42.8417, 3.8756, 50.5018, 4.2389, 58.1664, 4.5417, 65.6606, 4.7839, 72.8638, 4.9656, 79.7183, 5.0867, 86.2011, 5.2078, 92.3078, 5.2683, 103.435, 5.3289, 113.246, 5.45, 117.722, 5.5106, 121.948, 5.5348, 125.949, 5.5711, 133.371, 5.6074, 136.832, 5.6317, 143.343, 5.668, 149.395, 5.6922, 155.08, 5.7164, 160.468, 5.7528])

Fracture energy
setParameter(”MATERIAL”, ”Concrete”, ”TENSIL/MATURI/MATGF1”, [0, 0, 2.01733, 0, 4.06923, 0, 6.17812, 0, 8.38563, 0, 10.7804, 0.01467, 13.6179, 0.03111, 17.4992, 0.04299, 22.4795, 0.05483, 28.5123, 0.06351, 35.4129, 0.07147, 42.8417, 0.07743, 50.5018, 0.08171, 58.1664, 0.08516, 65.6606, 0.08786, 72.8638, 0.08984, 79.7183, 0.09115, 86.2011, 0.09245, 92.3078, 0.09309, 103.435, 0.09373, 113.246, 0.095, 117.722, 0.09564, 121.948, 0.09589, 125.949, 0.09627, 133.371, 0.09664, 136.832, 0.09689, 143.343, 0.09727, 149.395, 0.09752, 155.08, 0.09776, 160.468, 0.09814])

Concrete compressive behavior
setParameter(”MATERIAL”, ”Concrete”, ”COMPRS/COMCRV”, ”PARABO”)
setParameter(”MATERIAL”, ”Concrete”, ”COMPRS/COMSTR”, 86)
setParameter(”MATERIAL”, ”Concrete”, ”COMPRS/GC”, 22.5)

Compressive strength
setParameter(”MATERIAL”, ”Concrete”, ”COMPRS/MATURI/MATCST”, [0, 0, 2.01733, 0, 4.06923,

0, 6.17812, 0, 8.38563, 0, 10.7804, 3.63, 13.6179, 12.7, 17.4992, 21.77, 22.4795, 32.66, 28.5123, 41.73, 35.4129, 50.8, 42.8417, 58.06, 50.5018, 63.51, 58.1664, 68.04, 65.6606, 71.67, 72.8638, 74.39, 79.7183, 76.21, 86.2011, 78.02, 92.3078, 78.93, 103.435, 79.84, 113.246, 81.65, 117.722, 82.56, 121.948, 82.92, 125.949, 83.46, 133.371, 84.01, 136.832, 84.37, 143.343, 84.92, 149.395, 85.28, 155.08, 85.64, 160.468, 86.19])

Heat flow settings

```
setParameter( ”MATERIAL”, ”Concrete”, ”HEATFL/CONDUC”, 108 )
setParameter( ”MATERIAL”, ”Concrete”, ”HEATFL/CAPACI”, 2.675 )
setParameter( ”MATERIAL”, ”Concrete”, ”HEATFL/HEATHY/HYDRAT”, ”PREPRS” )
```

Adiabatic heat curve

```
setParameter( ”MATERIAL”, ”Concrete”, ”HEATFL/HEATHY/ADIAB”, [ 0, 20, 2.4, 32.46, 4.8, 40.42, 7.2, 46.54, 9.6, 51.36, 12, 54.66, 14.4, 57.96, 16.8, 59.95, 19.2, 61.94, 21.6, 63.14, 24, 64.34, 36, 65.07, 48, 65.79, 60, 66.15, 72, 66.5 ] )
setParameter( ”MATERIAL”, ”Concrete”, ”HEATFL/HEATHY/ARRHEN”, 4000 )
setElementClassType( ”SHAPE”, [ ”Concrete” ], ”STRSOL” )
assignMaterial( ”Concrete”, ”SHAPE”, [ ”Concrete” ] )
```

Reinforcement properties

```
createLine( ”Rebar”, [ 0, 50, 75 ], [ 1000, 50, 75 ] )
addMaterial( ”Reinforcement”, ”REINFO”, ”REBOND”, [] )
setParameter( ”MATERIAL”, ”Reinforcement”, ”REBARS/ELASTI/YOUNG”, 200000 )
setParameter( ”MATERIAL”, ”Reinforcement”, ”REBARS/PLATYP”, ”VMISES” )
setParameter( ”MATERIAL”, ”Reinforcement”, ”REBARS/PLASTI/TRESSH”, ”KAPSIG” )
setParameter( ”MATERIAL”, ”Reinforcement”, ”REBARS/PLASTI/KAPSIG”, [ 0, 500, 1, 550 ] )
setParameter( ”MATERIAL”, ”Reinforcement”, ”RESLIP/DSNY”, 130000 )
setParameter( ”MATERIAL”, ”Reinforcement”, ”RESLIP/DSSX”, 13000 )
setParameter( ”MATERIAL”, ”Reinforcement”, ”RESLIP/SHFTYP”, ”BONDS6” )
setParameter( ”MATERIAL”, ”Reinforcement”, ”RESLIP/BONDS6/SLPVAL”, [ 5.5, 2.2, 0.1, 0.6, 0.601, 2.5, 0.4 ] )
addGeometry( ”Reinforcement”, ”RELINE”, ”REBAR”, [] )
setParameter( ”GEOMET”, ”Reinforcement”, ”REITYP”, ”REITRU” )
setParameter( ”GEOMET”, ”Reinforcement”, ”REITRU/RDITYP”, ”RDIAME” )
setParameter( ”GEOMET”, ”Reinforcement”, ”REITRU/DIAMET”, 16 )
setShapeType( ”REINFORCEMENTSHAPE”, ”Rebar” )
setReinforcementType( ”REINFORCEMENTSHAPE”, ”Rebar”, ”TRUSS BOND SLIP” )
assignMaterial( ”Reinforcement”, ”REINFORCEMENTSHAPE”, [ ”Rebar” ] )
assignGeometry( ”Reinforcement”, ”REINFORCEMENTSHAPE”, [ ”Rebar” ] )
```

Dead weight

```
addSet( ”GEOMETRYLOADSET”, ”Dead weight” )
createModelLoad( ”Dead weight”, ”Dead weight” )
```

Interface boundary elements to model convection

```
addMaterial( ”Lateral convection”, ”HEATFL”, ”BOUNDA”, [] )
setParameter( ”MATERIAL”, ”Lateral convection”, ”HTBOUN/CONPAR/CVTYPE”, ”TIMDEP” )
setParameter( ”MATERIAL”, ”Lateral convection”, ”HTBOUN/CONPAR/CONVEC”, 108 )
setParameter( ”MATERIAL”, ”Lateral convection”, ”HTBOUN/CONPAR/TIMDEP/TIMCNV”, [ 0, 0.108, 18, 0.108, 18.0001, 50.4, 144, 50.4 ] )
createConnection( ”Lateral convection”, ”BOUNDA”, ”SHAPEFACE” )
setParameter( ”GEOMETRYCONNECTION”, ”Lateral convection”, ”MODE”, ”CLOSED” )
setElementClassType( ”GEOMETRYCONNECTION”, ”Lateral convection”, ”HEABOU” )
assignMaterial( ”Lateral convection”, ”GEOMETRYCONNECTION”, ”Lateral convection” )
setParameter( ”GEOMETRYCONNECTION”, ”Lateral convection”, ”FLIP”, False )
attachTo( ”GEOMETRYCONNECTION”, ”Lateral convection”, ”SOURCE”, ”Concrete”, [ [ 573.573, 57.3573,
```

```
150 ] ] )
attachTo( ”GEOMETRYCONNECTION”, ”Lateral convection”, ”SOURCE”, ”Concrete”, [ [ 573.573, 0,
63.96405 ] ] )
attachTo( ”GEOMETRYCONNECTION”, ”Lateral convection”, ”SOURCE”, ”Concrete”, [ [ 573.573, 100,
86.03595 ] ] )
attachTo( ”GEOMETRYCONNECTION”, ”Lateral convection”, ”SOURCE”, ”Concrete”, [ [ 426.427, 57.3573,
0 ] ] )
```

External temperature

```
addSet( ”GEOMETRYBCSET”, ”External temperature” )
createSurfaceBoundaryCondition( ”THERMAL”, ”External temperature”, ”External temperature” )
setParameter( ”GEOMETRYBC”, ”External temperature”, ”BOUTYP”, ”EXTEMP” )
setParameter( ”GEOMETRYBC”, ”External temperature”, ”EXTEMP/VALUE”, 20 )
setParameter( ”GEOMETRYBC”, ”External temperature”, ”EXTEMP/CONNEC”, [ ”Lateral convection”
] )
```

Intial temperature

```
addSet( ”GEOMETRYINIFIELDSET”, ”Initial temperature” )
createBodyInitialField( ”Initial temperature”, ”Initial temperature” )
setParameter( ”GEOMETRYINIFIELD”, ”Initial temperature”, ”INITYP”, ”TEMPER” )
setParameter( ”GEOMETRYINIFIELD”, ”Initial temperature”, ”TEMPER/VALUE”, 20 )
attach( ”GEOMETRYINIFIELD”, ”Initial temperature”, [ ”Concrete” ] )
```

Supports

```
createPointSupport( ”Support”, ”Support set 1” )
setParameter( ”GEOMETRYSUPPORT”, ”Support”, ”AXES”, [ 2, 2 ] )
setParameter( ”GEOMETRYSUPPORT”, ”Support”, ”TRANSL”, [ 1, 1, 1 ] )
setParameter( ”GEOMETRYSUPPORT”, ”Support”, ”ROTATI”, [ 0, 0, 0 ] )
attach( ”GEOMETRYSUPPORT”, ”Support”, ”Rebar”, [ [ 1000, 50, 75 ], [ 0, 50, 75 ] ] )
```

Mesh

```
setElementSize( [ ”Concrete” ], 20, 0.5, True )
setMesherType( [ ”Concrete” ], ”HEXQUAD” )
clearMidSideNodeLocation( [ ”Concrete” ] )
generateMesh( [] )
hideView( ”GEOM” )
showView( ”MESH” )
```

Transient staggered thermo-structural analysis

```
addAnalysis( ”Analysis1” )
addAnalysisCommand( ”Analysis1”, ”PHASE”, ”Phase” )
setActivePhase( ”Analysis1”, ”Phase” )
```

Transient heat analysis part

```
addAnalysisCommandDetail( ”Phased”, ”Transient heat transfer”, ”INITIA/TEMPER” )
setAnalysisCommandDetail( ”Phased”, ”Transient heat transfer”, ”INITIA/TEMPER”, True )
setAnalysisCommandDetail( ”Phased”, ”Transient heat transfer”, ”INITIA/ANATYP”, ”NONLIN” )
addAnalysisCommandDetail( ”Phased”, ”Transient heat transfer”, ”INITIA/NONLIN/HYDRAT” )
setAnalysisCommandDetail( ”Phased”, ”Transient heat transfer”, ”INITIA/NONLIN/HYDRAT”, True )
addAnalysisCommandDetail( ”Phased”, ”Transient heat transfer”, ”INITIA/NONLIN/EQUAGE” )
setAnalysisCommandDetail( ”Phased”, ”Transient heat transfer”, ”INITIA/NONLIN/EQUAGE”, True )
setAnalysisCommandDetail( ”Phased”, ”Transient heat transfer”, ”EXECUT/SIZES”, ”1(72)” )
setAnalysisCommandDetail( ”Phased”, ”Transient heat transfer”, ”EXECUT/NONLIN/ITERAT/MAXITE”,
25 )
```

Structural non-linear analysis part

```
addAnalysisCommand( ”Analysis1”, ”NONLIN”, ”Structural nonlinear” )
removeAnalysisCommandDetail( ”Analysis1”, ”Structural nonlinear”, ”EXECUT(1)” )
setAnalysisCommandDetail( ”Analysis1”, ”Structural nonlinear”, ”EXECUT(1)/EXETYP”, ”TIME” )
setAnalysisCommandDetail( ”Analysis1”, ”Structural nonlinear”, ”EXECUT(1)/TIME/STEPS/EXPLIC/SIZES”,
”1.00000” )
setAnalysisCommandDetail( ”Analysis1”, ”Structural nonlinear”, ”EXECUT(1)/TIME/STEPS/EXPLIC/SIZES”,
”1(72)” )
setAnalysisCommandDetail( ”Analysis1”, ”Structural nonlinear”, ”EXECUT(1)/ITERAT/MAXITE”, 10 )
setAnalysisCommandDetail( ”Analysis1”, ”Structural nonlinear”, ”EXECUT(1)/ITERAT/MAXITE”, 500 )
addAnalysisCommandDetail( ”Analysis1”, ”Structural nonlinear”, ”EXECUT(1)/ITERAT/CONVER/ENERGY”
)
setAnalysisCommandDetail( ”Analysis1”, ”Structural nonlinear”, ”EXECUT(1)/ITERAT/CONVER/ENERGY”,
True )
setAnalysisCommandDetail( ”Analysis1”, ”Structural nonlinear”, ”EXECUT(1)/ITERAT/CONVER/ENERGY/NOCONV”,
”CONTIN” )
setAnalysisCommandDetail( ”Analysis1”, ”Structural nonlinear”, ”EXECUT(1)/ITERAT/CONVER/FORCE”,
True )
setAnalysisCommandDetail( ”Analysis1”, ”Structural nonlinear”, ”EXECUT(1)/ITERAT/CONVER/FORCE/NOCONV”,
”CONTIN” )
setAnalysisCommandDetail( ”Analysis1”, ”Structural nonlinear”, ”EXECUT(1)/ITERAT/CONVER/DISPLA”,
False )
```

Set User Output Crack width

```
setAnalysisCommandDetail( ”Analysis1”, ”Structural nonlinear”, ”OUTPUT(2)/SELTYP”, ”USER” )
renameAnalysisCommandDetail( ”Analysis1”, ”Structural nonlinear”, ”OUTPUT(2)”, ”Crack width” )
addAnalysisCommandDetail( ”Analysis1”, ”Structural nonlinear”, ”OUTPUT(2)/USER” )
addAnalysisCommandDetail( ”Analysis1”, ”Structural nonlinear”, ”OUTPUT(2)/USER/STRAIN(1)/CRKWDT”
)
```

Run analysis

```
runSolver( [ ”Analysis1” ] )
```

Bibliography

[1] EN 1992-1-1: Eurocode 2: Design of concrete structures - Part 1-1: General rules and rules for buildings. Technical report, 2004.

[2] EN 1992-3: Eurocode 2: Design of concrete structures - Part 3: Liquid retaining and containment structures. 2006.

[3] P. B. Bamforth and Construction Industry Research and Information Association. *Early-age thermal crack control in concrete*. CIRIA, 2007. ISBN 9780861076602.

[4] Phil Bamforth. The development of a revised unified approach for the design of reinforcement to control cracking in concrete resulting from restrained contraction. Technical report, 2010.

[5] G D Base, J B Read, A W Beeby, and H P J Taylor. An Investigation of the Crack Control Characteristics of Various Types of Bar in Reinforced Concrete Beams. Technical report, ACI American Concrete Institute, 1966.

[6] A W Beeby. The prediction of crack widths in hardened concrete. Technical report, 1979.

[7] N Brattström and O Hagman. Reinforced Concrete Subjected To Restraint Forces A comparison with non-linear numerical analyses KTH ROYAL INSTITUTE OF TECHNOLOGY SCHOOL OF ARCHITECTURE AND THE BUILT ENVIRONMENT. Technical report, 2017.

[8] José CAMARA Associated Professor ISTécnico Av Rovisco and Ricardo Luis Jsj. Crack Control for Imposed Deformations Lisboa. Technical report.

[9] CROW-CUR. Scheurwijdtebeheersing van betonconstructies. Technical report, 2021. URL `www.crow.nl/shop`.

[10] Fédération internationale du béton. *Model code 2010*. Fédération internationale du béton, 2010. ISBN 9782883940963.

[11] A. W. Gutsch. Stoffeigenschaften jungen Betons-Versuche und Modelle. Technical report, Technical University Braunschweig, Braunschweig, 1998.

[12] A. K.H. Kwan and F. J. Ma. Crack width analysis of reinforced concrete under direct tension by finite element method and crack queuing algorithm. *Engineering Structures*, 126:618–627, 11 2016. ISSN 18737323. doi: 10.1016/j.engstruct.2016.08.027.

[13] Lokhorst. Deformational behaviour of concrete influenced by hydration related changes of the microstructure. *Rapport 25-5-99-05*, 2001.

[14] M. Micallef. Crack control in base-restrained reinforced concrete walls. Technical report, Department of Civil and Environmental Engineering, Imperial College of Science, Technology and Medicine, London, 2015.

[15] H Nakamura and T Higai. Compressive Fracture Energy And Fracture Zone Length of Concrete. Technical report, 2001.

[16] R Nirmalsingh. FEM analysis of the cracking behavior of a beam subjected to bending: A discrete crack width calculation using DIANA. Technical report, 2016.

[17] Ana Patrícia, Jorge Santos, José Manuel, and Matos Noronha Da Câmara. Evaluation of the indirect control method of cracking Extended Abstract. Technical report, 2016.

[18] Putter. Towards a uniform and optimal approach for safe NLFEA of re-inforced concrete beams. Technical report, 2020. URL `http://repository.tudelft.nl/`.

[19] Rijkswaterstaat. Guidelines for Nonlinear Finite Element Analysis of Concrete Structures. Technical report, 2017.

[20] F. S. Rostasy. Mechanical models of the stress-strain behaviour of young concrete in axial tension and compression. Technical report, Technical University Lulea, Lulea, 2001.

[21] S. Sule. *Effect of Reinforcement on Early-Age Cracking in High Strength Concrete*. PhD thesis, TU Delft, Delft, 3 2003.

[22] R. Salinger. High-grade steel in reinforced concrete. *Second Congress of the International Association for Bridge and Structural Engineering (IABSE)*, 1936.

[23] J R Van Bokhorst. Early-age cracking of concrete A study into the influence of stress relaxation on early-age cracking of concrete structures under imposed deformations. Technical report, 2020. URL `http://repository.tudelft.nl/.`

[24] Van Breugel, Van Der Veen, Braam, and Walraven. Concrete Structures under Imposed Thermal and Shrinkage Deformations Theory and Practice. Technical report, 2013.

[25] R Verschuur. Effective concrete tension zone. Technical report, 2018. URL `http://repository.tudelft.nl`.

[26] Y Zondag. Control of early-age cracking aimed at a test case for bacterial self-healing concrete. Technical report, 2021. URL `http://repository.tudelft.nl/.`